UNIVERSIDADE ESTADUAL DE MARINGÁ
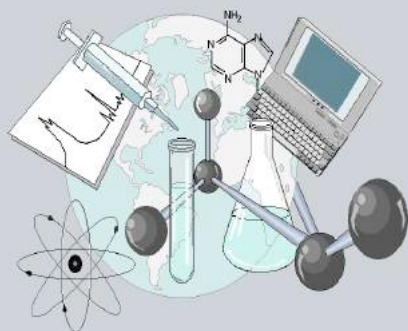
CENTRO DE CIÊNCIAS EXATAS

DEPARTAMENTO DE QUÍMICA

PROGRAMA DE PÓS-GRADUAÇÃO EM QUÍMICA

"Materiais híbridos magnéticos: preparação, caracterização e aplicação na área biomédica"

Tese apresentada por **Ernandes Taveira Tenório Neto** ao Programa de Pós-Graduação em Química do Departamento de Química do Centro de Ciências Exatas da Universidade Estadual de Maringá como parte dos requisitos para a obtenção do título de Doutor em Química.

CCE

Centro de Ciências Exatas

MARINGÁ, JUNHO/2016

UNIVERSIDADE ESTADUAL DE MARINGÁ
CENTRO DE CIÊNCIAS EXATAS – CCE
DEPARTAMENTO DE QUÍMICA
PROGRAMA DE PÓS-GRADUAÇÃO EM QUÍMICA

"Materiais híbridos magnéticos: preparação, caracterização e aplicação na área biomédica"

Orientador: Prof. Dr. Marcos Hiroiuqui Kunita
Dourorando: MSc. Ernandes Taveira Tenório Neto

Junho / 2016

Ernandes Taveira Tenório Neto

"Materiais híbridos magnéticos: preparação, caracterização e aplicação na área biomédica"

Tese apresentada ao Programa de Pós-Graduação em Química do Departamento de Química do Centro de Ciências Exatas da Universidade Estadual de Maringá como parte dos requisitos para a obtenção do título de Doutor em Química.

Orientador:
Prof. Dr. Marcos Hiroiuqui Kunita

Maringá – PR

2016

Este é o exemplar definitivo da Tese apresentada por **Ernandes Taveira Tenório Neto**, perante a Comissão Julgadora do Programa de Pós-Graduação em Química em 24 de junho de 2016.

COMISSÃO JULGADORA:

Prof. Dr. Adley Forti Rubira
PRESIDENTE - DQI/UEM

Profa. Dra. Ana Adelina Winkler Hechenleitner
MEMBRO -DQI/UEM

Prof. Dr. Eduardo Radovanovic
MEMBRO - DQI/UEM

Prof. Dr. Roberto de Matos
MEMBRO - UEL

Profa. Dra. Stephani Caroline Beneti
MEMBRO - UTFPR

Aos meus pais,

e à Michele

AGRADECIMENTOS

À minha querida esposa Michele Karoline Lima Tenório que está sempre ao meu lado; obrigado pelo carinho e amizade. Esta é mais uma etapa de nossas vidas e sei, que juntos, iremos realizar muitos sonhos.

À toda minha família, obrigado por tudo!

Enfim, à todos que, de alguma forma, contribuíram para a realização e conclusão deste trabalho.

Muito obrigado!

Ernandes Taveira Tenório Neto

"Os sábios buscam a sabedoria; os néscios pensam já tê-la encontrado".

Napoleão Bonaparte

RESUMO

Os materiais híbridos têm atraído muita atenção devido, principalmente à sua ampla faixa de aplicações, incluindo, liberação controlada de fármacos, captura de células e biossensores. Estes materiais podem ser obtidos a partir da combinação de polímeros com partículas magnéticas. Nesta tese, são apresentados a síntese e caracterização de dois diferentes materiais híbridos magnéticos: i) hidrogéis e ii) nanopartículas. No caso dos hidrogéis, este trabalho reporta a síntese e caracterização de um novo material, com propriedades pH-responsivas, baseado em poli(etileno glicol). A composição dos hidrogéis obtidos, que apresentaram um maior grau de intumescimento em função da variação de pH, foram utilizados como base para a obtenção de um material pH- e magneto-responsivo para aplicação na liberação controlada de Prednisolona (fármaco modelo). O potencial farmacológico desses hidrogéis foi avaliado a partir dos estudos de transporte de água, liberação de fármaco e ensaios de citotoxicidade. Além disso, demonstrou-se que a alteração dos grupos químicos, presente na estrutura polimérica dos hidrogéis, é uma importante característica para a liberação de moléculas encapsuladas. No caso das partículas híbridas magnéticas, avaliaram-se as condições experimentais utilizadas na síntese de partículas com o núcleo magnético e uma casca de poli(estireno-*co*-divinilbenzeno). Em seguida, essa condição experimental foi adaptada de modo a obter-se partículas magneto- e eletro-responsivas do tipo *core-shell* baseados em poli(pirrol-*co*-pirrol-2-ácido carboxílico). As partículas obtidas apresentaram um alto teor de óxido de ferro. Além disso, as partículas contendo grupos carboxílicos na sua superfície apresentaram uma boa condutividade sendo promissores para aplicações de detecção e captura de analitos específicos (como por exemplo sulfapiridina) em laboratórios em miniatura (*lab-on-a-chip*).

Palavras-chave: Poli(etileno glicol), hidrogel, dual-responsivo, partículas magnéticas e materiais híbridos.

ABSTRACT

Hybrid materials have been attracted much attention due to their wide range of applications including drug release, cell sorting, biosensors, and so on. These materials can be obtained combining polymers with magnetic nanoparticles. Herein, two different types of dual-responsive hybrid materials have been developed: i) hydrogels, and ii) nanoparticles. In case of the hydrogels, a novel pH-responsive material based on poly(ethylene glycol) was synthesized and characterized. Then, the samples which showed the best response in swelling under pH-changing were used as reference for obtaining a magnetic- and pH-responsive hydrogel for Prednisolone release (drug model). The pharmacological potential of these hydrogels were demonstrated by determining their water transport profile, drug release behavior, and cytotoxicity. In addition, the structural changes in their polymer network, in response to pH, which is an important characteristic for stimuli-triggered release of guest molecules were demonstrated. For magnetic hybrid nanoparticles, the experimental conditions used to obtain the poly(styrene-*co*-divnylbenzene) shell with magnetic core were studied. Afterwards, the same experimental procedure was adapted in order to obtain a magnetic- and electric-responsive core-shell particles based on poly(pyrrole-*co*-pyrrole-2-carboxylic acid). The desired perfect magnetic core and polymer shell morphology were successfully obtained exhibiting high iron oxide content. Moreover, the obtained particles are found to be conducting material bearing carboxylic groups on their surface. These promising conducting magnetic particles can be used for both transport and lab-on-a-chip detection.

Keywords: Poly(ethylene glycol), hydrogel, dual-responsive, magnetic particles, and hybrid materials.

SUMÁRIO

LISTA DE FIGURAS

LISTA DE TABELAS

LISTA DE ABREVIATURAS

Sigla	Nome
^{13}C-CP/MAS NMR	13C Cross-polarization magic angle spinning
MEO$_2$MA	2-(2-methoxyethoxy)ethyl methacrylate
HEMA	2-hydroxyethyl methacrylate
AAc	Acrylic acid
AMF	Alternating magnetic field
ATRP	Atom transfer radical polymerization
AAS	Atomic absorption spectroscopy
ATR	Attenuated total reflexion
N_A	Avogadro's number
BSA	Bovine serum albumin
HCl	Chloridric acid
CC$_{50}$	Concentration necessary to reduce the cell viability to 50%
C_t	Concentration of the drug at any time
C_∞	Concentration of the drug at equilibrium
CPs	Conducting polymers
CE	Counter electrode
CMC	Critical micelle concentration
CV	Cyclic voltametry
λ_D	Debye length
DTG	Derivative of thermogravimetric curves
DSC	Differential scanning calorimetry
DVB	Divinylbenzene
EIS	Electrochemical impedance spectroscopy
FDA	Food and drug administration
FTIR	Fourier transform infrared spectroscopy
GPC	Gel permeation chromatography
GMA	Glycidyl methacrylate
MHs	Hybrid materials
D_h	Hydrodynamic size

HG	Hydrogels
HPC	Hydroxypropyl cellulose
M_0	Initial mass of the hydrogel
IS	Ionic strength
$FeCl_3.H_2O$	Iron chloride hexahydrate
IONPs	Iron oxide nanoparticles
IPDI	Isophorone diisocyanate
LOC	Lab-on-a-chip
LBL	Layer-by-layer
LCST	Lower critical solution temperature
ME	Magnetic emulsion
MES	Magnetic emulsion seed
MF	Magnetic field
MHNC	Magnetic hydrogels nanocomposites
ML	Magnetic latex
MNPs	Magnetic nanoparticles
Fe	Magnetite
M_t	Mass of the hydrogel at any time
M_{eq}	Mass of the hydrogel at equilibrium
MMP	Matrix metalloproteinase
μ-TAS	Micro-total analysis systems
E	Modulus of elasticity
M_W	Molecular weight
M_WD	Molecular weight distribution
DMAAm	N,N'-dimethyl acrylamide
ODLAG	Oligo(DL-allylglycine)
OEGMA	oligo(ethylene glycol) methacrylate
GMAPEG	PEG modified with GMA
PBS	Phosphate buffer solution
PLGA	Poly(D,L-lactide-co-glycolide)
PDMS	Poly(dimethylsiloxane)
PEG	Poly(ethylene glycol)
PEGDA	Poly(ethylene glycol) diacrylate

PEGDMA	Poly(ethylene glycol) dimethacrylate
PEGMA	Poly(ethylene glycol) methacrylate
PHEMA	Poly(hydroxyethyl methacrylate)
PIA	Poly(itaconic acid)
PNIPAM	Poly(N-isopropylacrylamide)
PVA	Poly(vinyl alcohol)
PBAE	Poly(β-amino ester)-*co*-poly(ethylene glycol)
PCL	Poly(ε-caprolactone)
PAA	Polyacrylate
PANI	Polyaniline
PPy	Polypyrrole
PVP	Polyvinylpyrrolidone (Povidone)
KI	Potassium iodide
pH	Potencial hidrogeniônico
NMR-^{1}H	Proton nuclear magnetic resonance
Py	Pyrrole
Py-2-COOH	Pyrrole-2-carboxylic acid
RE	Reference electrode
RO	Reverse osmosis
RhB	Rhodamine B
Ms	Saturation magnetization
SEM	Scanning electron microscopy
SN	Second nucleation
SA	Sodium acrylate
SDS	Sodium dodecyl sulfate
NaOH	Sodium hydroxyde
$Na_2S_2O_8$	Sodium persulfate
KPS	Potassium persulfate
St	Styrene
SIONPs	Superparamagnetic iron oxide nanoparticles
SW	Swelling degree
TGA	Thermogravimetric analysis
TG	Thermogravimetry

3D	Three dimensional
t_{50}	Time where 50% of drug is released
t_{90}	Time where 90% of drug is released
TEM	Transmission electron microscopy
TEGDMA	Triethylene glycol dimethacrylate
UV	Ultraviolet
VSM	Vibrating sample magnetometer
WE	Working electrode
XRD	x-ray diffraction
αClεCL	α-cloro-ε-caprolactone

INTRODUÇÃO, MOTIVAÇÃO E OBJETIVOS

Os materiais híbridos (MHs) são aqueles obtidos a partir da combinação de materiais de origem orgânica e inorgânica. Geralmente, as substâncias utilizadas na obtenção desses materiais híbridos, devem possuir propriedades complementares dando origem a um único material com propriedades diferenciadas daqueles que lhe deram origem. Por exemplo, os MHs podem ser sintetizados a partir da combinação de polímeros (de origem natural ou sintética) com metais, óxidos metálicos ou cerâmicas[1]

Um exemplo de MHs que vêm sendo estudados são aqueles obtidos a partir da combinação de polímeros sintéticos com óxidos magnéticos. Estes materiais apresentam as propriedades magnéticas, proveniente dos óxidos, além das propriedades intrínsecas do polímero podendo ser aplicados em diversas áreas, incluindo em sensores, catalisadores, membranas, revestimentos, adsorventes e na liberação controlada de fármacos.

Os materiais magnéticos são conhecidos por apresentar uma resposta frente a um campo magnético. Contudo, o magnetismo é uma propriedade básica de qualquer material. A origem desta propriedade vem da combinação do momento angular orbital e momento angular de spin dos átomos fazendo com que cada átomo se comporte como um pequeno ímã (domínios magnéticos). Esses materiais podem ser classificados como paramagnético, diamagnético, antiferromagnético, ferrimagnético ou ferromagnético[2].

Os materiais paramagnéticos e diamagnéticos apresentam comportamento, em termos vetoriais, semelhante. Em um material paramagnético, os momentos dos átomos alinham-se na mesma direção e sentido do campo magnético (CM) enquanto que nos materiais diamagnéticos os momentos são alinhados na mesma direção e sentido oposto ao campo. Além disso, na ausência do CM, esses materiais apresentam uma magnetização residual, uma vez que, somente uma parte desses momentos retornam ao seu estado original. O comportamento antiferromagnético é observado quando o material não apresenta uma resposta aparente ao CM. Isso ocorre devido à posição antiparalela dos seus momentos. Em materiais ferromagnéticos todos os momentos estão alinhados, mesmo na ausência de um campo magnético externo, como consequência, esses materiais apresentam um "magnetismo natural", enquanto que no estado ferrimagnético, a combinação dos momentos de átomos diferentes é diferente de zero.

Dentre os materiais magnéticos, destaca-se o óxido de ferro principalmente devido à sua biocompatibilidade, baixa toxicidade, fácil preparação e baixo custo[3]. Além disso, o oxido de ferro, na escala nanométrica, pode apresentar propriedades superparamagnéticas (propriedade magnética semelhante ao paramagnetismo sem exibir magnetização residual)[4], característica essa, que é muito importante no desenvolvimento de materiais híbridos.

Um exemplo de materiais híbridos que utilizam o óxido de ferro são os hidrogéis (HG). Esses, são constituídos de uma rede polimérica reticulada tridimensionalmente que pode reter grandes quantidades de água ou fluídos biológicos permitindo a difusão de nutrientes ou fármacos[5]. Essa característica torna os HG importante para diversas aplicações incluindo biossensores, lentes de contato, carreador de nutrientes/fármacos, substrato para cultura celular, membranas, engenharia de tecidos entre outros. Quando combinado com partículas magnéticas, as propriedades de intumescimento do hidrogel podem ser controladas por estímulos externos, sendo extremamente útil na área biomédica[6].

Uma outra classe de materiais baseados em polímeros e óxidos metálicos combinados que tem atraído a atenção são as partículas híbridas coloidais. Essas partículas podem ser classificadas como *core-shell* ou *Janus*. Nas partículas do tipo *core-shell* a casca polimérica protege todo o núcleo magnético além de conferir grupos funcionais específicos às partículas[3]. Por outro lado, as partículas do tipo *Janus* possuem a superfície com dois hemisférios distintos, no qual, o polímero reveste parcialmente a superfície da partícula magnética. Esses materiais podem ser utilizados para acelerar processos de separação de misturas (que contém o analito de interesse) e de diagnóstico que muitas vezes são dispendiosos e necessitam de muito tempo. Além disso, as partículas híbridas magnéticas podem ser aplicadas em seleção de células, liberação controlada de fármacos e imunoensaios[7-9].

Embora hidrogéis e partículas coloidais, de certa forma, possam ser considerados materiais diferentes entre si, suas aplicações não o são. Ambos os materiais podem ser aplicados tanto na liberação controlada de fármacos quanto em biossensores, ou qualquer outra aplicação situada entre esses dois exemplos. Por este motivo, esses materiais são de extrema importância para a área biomédica.

Assim sendo, neste trabalho, objetivou-se a síntese de novos materiais híbridos que possuam propriedades magnéticas combinadas com outras propriedades responsivas

específicas (multi-responsivas) voltadas para aplicações na área biomédica. Como objetivos específicos, sintetizou-se hidrogéis magneto- e pH-responsivos, com o objetivo de obter-se um material multi-responsivo voltado para aplicações biomédicas. Além disso, objetivando as aplicações em biossensores, estudaram-se as rotas de síntese de partículas do tipo "*core-shell*", caracterizaram-se as propriedades do material e, a partir dos dados obtidos, obteve-se partículas com propriedades multi-responsivas (elétricas e magnéticas).

PARTE I *– SÍNTESE E CARACTERIZAÇÃO DE HIDROGÉIS COM PROPRIEDADES MAGNETO E PH RESPONSIVOS BASEADOS EM POLI(ETILENO GLICOL) PARA APLICAÇÃO NA LIBERAÇÃO CONTROLADA DE FÁRMACOS*

RESUMO - PARTE I

Os hidrogéis (HG) são redes poliméricas ligadas tridimensionalmente entre si capazes de reter grandes quantidades de água ou fluídos biológicos. Essas redes, podem ser compostas de homopolímeros ou copolímeros. Embora apresentem grande afinidade com a água, os HG são insolúveis nesse meio, devido à presença de ligações cruzadas de caráter químico ou físico.

Os hidrogéis podem ser classificados de acordo com: (*i*) a natureza dos seus grupos químicos (neutro ou iônico), (*ii*) tipo de ligação cruzada (física ou química), (*iii*) método de preparação (homopolímero ou copolímero) e (*iv*) cristalinidade (amorfo ou semicristalino).

De um modo geral, as aplicações dos hidrogéis são voltadas tanto para a área farmacêutica quanto para a área biomédica. Os hidrogéis se assemelham ao tecido natural mais do que qualquer outra classe de biomateriais sintéticos. Por este motivo, esses materiais podem ser aplicados em revestimentos de corações e peles artificiais, podendo também, ser utilizados em dispositivos de entrega de fármacos. Além disso, devido à sua consistência maleável e a capacidade de reter água, os HG também podem ser aplicados na agricultura, em lentes de contato, membranas, biossensores e armações de suporte para crescimento de tecidos.

A capacidade de absorção de água dos hidrogéis pode ser ajustada de modo que o seu intumescimento responda a estímulos externos, tais como, pH, força iônica, temperatura e campo magnético. Assim sendo, estes sistemas tendem a apresentar mudanças drásticas em seu perfil de intumescimento, o que permite desenvolver materiais com propriedades e aplicações únicas, dentre as quais, destacam-se aquelas utilizadas para a liberação controlada de fármacos.

Um sistema de liberação de fármaco ideal deve ser biocompatível, não tóxico, além de ser suficientemente estável de modo a prevenir a sua excreção pelo corpo humano. Os sistemas baseados em poli(etileno glicol) (PEG) estão entre os mais estudados e utilizados em aplicações biomédicas. O PEG é um polímero biodegradável, possui baixa toxicidade e é aprovado pela *U. S. Food and Drug Administration* (FDA) para uma variedade de usos clínicos. De um modo geral, os hidrogéis que utilizam PEG

em sua estrutura, apresentam uma boa biocompatibilidade e têm sido utilizados em encapsulamento de insulina, fibroblastos e na obtenção de membranas.

Como forma de modificação das cadeias do polietileno glicol, a adição de grupos vinílicos à grupos terminais da estrutura do PEG permite que este polímero possa reagir novamente como um macromonômero. Uma das formas de modificação é a reação dos grupos hidroxilas deste polímero com anéis epóxidos. Contudo, algumas rotas de síntese propostas requerem muitas etapas e/ou apresentam alto custo. Na Parte I desta tese, foram investigados a rota de modificação química do PEG com metacrilato de glicidila (GMA) de modo a obter-se um macromonômero que possa atuar como agente de reticulação entre cadeias poliméricas. A rota de modificação química proposta para o poli(etileno glicol) consiste na sua modificação com o metacrilato de glicidila via reação de abertura de anel epóxido. Os hidrogéis baseados em PEG foram sintetizados após a copolimerização do macromonômero de PEG modificado com GMA (^{GMA}PEG) juntamente com os monômeros *N,N'*-dimetil acrilamida e acrilato de sódio. Estes comonômeros foram empregados de modo a obter-se um hidrogel com propriedades pH-responsivas. No capítulo I, avaliou-se a influência da composição inicial dos monômeros nas propriedades dos hidrogéis, tais como, perfil e cinética de intumescimento, citotoxicidade e resistência mecânica. Parte dos resultados desta investigação foram publicados na revista "*Colloids and Polymer Science,* **2015***, 293, 3611-3622*".

No capítulo II obteve-se hidrogéis com propriedades magnéticas e pH-responsivas. Para alcançar este objetivo, as melhores condições experimentais investigadas no estudo anterior foram combinadas com nanopartículas de óxido de ferro comercial. Esta última, foi dispersa no meio reacional por ultrassom de ponta, para conferir propriedades magnéticas aos HG. Após a investigação da influência do campo magnético no intumescimento do material, a sua citotoxicidade foi avaliada. Em seguida, utilizou-se a prednisolona como fármaco modelo para realizar os ensaios de liberação controlada na presença e ausência de campo magnético. Os resultados deste trabalho estão em fase final de edição para a sua posterior submissão.

REVISÃO BIBLIOGRÁFICA

Poly(ethylene glycol)-based hydrogels from preparation methods to applications

1. Introduction

Hydrogels (HGs) are polymers with (3D) three-dimensional network structure which are able to swell, absorbing a huge amount of either water or biological fluids without the 3D structure being dissolved into liquid[10, 11]. Such a structure consists of either physically or chemically cross-linked polymers. Physically cross-linked HGs are obtained when their polymeric chains hold together by physical interactions, such as electrostatic interactions, Van der Waals forces, and/or hydrogen bonds. On the other hand, the chemically cross-linked HGs show as main characteristic the irreversible covalent bonds formed among polymeric chains[12]. The cross-linking can be formed either *in vitro* (during preparation) or *in vivo* (after application at a specific location inside the body)[13]. Furthermore, HGs can be classified based on their source (synthetic or natural), configuration (crystalline or amorphous), physical appearance (matrix, film, or microsphere), network electrical charge (ionic, neutral, zwitterionic), or according to their polymeric composition (homopolymer, copolymer, or interpenetrating polymeric network)[14].

HGs have been received considerable attention due to their great promise that they hold for a wide range of applications. The ability to swell under biological conditions, allowing nutrients diffusion, makes HGs very similar to natural tissues. This characteristic is of great importance for HGs applications, especially in biosensors, controlled release of drug, and tissue engineering[14-16]. They can also find efficient applications in the agriculture, both as soil conditioners and as nutrient carriers [12, 17].

The capability of water absorption (swollen weight per dry weight) depends on the porosity, cross-linking density, and chemical nature of the polymer chains carrying functional groups such as $-NH_2$, $-COOH$, $-CONH_2$, and $-SO_3H$. Hydrogels may be prepared so that their physical–chemical characteristics (equilibrium swelling and absorption kinetic) respond to changes in their external environment, such as temperature,

pH, ionic strength, and so on[18, 19]. These materials show a wide variety of applications, specially, for drug delivery systems[20, 21].

Both natural or synthetics hydrogels can be addressed to those proposes. Cell adhesion, and biodegradation are the main advantages of natural hydrogels. However, such materials have poor mechanical properties besides having potential immunogenic reactions restricting their applications[22]. Thus, synthetic hydrogels have been emerged as an alternative due their well-defined structure which can be modified yielding tailor able degradability and functionality[14].

Water-soluble polymers, such as, poly(acrylic acid), poly(vinyl alcohol), poly(vinyl pyrrolidone), poly(ethylene glycol), and poly(acrylamide) are often used in hydrogel synthesis[23]. Among them, the systems based on poly(ethylene glycol) are the most studied and used in biomedical applications owing to their biocompatibility and low toxicity[24]. The chemical structure of this polymer and its derivatives is shown in Figure 1.
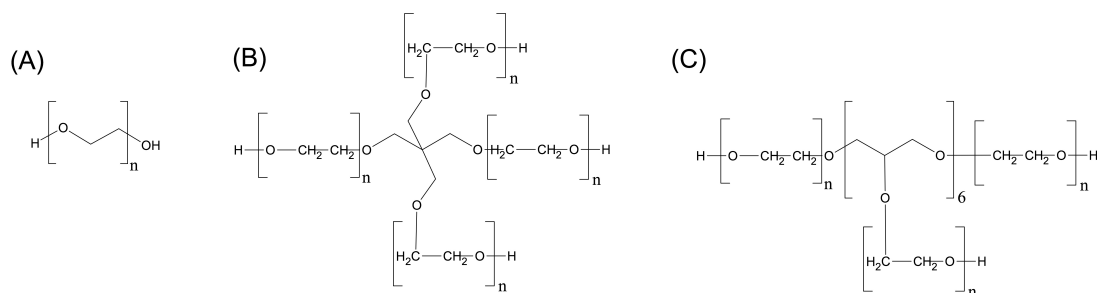
Figure 1. Chemical structure of poly(ethylene glycol) and its derivatives: (A) linear PEG, (B) 4-arm PEG, and (C) 8-arm PEG.

The PEG is a biodegradable polymer, has low toxicity and was approved by the U.S. Food and Drug Administration (FDA) for a variety of clinical uses[25, 26]. PEG has two hydroxyl end-groups, which can be easily converted to other reactive groups, such as, methyloxyl, carboxyl, amine, thiol, azide, vinyl sulfone, azide, acrylate, and so on[21]. In addition, due -CH_2CH_2O- segments, PEG has both hydrophilic and hydrophobic properties[27]. These characteristics plays an important role in designing of new materials. Currently, a variety of excellent books and reviews describe the preparation

and properties of hydrogels using either 4-arm PEG or 8-arm PEG. However, there are few works exploiting only hydrogels based on the linear PEG.

Herein, the main focus of this work is given to hydrogels based on linear PEG copolymerized with synthetic polymers. Thus, a number of interesting works which not follow this definition, such as, hydrogels containing natural polymers, 4-arm PEG, 8-arm PEG will not be covered in this review.

For obtaining PEG-based hydrogels the poly(ethylene glycol) can be used as macromonomers, cross-linking agent, or just as a segment in polymer backbone. These synthetic hydrogels are either chemically cross-linked or physically cross-linked and may be applied in biomedical field as drug carriers, scaffolds, or membranes.

2. Chemically cross-linked PEG-based hydrogels

2.1. Synthesis of PEG-based macromers

Although different structures of synthetic polymers can form hydrogels via chemical cross-linking, PEG has been one of the most investigated systems[28, 29]. The hydroxyl end-groups of poly(ethylene glycol) can be easily modified by other groups of interest. In addition, the properties of this polymer, such as, high hydrophilicity, and biocompatibility can be used for tuning the desired material. PEG also exhibits the ability to suppress cellular and protein adsorption[30]. Moreover, if compared to natural polymers, PEG offers a high control over engineering properties (i. e. elastic modulus, and degradation rate). These features make PEG an excellent candidate for developing new devices applied in biomedical field. Some examples of PEG-based macromonomers (cross-linkers) are shown in Table 1.

Table 1. Examples of chemical routes used in the preparation of PEG-based cross-linkers.

PEG	Reactant	Macromonomers / cross-linkers	References
			[21]
			[26, 31]
			[27, 32-36]
	(1) NaH ; (2)		[37]
		+	[38]
			[39, 40]
			[28, 41]
			[42]
			[29, 43]
			[44]
			[45]
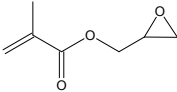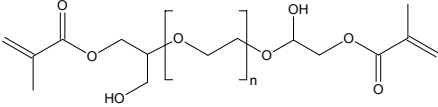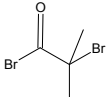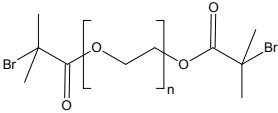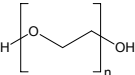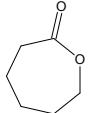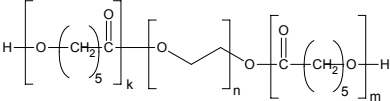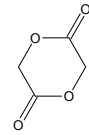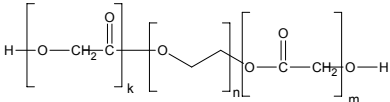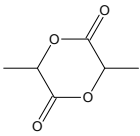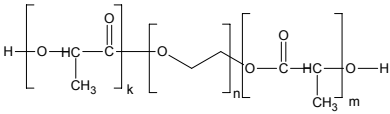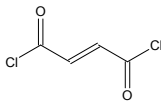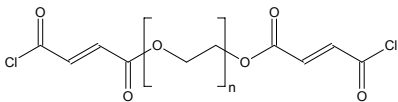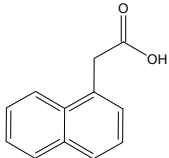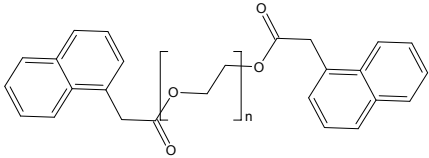
2.2. PEG containing acrylate end-groups

PEG macromers containing acrylate (or methacrylate) end-groups are the most common cross-linking agents. Such a structure can be easily polymerized by a variety of methods including UV photoirradiation[28]. Usually, the modification of PEG to PEG diacrylate (PEGDA) is achieved by reacting the poly(ethylene glycol) with acryloyl in the presence of triethylamine. For example, Berdichevski and co-workers have preprared PEGDA macromonomer using this technique[46]. In that work, the hydrogel was obtained by photo-polymerization of PEGDA with fibrogen, gelatin, albumin, and gadolinium triacrylate. Those hydrogels were used for studying the *in vivo* mechanisms of hydrogel swelling and their biodegradation properties. Lee, B. H. *et al*. have also reported the synthesis of PEGDA using the same chemical route[27]. According to the authors, after photopolymerization, PEG-based hydrogels could be obtained. They have investigated the influence of hydrogel modulus on spheroid formation and its functionality obtaining an important insight about mechanobiology of healthy liver cells and tissues.

Recently, Kar, M. and co-workers have reported the synthesis of several acrylate macromonomers, including PEGDA, obtained through various pathways[47]. The authors have investigated whether the incorporation of disulfide moieties onto backbone of hydrogels could impart them degradation properties. For performing this investigation the synthesis of disulfide-modified poly(ethylene glycol) diacrylate was carried out. Firstly, the monoacrylate poly(ethylene glycol) was synthesized by reacting PEG with acryloyl chloride in presence of silver oxide and potassium iodide (KI). Then, the obtained product was used as precursor for synthesizing disulfide-modified poly(ethylene glycol) diacrylate. The reaction scheme of this synthesis is shown in Figure 2.

i) Silver oxide, KI, Acryloyol chloride

ii) Disuccinimidyl carbonate, Pyridine, Cystamine dihydrochloride
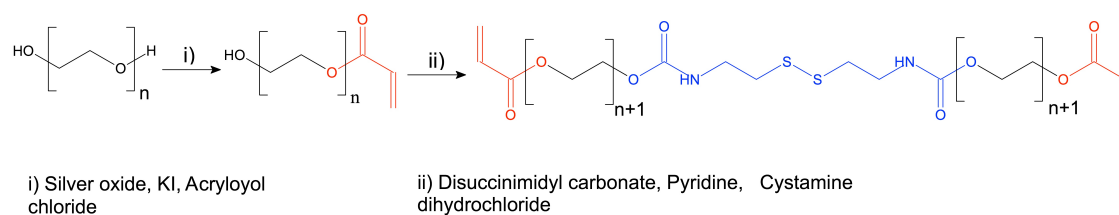
Figure 2. Reaction scheme for the synthesis of disulfide-modified poly(ethylene glycol) diacrylate[47].

2.3. PEG containing methacrylate end-groups

The nature of cross-linker end-groups confers the ability tune the physical properties of PEG hydrogels. The poly(ethylene glycol) dimethacrylate (PEGDMA) has slower reaction kinetics than PEGDA[38]. In a polymerization, an acrylate group forms secondary radicals while methacrylate groups forms tertiary one. Thus the stability of tertiary radicals confer the lower reactivity if compared to acrylate groups. However, the cross-linking reaction for PEGDMA is still rapid, occurring in minutes, and achieves greater macromer conversion than PEGDA as the increased hydrophobicity of the methacrylate group increases functional group aggregation in solution, thereby increasing the probability of radical transfer and methacrylate conversion. PEGDMA hydrogels are also associated with increased cellular viability and growth when compared to PEGDA hydrogels. This is associated with decreasing in reaction rate, at any given time, which reduces radical concentration and unreacted macromers present[28].

For synthesizing PEG functionalized with methacrylate groups different chemical routes can be used. Koushabi, A. and co-authors have investigated the influence of nanofibrillated cellulose addition to the poly(ethylene glycol) dimethacrylate hydrogel. In such work, PEGDMA could be obtained after reacting PEG with methacrylic anhydride, during five days, in triethanolamine[48]. While many variations of this approach exist, all of them are time-consuming. Depending on the method employed for synthesis it will be required 24 hours or days. In order to decrease the reaction time, Hove, A. H. and co-authors have demonstrated that PEGDMA could be obtained in 5 minutes using microwave-assisted method[38]. This method is also solvent-free and can be employed as an excellent strategy for PEG modification.

2.4. PEG containing others end-groups

PEG end-groups can be used for nicely coupling either reactive ligands or polymers in their extremities. This polymer can be readily modified with a variety of functional groups depending on desired application. For example, Tenório-Neto, et al. have shown PEG modification with glycidyl methacrylate (GMA) through an epoxide ring-opening reaction. In that work, PEG was vinyl-modified with GMA and subsequently polymerized with sodium acrylate (SA) and *N,N'*-dimethyl acrylamide (DMAAm) for obtaining pH-responsive hydrogels[21]. Peng, L. et al. have synthesized a difunctional PEG macroinitiator (Br-PEG-Br) for using in Atom Transfer Radical

Polymerization (ATRP) technique. The thus obtained hydrogel temperature-responsive properties and was used for bovine serum albumin (BSA) release[26]. PEG also can be functionalized with alkine end-group after reaction with propargyl bromide as reported by Pahimanolis, N. et al[37]. Moreover, PEG porogens can be obtained by an esterification reaction using naphthyl acetic acid[44]. In addition, for synthesizing hydrogels, PEG can also be modified by polymers, such as, poly(glycolic acid)[41], poly(L-lactic acid)[42], poly(latic-co-glycolic acid)[49], poly(ε-caprolactone)[50], and so on.

3. Physically cross-linked PEG-based hydrogels

Physically cross-linked hydrogels, generally, are obtained by ionic interactions, crystallization process, stereocomplex formation, hydrogen bond, freeze-thawing, and so forth[51]. These HGs can also be obtained from either multiblock copolymers or graft copolymers[52]. Due their noncovalent nature, these systems are inherently responsive to external stimulus, such as, pH and temperature. Furthermore, the physically cross-linked hydrogels are self-healing by nature, and they can be processed under mild conditions, at room temperature, and/or physiological pH. For example, poly(acrylic acid) and poly(methacrylic acid) form complexes with PEG by hydrogen bonds in a process involving crystallization by freezing-thawing creating a strong and elastic gel[53]. In addition, the interaction between PEG backbone and cyclodextrin produces hydrogel simply by mixing[54].

PEG-conjugated with proteins have been used for synthesizing physically cross-linked hydrogels by ß-sheets interaction[55]. The advantage of these systems consist on the inherent biocompatibility and biodegradability of peptides. Protein interactions involve hydrogen bonding and hydrophobic interactions facilitating the gelification process. Several ß-sheet forming hydrogels have a great potential to be applied in medicine regenerative and tissue engineering.

4. Smart PEG-based hydrogels

Polymeric networks which are able to change their properties in response to physical, chemical, and/or biochemical stimuli, are known as "smart hydrogels". Physical stimuli consist of temperature, pressure, light, electric, magnetic, and sound fields, while chemical or biochemical stimuli involve pH, ionic strength, ions, or specific molecular

recognition events[26, 56]. In addition, the possibility of using temperature, magnetic field, and pH stimuli to control the response of a single system is considered to be highly advantageous for their future exploitation in the biomedical field[57].

4.1. Magnetic-responsive

Magnetic hydrogels nanocomposites (MHNC) containing magnetic nanoparticles embedded in cross-linked hydrogels networks have attracted much attention. These nanocomposites have potential to be used in a wide range of applications, such as, hyperthermia therapy, drug delivery devices, tissue repair, and so forth. The methods for MHNC fabrication are shown in Figure 3 and can be defined as follows: i) *Blending method*: where the prepared MNPs is mixed with a hydrogel precursor solution at a certain molar ratio and cross-link hydrogels to entrap the MNPs (Figure 3A), ii) *in situ precipitation method*: MNPs are fabricated via an *in situ* precipitation reaction in the network of the polymer hydrogels after cross-linking reaction (Figure 3B), and iii) *grafting-onto method*: MNPs are grafted with functional groups acting as nanocross-linkers (Figure 3C)[58].
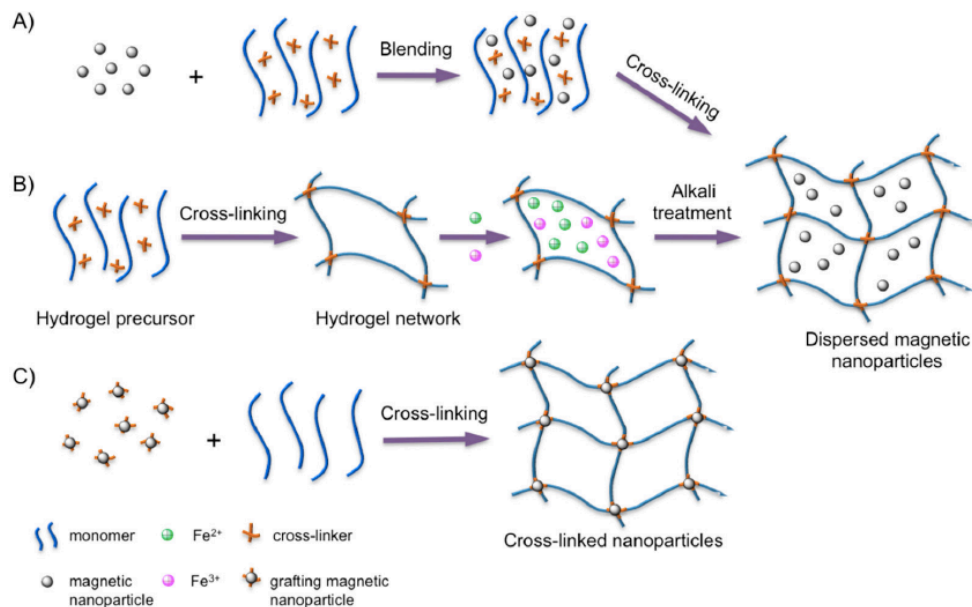
Figure 3. Schematic representation of preparation methods of magnetic hydrogels. A) The blending method B) The *in situ* precipitation method, and C) The grafting-onto method. Reprinted with permission from reference [58]. Copyright© 2016.

The formed MHNC combine properties of hydrogels and magnetic nanoparticles providing a system with unique properties enhancing and increasing the versatility of their applications. In addition, hydrogels can provide increased biocompatibility over exposed, uncoated nanoparticulates (they can encapsulate the particulate in the composite matrix providing a barrier between sensitive tissues and the more harmful nanoparticulates). The incorporation of magnetic nanoparticles such as iron oxide nanoparticles (IONPs) into hydrogels can create tunable nanocomposites that can be remotely controlled by an alternating magnetic field, for example, magnetically modulated drug delivery systems with capabilities of delivering drugs at increased rates[59, 60].

For example, MHNCs have been used in designing new materials for hyperthermia treatment. The temperature of cancerous tissue needs to reach 42 – 45°C for effective therapy. Moreover, temperatures higher than 50°C may cause damage to cells via thermoblation. Alternating magnetic field (AMF) can control the temperature of hydrogels. As can be seen in Figure 4, the heating mechanisms are based on Brownian relaxation (rotation of the particle as a whole according to an external magnetic field), the Néel effect (reorientation of the magnetization vector inside the magnetic core against an energy barrier), and often some minimal hysteresis losses[61].
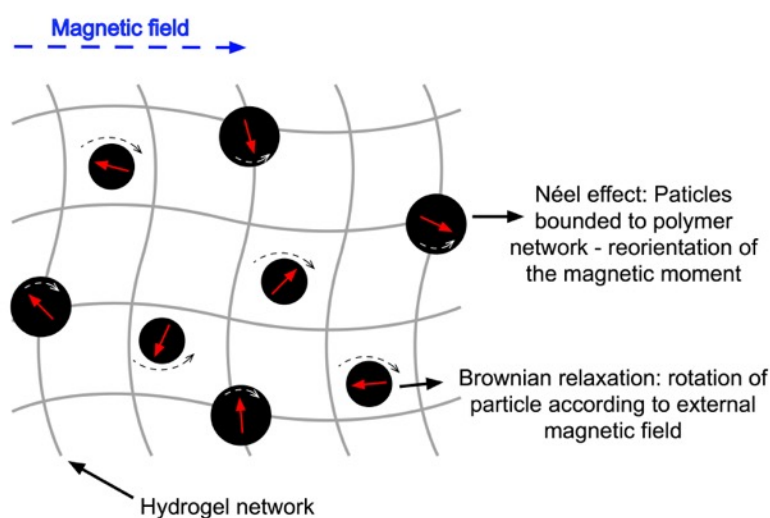
Figure 4. Schematic representation of nanoparticles in hydrogel networks with Néel effect and Brownian relaxation.

Poly(ß-amino ester) macromers composed of poly(ethylene glycol) diacrylate

have been used for obtaining MHNC focusing in hyperthermia applications. The synthesis of PBAE macromers consist on reacting excess of PEGDA with isobutylamine as shown in Figure 5. Meenach and co-workers have exposed the swollen hydrogels to an electromagnetic filed in different conditions (dried hydrogels and hydrogels after degradation at various time points). For all conditions, the temperature reached were well beyond the required values for hyperthermia applications. In addition, the authors could control the heating of hydrogel just adjusting the power of AMF[61].
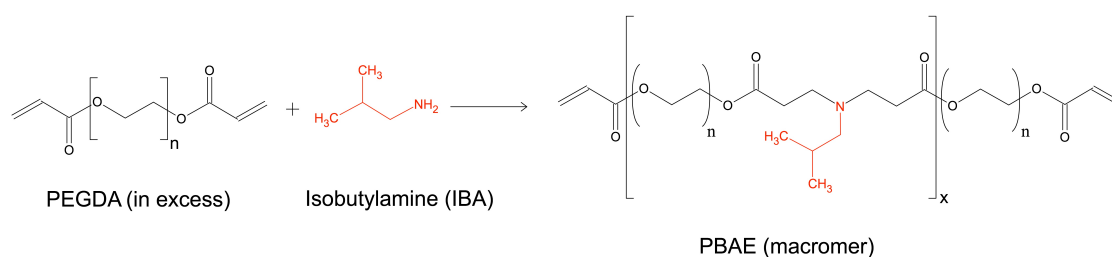
Figure 5. Schema demonstrating the synthesis reaction of PBAE macromers.

4.2. Temperature-responsive

Temperature-responsive hydrogels exhibit a reversible sol-gel phase transition with the temperature changing. This transition is defined by lower critical solution temperature (LCST). Polymers which undergo the sol-gel transition as the temperature increases, have received considerable attention for use in a wide variety of fields, particularly in biomedical applications. Generally, these polymer aqueous solutions are low viscous sol at room temperature or below the sol-gel transition temperature becoming a gel at body temperature[62]. Poly(N- isopropylacrylamide) (PNIPAM), poly(hydroxyethyl methacrylate) (PHEMA), polyvinylpyrrolidone (PVP), and hydroxypropyl cellulose (HPC) are the most common thermosensitive polymers. Among them PNIPAM, which displays a LCST in water around 32°C, has been the most studied thermosensitive polymer[63]. However, in an interesting work, Lutz J-F et al. have reported a series of 2-(2-methoxyethoxy)ethyl methacrylate and oligo(ethylene glycol) (P(MEO$_2$MA-*co*-OEGMA)) which exhibit LCST between 30°C to 50°C. They could predict the LCST by adjusting the fraction of OEGMA units in the copolymer chains[64]. The presence of oligo(ethylene glycol) side chains on the copolymer can form H-bonds with water molecules while the backbones are hydrophobic at room temperature. Thus the balance between hydrophilic and hydrophobic moieties, in copolymer structure, plays

a key role on their LCST properties[62].

PEG can be combined with poly(ε-caprolactone) (PCL), which is non-toxic and biodegradable, for obtaining a triblock copolymer with temperature responsive properties. PCL-PEG-PCL blocks exhibits low solubility in water beyond exist only in a micelle form in aqueous solution. In order to overcome these drawbacks α-cloro-ε-caprolactone (αClεCL) have been used for synthesizing poly(αClεCL)-PEGb-(αClεCL) copolymers. This copolymer has active chlorine facilitating the poly(MEO$_2$MA-*co*-OEGMA) graftization as have been reported by Wang, Q. and co-workers[62]. In such work, they could adjust the LCST of [PCL-*g*-poly(MEO$_2$MA-*co*-OEGMA)]-*b*-PEG-*b*-[PCL-*g*-poly(MEO$_2$MA-*co*-OEGMA)] (tBG) to 35 °C by controlling the feed ratio of the MEO$_2$MA and OEGMA. Furthermore, they found that tBG polymer could become micelles or hydrogel depending on the concentration. A scheme proposing the gelation and micellization mechanism can be seen in Figure 6.
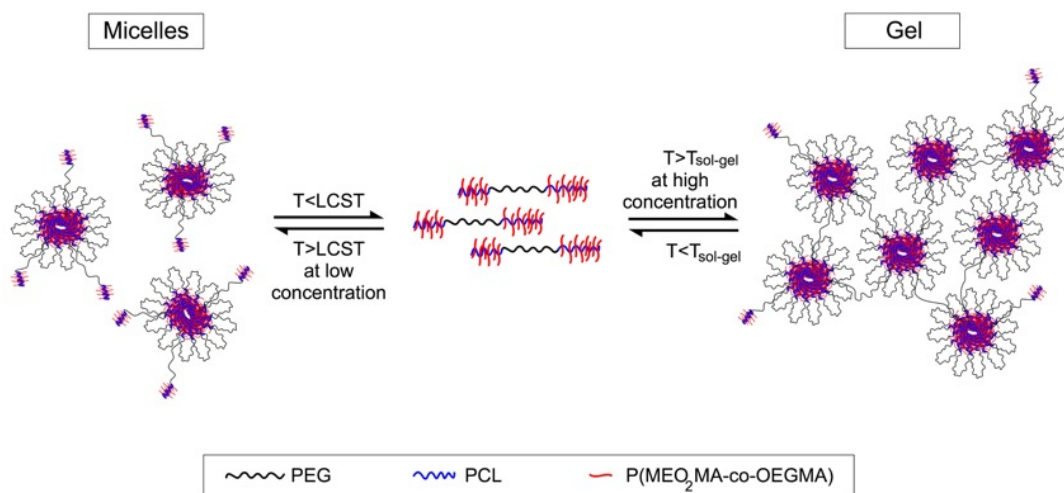
Figure 6. Gelation and micellization mechanism of tBG in aqueous solution.

Due to the thermo-responsive properties of hydrogels based on MEO$_2$MA- and OEGMA have been extensively studied. Xia, M. et al. have combined clay with MEO$_2$MA and OEGMA for obtaining a hydrogel nanocomposite where the swelling properties were thermo-dependent. All swollen hydrogels tended to shrink and lose water after immersing in water at higher temperature (~50°C). This effect was associated to the disruption of hydrophilic / hydrophobic balance in nanocomposite hydrogels[65].

Another strategy for obtaining PEG-based hydrogels with thermo-responsive properties consist on using poly(D,L-lactide-co-glycolide)-poly(ethylene glycol)-poly(D,L-lactide-co-glycolide) triblock copolymers. In the aqueous solution, the hydrogel is formed by micelles with intermicellar bridges, where these micelles are formed by the PLGA block (core) and the PEG block (shell). Chen, L. and collegues have studied the effects of molecular weight and thermogellability of PLGA-PEG-PLGA copolymer aqueous solutions[66]. A schematic presentation of PLGA−PEG−PLGA transition phase as function of temperature and molar mass is shown in Figure 7.
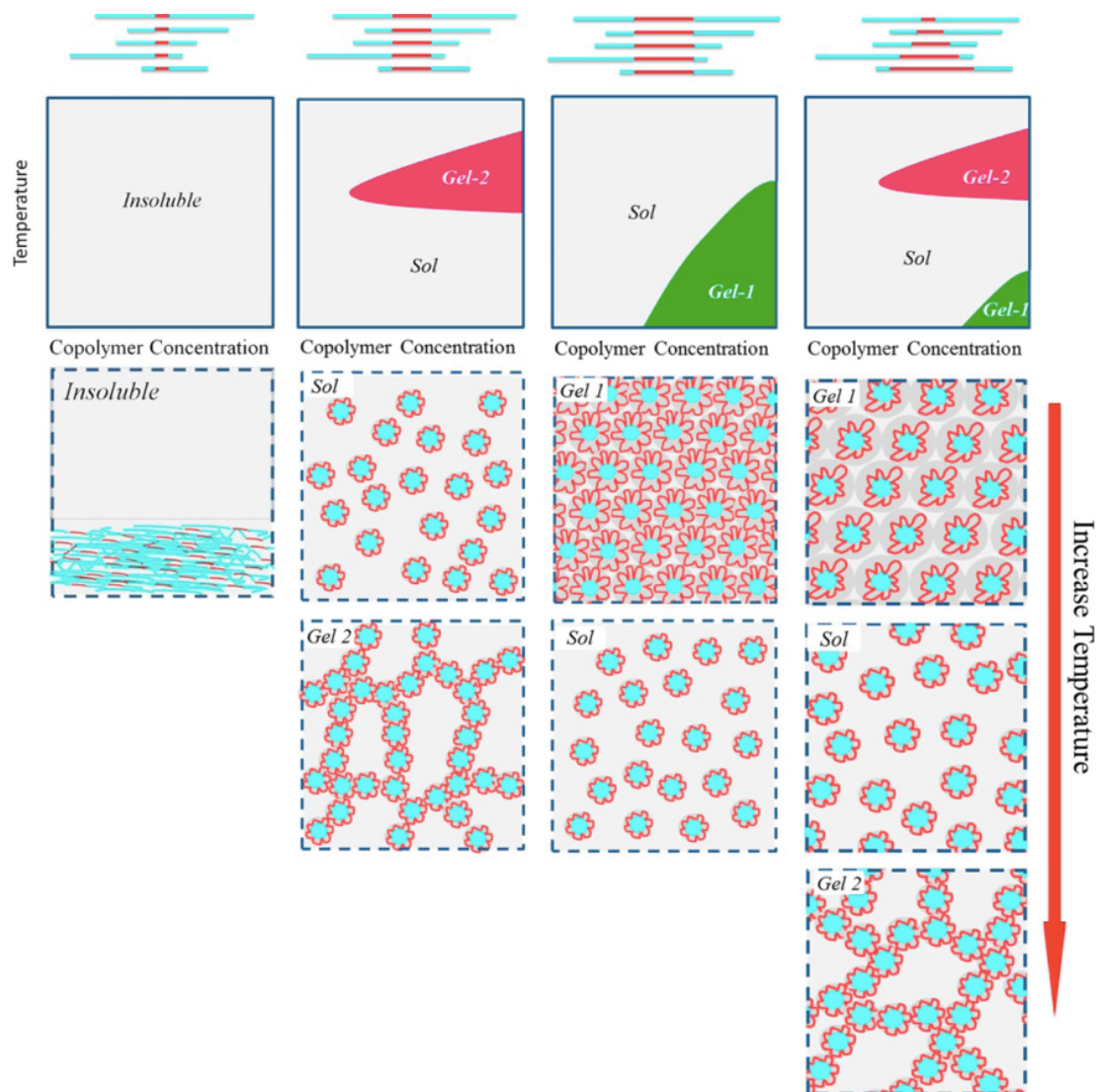
Figure 7.Schematic presentation of the phase transition of aqueous systems of copolymer PLGA−PEG−PLGA with different M_W or different M_WD of the PEG block at different temperatures. Reprinted with permission from reference [66]. Copyright$^{©}$ 2016.

In this Figure, the first row shows that copolymers have similar average length of PLGA block but different chain lengths or molecular weight distribution (M_WD) of the PEG block. The second row demonstrates the state diagrams of these copolymers in water. All of pictures below show the internal mesoscopic structures with respect to those macroscopic states. The copolymer with a small PEG block cannot be dissolved in water at any temperature. The solubility of PLGA-PEG-PLGA copolymer increase in water when the PEG block length increases. The solution of copolymer with a narrow MWD of the PEG block is a sol at low temperatures and can spontaneously gel at body temperature. However, for longer PEG block, the aqueous system presents a gel state at low temperature and becomes a sol upon heating. For copolymers with a wider MWD of the PEG block, its aqueous system exhibits, upon heating, a normal gel due to micelle jamming, to a sol (micelle dispersion), and then to a thermogel with a percolated micelle network. In addition, PLGA-PEG-PLGA copolymer have been shown to be biocompatible and biodegradable. Thus, sustained release behaviors of several protein and anti-cancer drugs from the injectable PLGA-PEG-PLGA hydrogels have been investigated[67]. For example, Yan, Q. and colleagues have synthesized PLGA-PEG-PLGA hydrogels containing simvastatin and studied their drug-release properties[68]. Yuan, B. and co-authors investigated the influence of PLGA-PEG-PLGA hydrogels loaded with 5-fluorouracil for the prevention of postoperative Achilles tendon adhesion.

PEG also have been combined with PNIPAM for obtaining a thermo-responsive hydrogel as was demonstrated by Graaf, A. J. and co-workers[69]. The poly(N-isopropylacrylamide)-poly(ethylene glycol)-poly(N-isopropylacrylamide) (PNIPAM-PEG-PNIPAM) was synthesized using Br-PEG-Br macroinitiator. The formed PNIPAM-PEG-PNIPAM hydrogels shown their gelling point near to 40°C. However, at 37°C in both *in vitro* and *in vivo* systems, the triblock co-polymer hydrogels slowly were interconverted into flower-like micelles when in contact with an aqueous environment releasing paclitaxel, as drug model, in an erosion-controlled mechanism.

4.3. pH-responsive

Generally, pH-sensitive hydrogels are polymers that contain ionic groups in their polymeric backbone. Their ability to swell responding to specific physiological stimuli makes them extremely important in biomedical field, especially, in drug release. pH-

responsive hydrogels are composed of polymeric backbones with ionic pendants groups including $-NH_2$, $-COOH$, $-CONH_2$, and $-SO_3H$[70]. These pendant groups can be divided in anionic and cationic one. In case of anionic-pendant groups the ionization occurs when the pH of the solution, where the hydrogel is immersed, is higher than the pK_a values from polymeric networks. On the other hand, when the pH is smaller than the pK_a the anionic-pendant groups remain un-ionized. The reverse is the case of cationic-pendant groups, where are ionized and un-ionized when $pH < pK_a$ and $pH > pK_a$ respectively[71]. In any event, when the polymeric-pendant groups are ionized, the repulsive forces repel each other increasing the mesh size of porous structure favoring the water-uptake. A schematic representation of swelling in a pH-responsive hydrogel is shown in Figure 8.
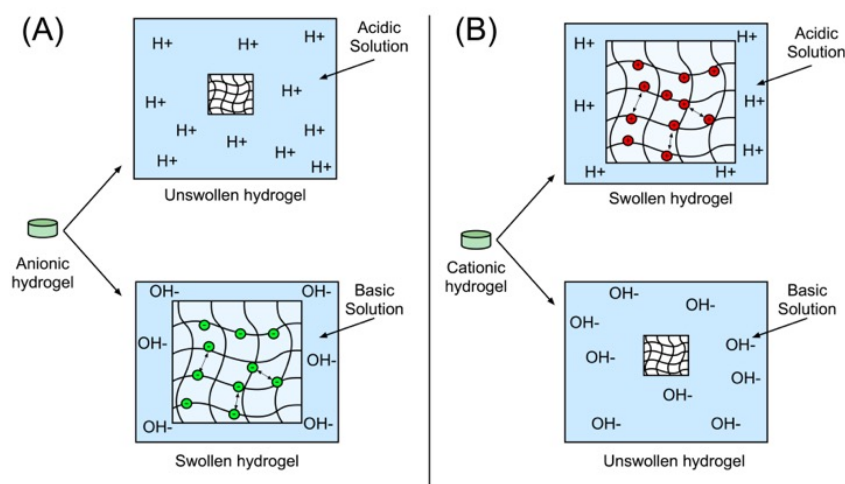
Figure 8.The pH-responsive swelling of (A) anionic and (B) cationic hydrogels.

Focusing on drug delivery through oral route, Tenório-Neto and co-workers have reported the synthesis of degradable and biocompatible PEG-based hydrogels with pH-responsive properties[21]. They investigated the influence of sodium acrylate (SA), *N,N'*-dimethyl acrylamide (DMAAm), and cross-linking agent, which consisted in PEG modified with GMA (GMAPEG), on swelling properties at pH 2, 7, and 10. It was found that carboxylic groups has more influence on the swelling properties than others ones. Some examples of swelling curves are show in Figure 9.
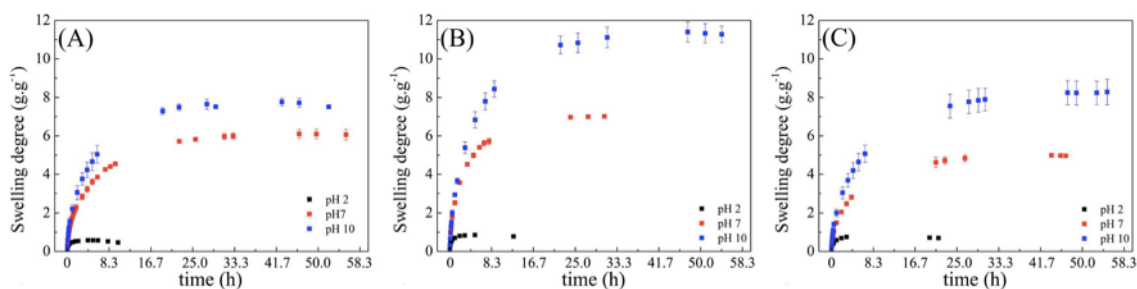
Figure 9. Time-dependent curves of hydrogels at the indicated pH at temperature of 36.5°C. The hydrogels were synthesized as follows: A) 5g of ^{GMA}PEG, 0.5g DMAAm, 0.6g SA (P1D1A1), B) 5g of ^{GMA}PEG, 0.5g DMAAm, 1.2g SA (P1D1A2), and C) 5g of ^{GMA}PEG, 1.0g DMAAm, 0.6g SA (P1D2A1). Reprinted with permission from reference [21]. Copyright$^©$ 2016.

Betancourt, T. and colleagues reported the synthesis of anionic hydrogels based on poly(itaconic acid-*g*-ethylene glycol) (PIA-*g*-PEG) for drug delivery applications[72]. The effect of monomer composition, and cross-linker on the resulting properties of the hydrogel was also investigated. The PIA-*g*-PEG hydrogels were designed for use as carriers for the delivery of proteins and other acid-labile molecules to the intestinal track. They have reported that hydrogen bonding interactions between carboxylic acid groups from poly(itaconic acid) and the ether groups from PEG play an important role for collapsing the polymer networks. Later, the same research group, reported the synthesis of poly(itaconic acid)-based hydrogels combined with several monomers including N-vinyl-pyrrolidone, PEGDMA, and TEGDMA for delivery proteins with high isoelectrical point. In addition, the bioavailability on proteins delivery was improved by adjusting the ionic strength of the loading solution.

The ionic strength (IS) can decrease the protein loading by two ways: i) the swelling behavior of a pH-responsive hydrogel is strongly affected by ionic strength, decreasing the swelling. Thus, the hydrogel swelling will increase by reducing IS allowing to absorb a huge amount of the protein. ii) the ionic strength affects the degree to which coulombic interactions take place, as described by the Debye length. The Debye length is the effective distance over which an ion's charge is offset by the charges of ions present in the surrounding medium. The Debye length (λ_D) can be calculated by Equation (1):

$$\lambda_D = \sqrt{\frac{\varepsilon k_B T}{2 N_A e^2 I}} \propto \sqrt{\frac{1}{I}} \tag{1}$$

where I is the ionic strength (mol m^{-3}), ε is the permittivity of the medium, k_B is the Boltzmann constant, T is the absolute temperature, N_A is Avogadro's number, and e is the elementary charge. Considering all parameters as constant, the λ_D is inversely proportional to the square root of the ionic strength. If the IS decreases the distance over ionic interactions are expected to increase, which mean, there is a greater likelihood of coulombic binding. During drug release, these interactions are undesirable, however, they can be used beneficially during protein loading[73].

The ability of some PEG-conjugated to undergo structural transitions by pH changing have been exploited to Ponnumallayan and Fee[55, 57]. They have reported the self-assembly of the peptide ELELELELELF (EL-5F) conjugated with PEG. A schematic representation is shown in Figure 10.
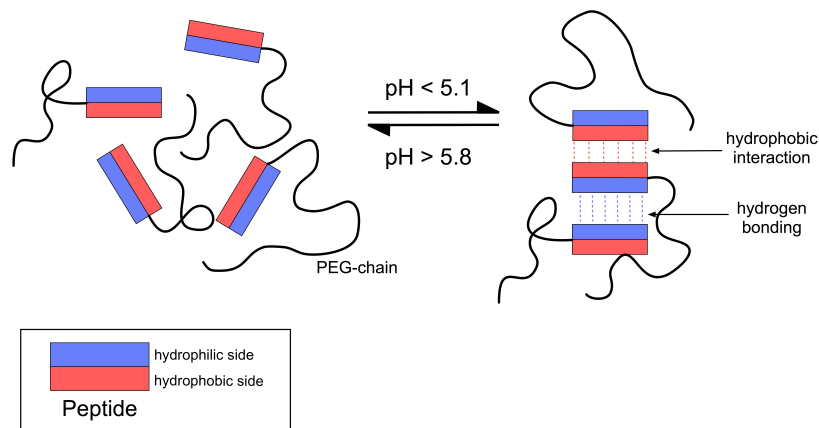
Figure 10. Structural view of pH-regulated, reversible self-assembly of EL-5F−PEG conjugates.

The self-assembly process is controlled by protonation and deprotonation of glutamic acid side chains which are present in structure of the peptide. According to the authors, the presence of PEG chains slightly decreased the pH range over which structural transition occurred. In addition, as the PEG molar mass increases this effect was more pronounced.

4.4. Multi-responsive

Multi-responsive hydrogels are a class of material which are able to respond to two or more environmental stimuli. Generally, such materials are pH-, thermo-, and/or magnetic responsive. The possibility of using temperature, magnetic field, and pH stimuli to control the response of a single system is considered to be highly advantageous for their future exploitation in the biomedical field. For example, Papaphilippou et al. reported synthesis and characterization of triple-responsive nano-composite networks. These hydrogels consisted of monomers with specific properties, such as, hexa(ethylene glycol) methyl ether methacrylate units (thermo-responsive), N-diethylaminoethyl methacrylate, and 2-(dimethylamino)ethyl methacrylate units (pH-responsive), and finally oleic acid-coated iron oxide nanoparticles (magnetic-responsive). The ability of these materials to adsorb and desorb benzoic acid in a controlled manner upon triggering the pH, combined with their tunable superparamagnetic behavior and thermo-responsive properties in aqueous media was investigated. In addition, the materials were capable of deswell responding to temperature changes[57].

Sheng, W. and colleagues reported synthesis and characterization of temperature- and pH- responsive hydrogels based on polyethylene glycol analogues and poly(methacrylic acid) via click chemistry. They have performed swelling-deswelling experiments varying both the pH and the temperature. The swelling behavior was observed in pH 9.0 at 25°C while deswelling was achieved in pH 4.0 at 45°C. In the same work, *in vitro* tests were made using bovine serum albumin (BSA) as a model drug in order to examine the release profile from hydrogels. As expected, the best condition which released huge amount of BSA was achieved in pH 4.0 at 45°C (deswelling conditions)[74].

A multi-responsive hydrogels using PEG derivatives was reported by Wooley's group[75]. A synthesis of oligo(DL-allylglycine)-block-poly(ethylene glycol)-block-oligo(DL-allylglycine) (ODLAG-*b*-PEG-*b*-ODLAG) was reported (Figure 11). This copolymer exhibited reversible and repeatable sol-to-gel and gel-to-sol transitions that can be triggered by heat and sonication, respectively. In presence of certain enzymes, the HG became sol. The process of hydrogelation is driven by a combination of oligopeptide ß-sheeting and a balance between PEG–PEG interactions and PEG–water interactions similar to observed in Figure 10.
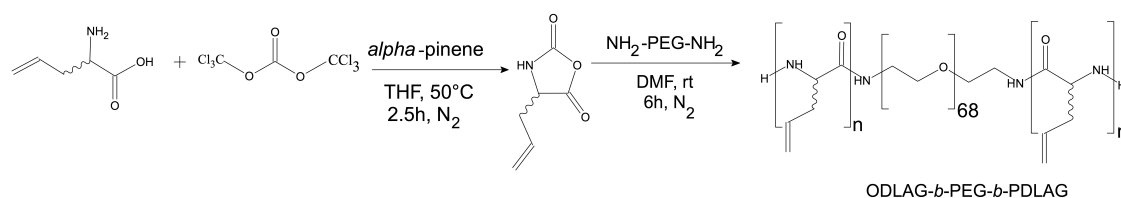
Figure 11. Synthesis of ODLAG-b-PEG-b-ODLAG.

The enzyme-responsiveness of such hydrogel was investigated by studying in vitro the weight loss profiles at 37°C and pH 8.0. Samples containing proteinase K or trypsin was used as the degradation medium, and the results were compared with the control. It was observed that hydrogels in presence of the enzymes were degradaded much faster than the control. The enzyme accelerated weight loss was associated to the surface erosion and the fast degradation of the oligopeptide chains.

4.5. Self-healing hydrogel

Self-healing hydrogels have attracted great attention because they can be biocompatible and have similar mechanical properties to natural tissues. For constructing the desired network structure, usually, these HGs are physically cross-linked by either hydrogen bonding, electrostatic interactions, host-guest recognition, hydrophobic association, and so on. Li and co-workers, in an interesting work, have prepared the synthesis of a double-network polymer hydrogel chemically cross-linked poly(ethylene glycol) (PEG) and physically cross-linked poly(vinyl alcohol) (PVA)[76]. Besides having self-healing properties, these HGs also shown shape memory response. It is important to highlight that shape memory hydrogels are difficult to obtain, especially, due to large amount of water present in the polymer network. The main strategy employed by the authors was to prepare a chemically cross-linked PEG interpenetrated by physical hydrogels of PVA. A schematic representation of this material and its properties is shown in Figure 12.
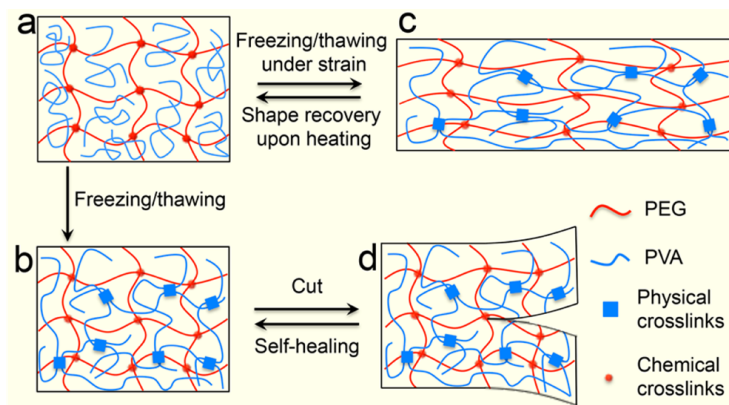
Figure 12. Schematic illustration of the PVA/PEG double-network hydrogel possessing the shape memory and self-healing functionalities. Reprinted with permission from reference [76]. Copyright© 2016.

The PEG networks are responsible for maintaining the basic structure of the hydrogel while PVA confers the self-healing properties. Furthermore, when the hydrogel (70 wt % of water) is subjected to freezing/thawing treatment under strain (Figure 12A to Figure 12C) , the enhanced physical network as a result of crystallization of PVA chains can stabilize the hydrogel deformation after removal of the external force at room temperature. Subsequent disruption of the physical network of PVA by heating allows for the recovery of the initial shape of the hydrogel (Figure 12A to Figure 12B).

5. Applications

The versatility of PEG-based hydrogels makes them important in different fields of research. In biomedical applications, stimuli-responsiveness, biocompatibility, and biodegradability are highly needed. The HG synthesis are relatively easy to perform, furthermore, such biomaterials can be readily modified to tune their physicochemical properties. The most investigated HG systems are those that are pH- and temperature-responsive. These multi-responsive HG provide high efficacy and better targeting in complex environments. Delivery via the oral route is a preferable method for drug administration. However, there are significant obstacles that have prevented oral delivery, specially, for protein therapeutics. Proteins are subject to enzymatic cleavage or acid-

catalyzed denaturation in the stomach, are further digested by enzymes in the small intestine, and are generally poorly absorbed across the intestinal epithelium into the bloodstream which decreases their bioavailability[77]. Due the difference between acid and neutral environment in the stomach (pH approx. 1.2) and the small intestine (pH approx. 7.0) respectively, proteins encapsulated by HG pH-responsive may be an excellent alternative for delivering one. HG may confer protection to the protein in acidic pH and the release mechanism can be triggered after increasing the pH.

Poly(ethylene glycol) hydrogels have also been applied for cell delivery[47, 78]. Stem cell can contribute to tissue regeneration and repair either by differentiating into tissue specific cells or by the secretion of trophic factors to rejuvenate the host tissue environment. In this sense, hydrogels which could be degraded by matrix metalloproteinase (MMP) plays an important role in delivering stem cells. This degradation can be achieved by incorporating two covalently bounded sulfur atoms, which can be reduced by gluthathione (a cell metabolite) is a key reaction in living systems as has been demonstrated by Vargheses research group. In addition, the mechanical properties of PEG-based hydrogels can be tailored to match of many soft tissues to be applied as scaffolds for development or regeneration of soft tissues. The regeneration of tissues may be achieved using either one of two principle approaches: i) the *in vitro* construction or ii) the *in vivo* induction of tissue[79]. In the first approach, the biomaterial scaffolds are combined with cells and the tissue is grown *in vitro* for being implanted into the host. The second one the scaffolds are implanted into the host and the body acts as a bioreactor regenerating the tissue of interest. Biomaterials based on PEG hydrogels acts as a blank slate upon which signals from extracellular matrix can be systematically introduced for controlling cell behavior and tissue regeneration.

PLGA-PEG-PLGA thermosensitive hydrogels have been used for wound healing. This HG containing transforming growth factor-beta1 encoding plasmid significantly increased the reepithealization in diabetic mices. Moreover, it was observed an organized collagen in wound[80].

For preparing contact lenses, Lin, C-H. and collegues have reported a hydrogel synthesized from poly(dimethylsiloxane) dialkanol (PDMS), isophorone diisocyanate (IPDI), 2-hydroxyethyl methacrylate (HEMA) and poly(ethylene glycol) methacrylate (PEGMA). They found that higher PEGMA content led to a lower contact angle, higher water content, lower elastic modulus, and higher glucose permeability. In addition, the

hydrogels exhibited not only relatively high oxygen permeability and relative optical transparency, but also hydrophilicity, and anti-protein adsorption which was correlated with PEGMA concentration[81]. More recently, the same research group improved the surface wettability and anti-protein adsorption of this hydrogel by assembling Chitosan and hyaluronic acid on the silicone hydrogels in a layer-by-layer self-assembly manner[82].

Alternatively, Tang, Q. and co-workers have synthesized polyacrylate/poly(ethylene glycol) (PAA/PEG) interpenetrated hydrogels for removing heavy metal ions and dye[83]. Based on swelling and deswelling properties the PAA/PEG hydrogels could adsorb 29.9 mg g^{-1} of methyl orange and released about 80% in 30 min after controlling the pH. Yuan, Z. and collegues have reported the synthesis of multiple stimulus-responsive organic/inorganic hybrid hydrogels based on poly(2-(2-methoxye-thoxy) ethyl methacrylate-co-oligo (ethylene glycol) methacrylate-co-acrylic acid) hydrogel with magnetic attapulgite/Fe_3O_4 nanoparticles for removing Rhodamine B (RhB) dye from wastewater. The absorption of RhB could reach over 95% after changing pH, temperature. The adsorption rate increased 250 min under magnetic field and the HG could be easily separated from wastewater[84].

Hydrophilic membrane coating materials synthesized from PEG-based hydrogels have been reported by Sharma's group. In water treatment, reverse osmosis (RO) membranes foul strongly in the presence of oily feed waters. However, proteins and human serum proteins adhere poorly to surfaces rich in PEG segments. Thus the authors have employed PEG-based hydrogels for preparing fouling-resistant coatings for being applied in RO membranes[85].

6. Conclusions

Poly(ethylene glycol) has attracted much attention, specially over the last twenty years. This polymer has been used for developing a wide range of new (bio)materials with tailored properties. Due to its biocompatibility, non-toxicity, and amphiphilic characteristics, PEG has also been utilized for the synthesis of hydrogels. The ability to swell under biological conditions, allowing nutrients diffusion, makes PEG-based hydrogels an ideal class of materials for biomedical applications. This review highlighted the synthesis of linear PEG-based hydrogels and their applications emphasizing the emerging works. For synthesizing such hydrogels, many cross-linking methods have been

developed including the modification of PEG for using as macromers. In addition, these HG may respond to external stimuli, which increases their efficacy for uses in biomedical field. The studies shown here have contributed for understanding the influence of linear-PEG properties in hydrogels. Despite these advances, there is still much to be done.

PARTE I – CAPÍTULO 1

Synthesis and characterization of a pH-responsive poly(ethylene glycol)-based hydrogel: Acid degradation, equilibrium swelling and absorption kinetic characteristics

1. Introduction

Hydrogels (called water-based gels or aqueous gels) are water absorbers of high performance because of their ability to absorb and retain a large volume of the liquid while maintaining a distinct 3D polymer network[86]. The capability of water absorption (swollen weight per dry weight) depends on the porosity, crosslinking density and chemical nature of the polymer chains carrying functional groups such as $-NH_2$, $-COOH$, $-CONH_2$ and $-SO_3H$[70]. Hydrogels may be prepared so that their physical-chemical characteristics (e.g., equilibrium swelling and absorption kinetic) respond to changes in their external environment, such as temperature[87], pH[18, 19], ionic strength[88], and so on. These materials show a wide variety of applications such as drug delivery[20], membranes for (bio)separation process[89], substrate for cell culture[90], and mucosal vaccines[91].

Polymer systems based on poly(ethylene glycol) (PEG) are among the most widely studied in the biomedical applications, owing to their biocompatibility and low toxicity[24]. PEG is a neutral, nontoxic, water-soluble polymer approved by the U.S. Food and Drug Administration (FDA) for a variety of clinical uses, such as carrier and excipient in the pharmaceutical, cosmetic and food products[19, 24]. PEG has also been used in drug delivery, tissue engineering scaffolds, surface functionalization, and so forth[92, 93]. Researchers in the area of biotechnology have focused on thermo-sensitive, pH-responsive, and (bio)degradable hydrogels that may be obtained from PEG[94]. An efficient strategy using polymers as starting monomers for creating hydrogel network is based on the chemical modification of functional groups. PEG has two hydroxyl end-groups, which can be converted to other polymerizable, reactive groups, such as methyloxyl, carboxyl, amine, thiol, azide, vinyl sulfone, acetylene, and acrylate[22, 37, 45].

This work aimed at creating a covalent hydrogel based on PEG, acrylic acid (AAc) and *N',N*-dimethylacrylamide (DMAAm) that shows pH-dependent equilibrium swelling degree, which is a valuable characteristic in drug delivery systems intended for aqueous environments such as biological organisms. For this end, it would be useful that the hydrogel chains degrade by acid catalyzed hydrolysis[95]. For this reason, PEG was chosen as key constituent acting as a pillar on polymer network. If its chains break, the polymer network crumbles. AAc is the ionic monomer and DMAAm was used owing to its good gel-forming capacity. On the scientific basis, it has not yet been found reports on hydrogel with such architecture.

To produce the hydrogels, PEG was vinyl-modified with GMA (^{GMA}PEG) and subsequently cross-linked/polymerized with sodium acrylate ((SA) respective acrylic acid salt)) and DMAAm. The modification of macromolecules with GMA occurs by transesterification and/or epoxide ring-opening reaction mechanism[96]. The occurrence of either mechanisms (or both mechanisms) strongly depends on pH and this has been clearly elsewhere.

The water transport profile of these hydrogels was studied by taking into account their absorption kinetic. Determining swelling degree gives an insight into other properties such as morphology, porosity, ability to interact with different media and so forth. The water transport data gives an understanding on interaction of the polymer devices with the physiological environment. In these studies, power law and Weibull equations, which are swelling-based models, were used for treating the experimental data.

2. Experimental

2.1. Materials

Poly(ethylene glycol) (PEG) Mw 950-1050 g mol^{-1}, glycidyl methacrylate (GMA), sodium persulfate ($Na_2S_2O_8$), *N',N*-dimethyl acrylamide (DMAAm), and acrylic acid (AAc) were purchased from Sigma-Aldrich. Acetone and sodium hydroxide (NaOH) in pellets were supplied by Fmaia. All chemicals were of analytical grades and used without further purification.

2.2. Evaluation of the chemical route for modifying PEG with GMA

2.2.1. The influence of time during chemical modification of PEG with GMA

The main strategy for synthesis of PEG-based hydrogels consisted on use PEG as cross-linker agent (macromere). For obtaining such macromere PEG was vinyl-modified with GMA by an epoxide ring-opening reaction using NaOH as catalyst. However, depending on the method employed, the reaction time of hydroxyl groups with epoxy rings may take between 24h to 42h[96]. Thus, a previous experiment was performed in order to evaluate the reaction time during chemical modification of PEG. Initially, PEG 9.75 g (9.75 mmol) was added to 35 mL of water at room temperature while stirring. The temperature of the mixture was increased up to 50 °C and the pH of the solution was adjusted to 10.5 with addition of 1.0 mol L^{-1} NaOH solution. Then, 2.7 mL (19.8 mmol) of GMA were introduced into the mixture. The solution of PEG with GMA was left to react for 24h under stirring (300 rpm). Aliquots of 5mL were collected from the solution at specific times, and then, they were freeze-dried for 24h for chemical characterization by NMR-^{1}H spectroscopy.

Figure 13 shows the ^{1}H-NMR spectra obtained from those aliquots taken at specific times during chemical modification of PEG with GMA. In the first 6h, two signals could be observed between 5.74 ppm and 6.17 ppm. These signals are attributed to the macromere obtained by epoxide-ring opening. After 6h of reaction, new signals (highlighted in the Figure 13) were observed at δ 5.67 and δ 5.36 indicating the presence of another macromere obtained from *trans*-esterification process (an additional discussion about results obtained from ^{1}H-NMR spectra will be addressed in great detail later in *section 4.1*). Thus, for obtaining a macromere with uniform properties, the time of reaction was set up to 6h.
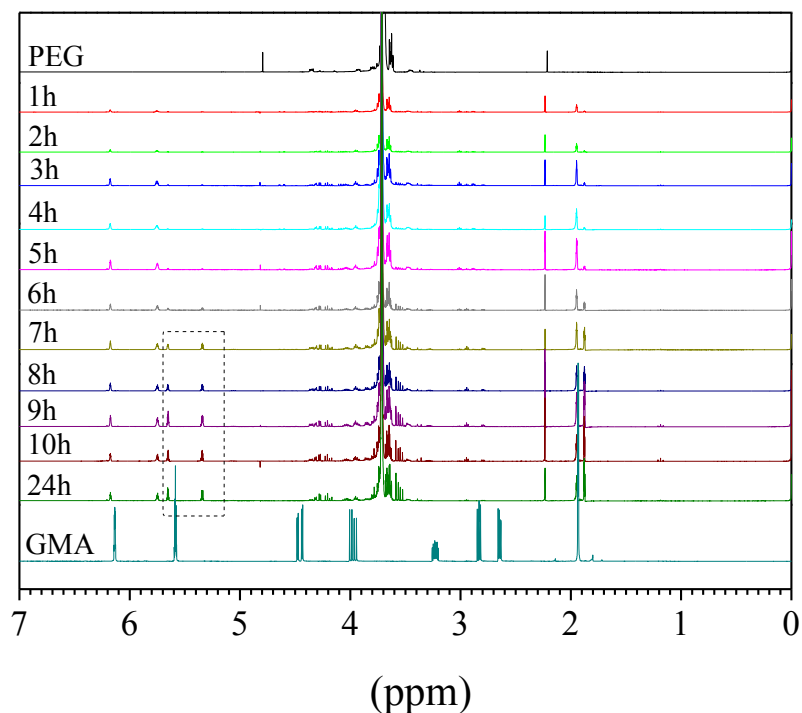
Figure 13. ^{1}H-NMR spectra of PEG, GMA, aliquots taken at specific times during the chemical modification of PEG with GMA.

2.2.2. The influence of pH on the chemical modification of PEG with GMA

For investigating the influence of pH on the chemical modification of PEG with GMA, the following experiment was performed: PEG (9.75 g) was added to 35 mL of water at room temperature while stirring. The temperature of the mixture was increased up to 50 °C and the pH was adjusted to 10.5 with addition of 1.0 mol L^{-1} NaOH solution. Then, 2.7 mL of GMA were introduced into the mixture. It was observed that the pH of the solution spontaneously decreased to approx. 7.0 after addition of GMA. In order to have more precise control over the reaction, two different investigations on the PEG modification were performed: i) at pH 7.0, which was the pH of the solution after addition of GMA, and ii) where pH of the solution was readjusted up to pH 10.5 by adding NaOH. The solution of PEG with GMA was left to react for 6 h under stirring (300 rpm). Later, the solution was labeled ^{GMA}PEG solution. The product was separated by centrifugation and

freeze-dried for 24 h for chemical characterization by FTIR and ^{1}H-NMR spectroscopy.

2.3. Preparation of sodium acrylate (SA) from acrylic acid (AAc)

In the hydrogel-forming solutions, acrylate salt was used instead of acrylic acid in order to prevent overheating, by acid addition, over gelation at 70 °C. In a common example of neutralization, 50 mL of AAc were solubilized in acetone at room temperature under continuous stirring (300 rpm). Then, 28.6 g (0.71 mols) of NaOH were slowly added to the stirred solution. After few minutes, the clear solution turned to a whitish suspension, as a result of the salt precipitation. The precipitate was filtered under vacuum and left to dry in a ventilated oven at 35°C for 48 h.

2.4. Synthesis of hydrogels based on GMA-modified PEG (^{GMA}PEG)

The experimental conditions of hydrogel synthesis were chosen on the basis of spectroscopic data for modification of PEG with GMA (^{GMA}PEG). Result from those studies motived us to use the ^{GMA}PEG synthesized during 6h of reaction at pH 7.0, as cross-linker agent, because in this condition, the ^{GMA}PEG is obtained only from epoxide ring-opening reaction (as shall be seen in results and discussions). For preparing the hydrogel, recently prepared ^{GMA}PEG solutions were employed. In view of this, a two-step synthesis was performed. In the first step, 16 g of PEG (16 mmol) were added to 80 mL of water at 50°C under stirring. The pH of the mixture was adjusted to pH 10.5 with NaOH solution at 1.0 mol L^{-1} concentration. After the solubilization, 4.8 mL of GMA (32.4 mmol) were introduced, causing a spontaneous decrease in pH to *ca*. 7. The solution of PEG with GMA was left to react for 6 h under mild stirring. In the second step, the ^{GMA}PEG solutions were used to produce the hydrogels using volumes of 5 and 10 mL, as shown in Table 2. The final volume of solvent used in the hydrogel-forming solutions was approximately 10 mL. In the case of hydrogels prepared with 5 mL of solution, the volume was made up to 10 mL with water. Then, DMAAm, SA (Table 2) and Na$_2$S$_2$O$_8$ (0.03 g) were added to ^{GMA}PEG solution at 70°C and left to react for 30 min, forming a transparent material. The thus obtained hydrogels were washed with distilled water and stored at 15°C before swelling experiments.

Table 2. Volumes of ^{GMA}PEG solution and amounts of DMAAm and SA used for gelation.

Sample Name	^{GMA}PEG solution (mL)[b]	DMAAm (g)	SA (g)
P1D1A1	5.0	0.5	0.6
P1D1A2	5.0	0.5	1.2
P1D2A1	5.0	1.0	0.5
P1D2A2	5.0	1.0	1.2
P2D1A1	10.0	0.5	0.6
P2D1A2	10.0	0.5	1.2
P2D2A1	10.0	1.0	0.6
P2D2A2	10.0	1.0	1.2
P2D2	10.0	1.0	0.0
P2A2[a]	10.0	0.0	1.2

a. Hydrogel not formed; b. A solution of ^{GMA}PEG (0.2 g mL^{-1}) was used

2.5. Stress-strain measurements

The mechanical tests were performed on the hydrogels free from air bubbles or physical imperfections. This was visually verified. Mechanical tests were considered as being the measured force for compressing the hydrogels to 1 mm deformation using a texture analyzer-TAX.T2i equipped with a 5 kg load cell. The apparatus was equipped with a circular probe of 0.5 mm diameter (P/0.5), which was programmed to descend onto gel surface moving at a constant speed of 2 mm s^{-1}. The hydrogels were cut into small pieces with 10 mm-height, 100 mm^2-surface dimensions. Their compressive strength was performed at 25°C. The stress-strain measurements were done in triplicate, shortly after polymerization. Each measurement was performed in less than 1 min to prevent water loss by the hydrogel over the experiment. The force necessary for compressing the hydrogels at 1 mm was recorded and the stress values were determined using the Eq. (2):

$$\sigma = \frac{F}{A} = E\varepsilon \tag{2}$$

where F is the force and A is the cross-sectional area of the hydrogel, E is the elastic modulus, and ε is relative deformation of the sample ($\Delta l/l_0$).

2.6. Swelling kinetics of ^{GMA}PEG hydrogels (water absorption capacity)

The swelling degree (SW) of the hydrogels were investigated by immersing 1 cm^3 dry samples of known mass into buffer solutions of pH 2.0, 7.0, and 10.0, in dependence on time at 36.5 °C. The hydrogels were withdrawn from the solution buffers, the excess water droplets on the surface were wiped off carefully, and the samples were weighed at each new time-step. This procedure was done until to achieve the swelling equilibrium. SW of ^{GMA}PEG hydrogels with different compositions was obtained from the Eq. (3), correlating the water mass within the hydrogel at any time (M_t) to the initial mass of hydrogel (M_0).

$$SW = \frac{M_t - M_0}{M_0} \tag{3}$$

2.7. Determination of swelling mechanism (water transport)

To have an insight into water transport through the hydrogels, the swelling mechanism was investigated. For water-swellable polymer networks, it can be described by power law model, applying the Eq. (4):

$$\frac{M_t}{M_{eq}} = kt^n \tag{4}$$

where, n represents the diffusion coefficient that describes the specific transport mechanism, k is a parameter related to diffusion coefficients. M_t and M_{eq} are the absorbed water masses by the hydrogel at a specific time and at equilibrium, respectively[97]. The plot of the relative mass of water diffused into hydrogel (M_t/M_{eq}) against time (t) gives both n and k values.

2.8. An empirical approach for predicting the entire water transport profile

The Eq. (4) is a semiempirical, mathematical model that describes only the first 60 % of the absorbed water, when the water diffusion inwards the hydrogel

linearly changes with time. Weibull function is an empirical equation that has been used as an alternative tool to describe overall profile of water absorption:

$$\frac{M_t}{M_{eq}} = 1 - e^{-[k_W(t-t_0)]^d}$$

(5)

where τ_0 represents the time-lag onset before swelling, d is related to mechanism and k_W is associated to swelling rate constant[98, 99]. The Eq. (5) gives an insight into the diffusional mechanism and swelling rate[100-102].

3. Characterizations

3.1. Fourier Transform Infrared Spectroscopy (FTIR)

The FTIR spectra were recorded in a Bruker spectrometer model Vertex-70V. Powdered samples were prepared into pellets with KBr. The scan range varied from 400 to 4000 cm^{-1}, and 128 scans were run for each spectrum. The resolution of the measurements was 4 cm^{-1}.

3.2. ^{1}H-NMR and Solid-State ^{13}C Cross-Polarization Magic Angle Spinning (^{13}C-CP/MAS-NMR)

The ^{1}H NMR spectra were recorded in a Varian spectrometer, model Mercury Plus BB 300 MHz, using a frequency of 300.059 MHz for ^{1}H nucleus, an angle pulse of 90° and a relaxation delay of 3 s. The spectra were obtained with CDCl$_3$ solutions containing 20 mg L^{-1} of sample. The chemical shift was reported as δ values (ppm). The solid-state ^{13}C-CP/MAS NMR spectra of the powdered hydrogels were obtained using an angle pulse of 37°, a frequency of 75.45 MHz for 13C nucleus, a contact time of 3 ms, and recicle delay of 3s. The samples were packed into a SiN$_4$ rotor of 7-mm diameter, which was spun at 4 kHz during the measurements. The chemical shifts were externally referenced by setting the methyl carbon resonance of hexamethylbenzene to 17.3 ppm.

3.3. Scanning Electron Microscopy (SEM)

The hydrogels were swollen to equilibrium in water prior to SEM imaging. They were withdrawn from water and immediately frozen by immersion in liquid

nitrogen before being lyophilized for 72 h. Under these conditions, it is supposed that the morphology of the swollen hydrogels is maintained. The samples were sputter-coated with a thin layer of gold and the SEM images were obtained in a scanning electron microscope (Shimadzu, model SS550 Superscan) by applying an acceleration voltage of 15 kV and a current intensity of 30 μA.

3.4. Cytotoxicity Measurement

Cytotoxic effects were evaluated against VERO line cells, originated from kidney of African green monkey. The cells were cultivated in DMEM (Dulbecco's Modified Eagle's Medium) with 10% fetal calf serum (FCS) at 37 °C and 5% CO_2. Approximately $2{,}5 \times 10^5$ cells were obtained by tripsinization and added to a 96-well plate for 24 h, using the same conditions described previously. Later, the compounds in different concentrations were added and incubated for 72 h. After that, MTT (Amresco®) solution at 2 mg mL^{-1} concentration was maintained in the wells for 4 h for reading of the absorbance at 570 nm, in a microplates spectrophotometer (Bio Tek-Power Wave XS).

4. Results and discussions

4.1. Characterization of PEG modified with GMA

Figure 14 shows the FTIR spectra of GMA, ^{GMA}PEG, and PEG in the spectral range of 2000 cm^{-1} to 800 cm^{-1}. The spectra of ^{GMA}PEG synthesized at pH 7.0 and 10.5 showed the same characteristics. The bands at 1720 and 1640 cm^{-1} in the spectra of ^{GMA}PEG were attributed to stretching vibrations of carbonyl groups (νC=O) and vinyl groups (C=C), respectively[103, 104]. These signals correspond to conjugated esters derived from GMA moieties. Furthermore, in the same spectrum, the bands at 910 and 860 cm^{-1}, owing to $ν_{as}$C-C and νC-O of the epoxy ring, respectively, completely disappeared[45, 105]. These spectral changes indicated that PEG reacted with GMA by an epoxide ring-opening mechanism.
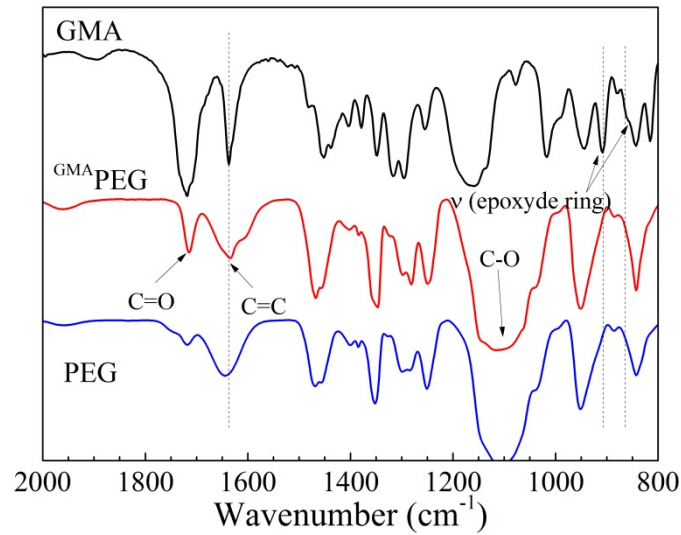
Figure 14. FTIR spectra of GMA, ^{GMA}PEG, and PEG in the spectral range of 2000 cm^{-1} to 800 cm^{-1}.

The chemical reaction of PEG with GMA was also analyzed by ^{1}H-NMR spectroscopy (Figure 15). For a more detailed analysis, a scheme of the products resultant of the PEG reaction with GMA were shown in inset.
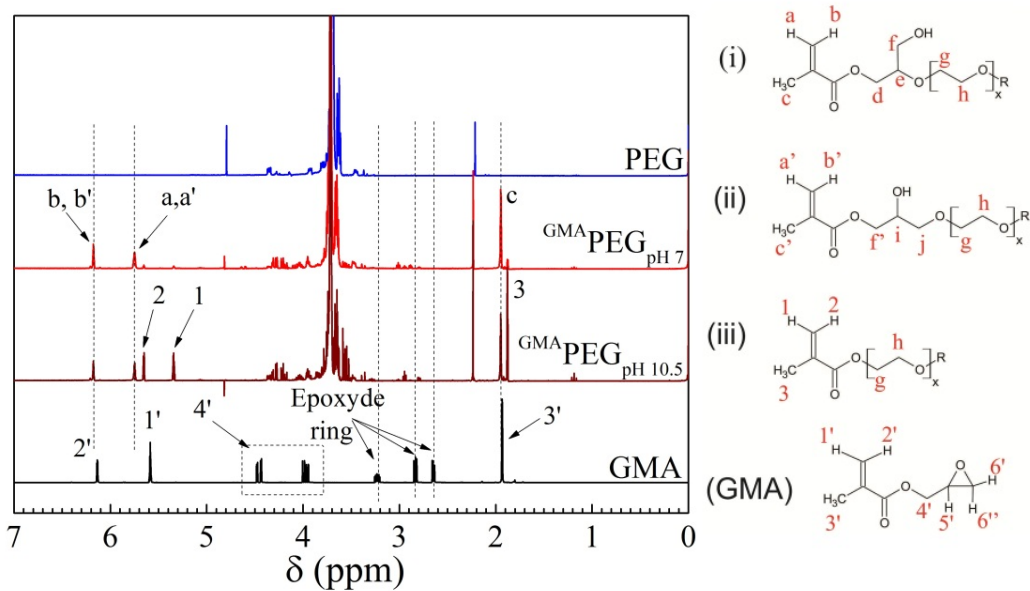
Figure 15. ^{1}H-NMR spectra of PEG, ^{GMA}PEG modified at pH 7.0 and 10.5, and GMA. Inset: products resultant of the PEG reaction with GMA at pH 7.0 and 10.5.

The signals at δ 2.67, δ 2.84, and δ 3.23 in the spectrum of GMA were attributed to hydrogen from epoxide ring (6', 6", and 5' respectively). These signals were not observed in the spectra of ^{GMA}PEG.

The signals at δ 6.17 and δ 5.74 in the spectra of ^{GMA}PEG modified at pH 7.0 were assigned to vinyl carbon-linked hydrogen from both (i) and (ii) molecules (inset). The signal at δ 1.94, in the same spectrum, corresponded to methyl carbon-linked hydrogen from vinyl carbons. These structures result of the epoxide ring-opening mechanism[22]. Other signals of the ^{GMA}PEG molecular structure were overlapped by hydrogen signals from PEG.

The signals that give information on the PEG reaction at pH 10 were observed at δ 5.67 and δ 5.36. They refer to hydrogen from vinyl groups of (iii) molecule (inset), which is a reaction product of the transesterification mechanism[96, 106]. A schema suggesting the chemical structure of the products resultant from PEG reaction with GMA as a function of pH was proposed in Figure 16.
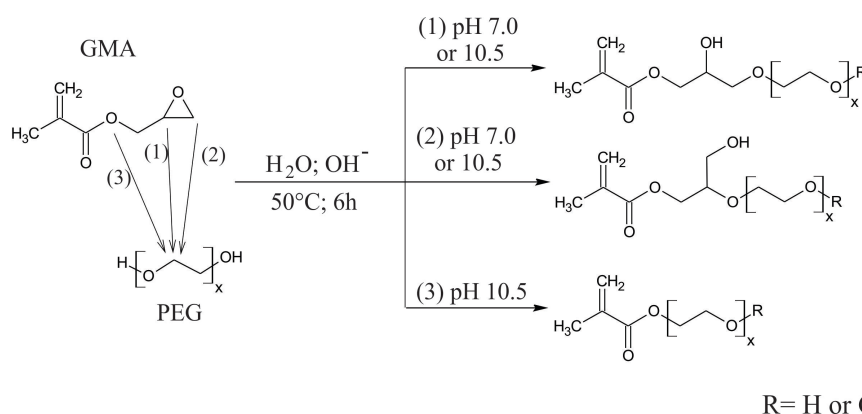
Figure 16. Scheme of the chemical structure of the products resultant from PEG reaction with GMA at pH 7.0 and 10.5.

At pH 10.5, three different chemical structures were obtained: (1) vinyl methacrylate of PEG, (2) 3-methacryloyl-1-glyceryl ether of PEG, and (3) 3-methacryloyl-2-glyceryl ether of PEG. The (1) and (2) structures result from ring-opening reaction, and the (3) structure originates from transesterification reaction. From a chemical point of view, the modification of PEG at pH 7.0 seems to be more interesting for further gelation, for two reasons. The first and most important

reason is that the PEG reaction with GMA may be processed at a pH close to that of the pure water. The second reason is that the two structures from epoxide ring-opening reaction (1,2) carry hydroxyl groups in their chemical structures which could interact with water by way of hydrogen bonds within the swollen hydrogel. Thus, for hydrogel synthesis, the modification of PEG was performed at pH 7.0 in order to obtain preferably only structures resulting from epoxide ring-opening reaction.

4.2. Characterization of hydrogels based on ^{GMA}PEG

Figure 17 shows the solid-state ^{13}C-CP/MAS spectra of the P2D2 and P2D2A2 hydrogels. The corresponding signal of carbonyl groups in the spectrum of P2D2 hydrogel was visualized at δ 178. This signal was attributed to C=O from both ^{GMA}PEG and DMAAm (f+h). The signal at δ 184 in the spectra of P2D2A2 was assigned to C=O from AAc (g)[107].
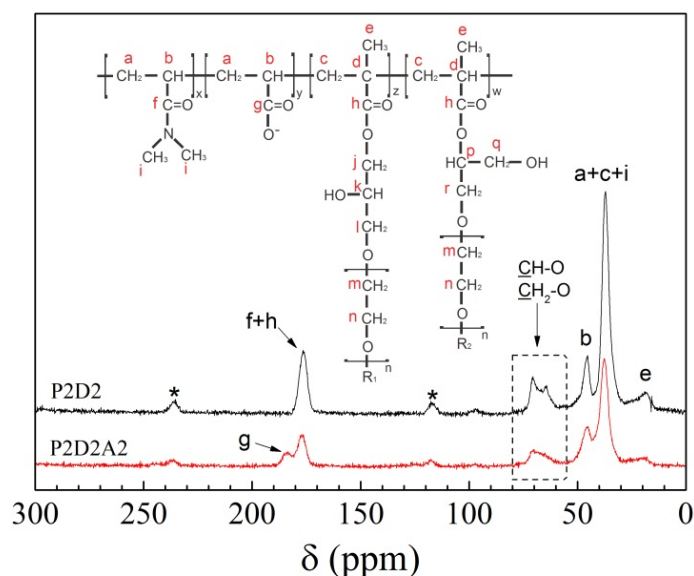
Figure 17. Solid state ^{13}C-CP/MAS NMR spectra of P2D2 and P2D2A2 hydrogels. (*) Side band spinning effect.

The signals between δ 60 and δ 80 were attributed to carbons linked to oxygen (CH-O and CH$_2$-O) and the signal at δ 19 (e) was ascribed to methyl group. Both of them were corresponded to ^{GMA}PEG structure[108]. In the same spectra, the signals at δ 45 and 37 ppm were assigned to carbons in the main chain of the

hydrogel network (CH and CH$_2$, respectively)[109, 110]. Moreover, side band spinning effect (*) was associated with signals at δ 235 and δ 119, which are symmetric to the carbonyl group at δ 178[111, 112]. From these spectroscopic data, a simplified schema suggesting the structure of the ^{GMA}PEG-based hydrogel was showed in Figure 18.
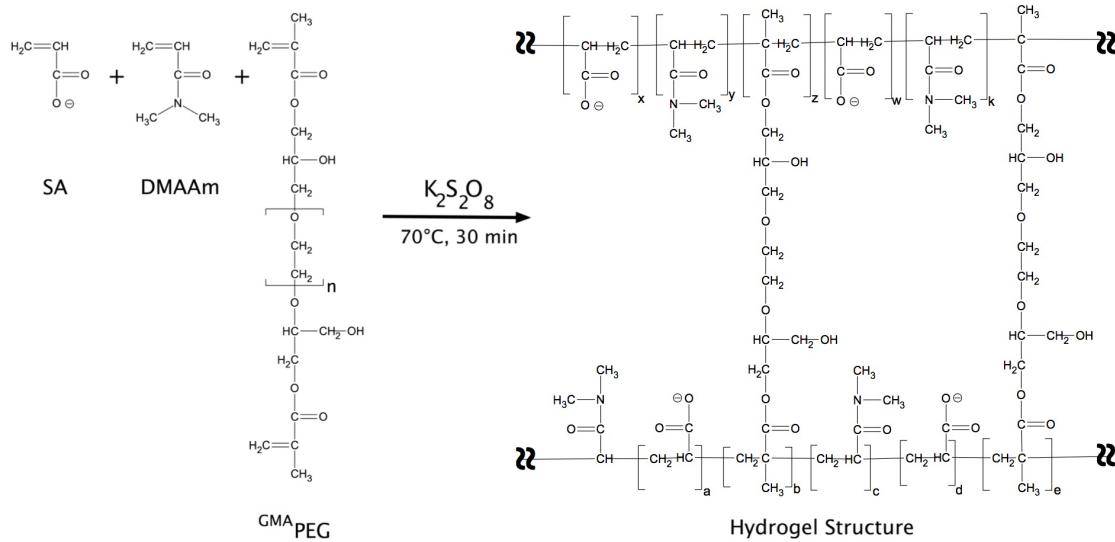
Figure 18. Scheme of the chemical structure of ^{GMA}PEG-based hydrogel.

4.3. Swelling performance

Figure 19 shows the swelling kinetics of the hydrogels in buffer solutions with pH 2.0, 7.0 and 10.0 at 36.5 °C. As a general trend, all hydrogels showed higher SW values at pH 10 and lower at pH 2. This effect may be associated with the ionization of the carboxylic groups (COOH) of AAc changing to acrylate ions (COO$^-$). In the alkaline medium, the COOH groups are ionized to form COO$^-$ generating electrostatic repulsion forces among the polymer chains. As a result, the hydrogel affinity for water increases. However, at pH 2, there is an excess of H$^+$ ions, and consequently, COO$^-$ is converted to form COOH, leading to network hydrophilicity reduction[113, 114]. This assumption is confirmed by comparing the hydrogels made of P2D2, P2D2A1, and P2D2A2 (Figure 19I, 19G, and 19H, respectively).
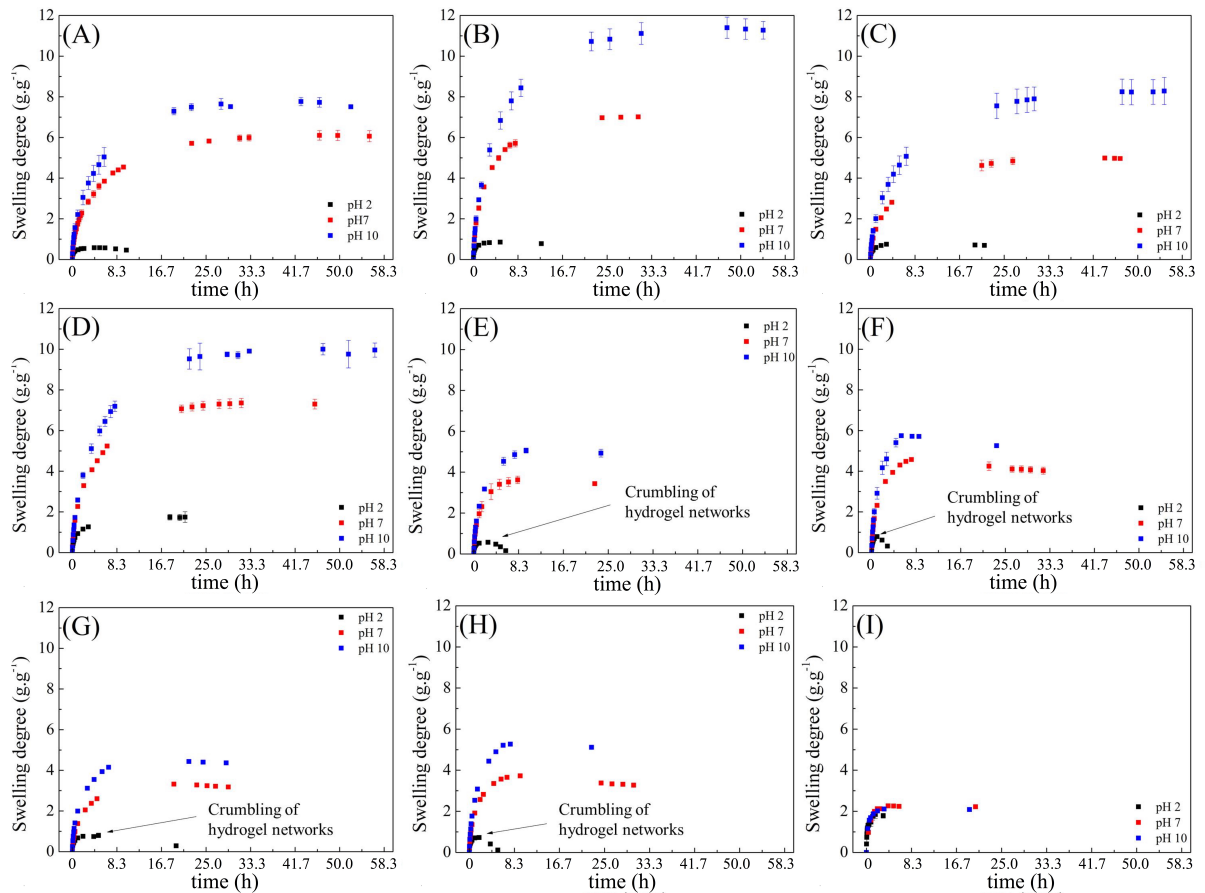
Figure 19. Time-dependent swelling curves of hydrogels at the indicated pH at a temperature of 36.5 °C: (A) P1D1A1, (B) P1D1A2, (C) P1D2A1, (D) P1D2A2, (E) P2D1A1, (F) P2D1A2, (G) P2D2A1, (H) P2D2A2, and (I) P2D2.

In Figure 19I, the P2D2 hydrogel (without AAc) did not show significant SW changes by changing the pH of the surrounding liquid. However, the P2D2A1 and P2D2A2 hydrogels (both with AAc) showed higher swelling degree at pH 7.0 and 10. At pH 2, both of them showed lower SW, as a result of hydrogen bonds between the COOH groups[115, 116].

The effect of ^{GMA}PEG on the swelling performance was also investigated. The water absorption capacity of the hydrogels increases when the amount of ^{GMA}PEG within them decreases. This effect can be better visualized at pH 10. For example, the P1D1A1 hydrogel (Figure 19A) showed SW value of *ca*.8 The P2D1A1 hydrogel (Figure 19E), which has higher amount of ^{GMA}PEG, showed SW value of *ca*. 5. The same effect also was found in both the P1D1A2 and the P2D1A2 hydrogels. The chemical nature of the polymer network forming the hydrogel

affects SW but the crosslinking density also changes its water absorption performance[117]. ^{GMA}PEG has potential crosslinking points, owing to vinyl groups introduced by modification reaction. Larger amount of ^{GMA}PEG added for gelation results in a more densely cross-linked PEG network and thus in a lower SW.

In the acidic solutions, the hydrogel networks with larger amount of ^{GMA}PEG (Figure 19E, 19F, 19G and 19H) started to crumble after achieving the swelling equilibrium. This fact may be associated to ester groups in ^{GMA}PEG. Under those conditions, the covalent bonds that form the main structure of the hydrogel can be unmade by decreasing the swelling pH, as a result of acidic hydrolysis of esters groups. In fact, hydrolysis can occur either in acid or in basic medium. However, in this work, the acid hydrolysis effect is more pronounced than the basic one. This is associated with concentrations of OH$^-$ and H$^+$ since, at pH 10, the concentration of OH$^-$ is a hundred times lower than H$^+$ concentration at pH 2.

The breakage of ^{GMA}PEG, which is a key constituent of network, causes degradation of the cross-linked polymer network. Poon and co-workers have reported the hydrolysis in hydrogels containing poly(ethylene glycol) dimethacrylate[118]. Giammona and co-authors investigated both enzymatic and chemical hydrolysis on the PEG-derivatives hydrogels[119]. In addition, Lee and co-workers reported the hydrogel degradation through ester bond hydrolysis resulting in the release of PEG and poly(acrylic acid-*co*-vinyl pyrrolidone)[120].

The hydrogel deconstruction seems to be similar to that reported by Lee and co-workers[120]. A schematic representation of the whole process of the hydrogel degradation is shown in Figure 20.
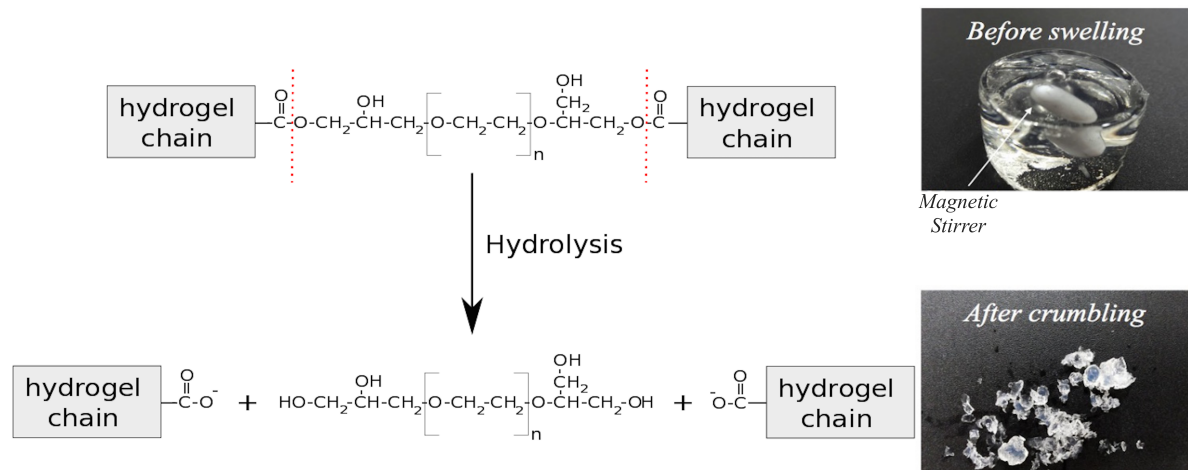
Figure 20. Schematic representation of ^{GMA}PEG hydrogel degradation upon ester hydrolysis at pH 2. Digital photos of sample P2D2A1 taken after 500 min of swelling.

4.4. Studies of water transport

The water transport through the hydrogels was investigated by adjusting the experimental data to both Eqs. (4) and (5). The fitting parameters were described in Table 3. The n and k parameters were obtained from Eq. (4) and the k_W parameter from Eq. (5). The n parameter has different conceptual meanings depending on geometrical shape of the material. For cylinder, which is the geometry of PEG-based hydrogels, when $n=0.5$ the swelling mechanism is termed as Fickian transport. This mechanism is characterized when the solvent diffusion rate is slower than relaxation rate. If $n=1$ (Case II transport), the diffusion is faster than relaxation.

Table 3. Fitting parameters of Eqs. (4) and (5) to swelling kinetics of hydrogels composed of ^{GMA}PEG, DMAAm and SA at different pH at 36.5 °C.

Hydrogel	pH	Power law model		Weibull model	
		n	k	d	k_W (min^{-1})
P1D1A1	2	0.100 ± 0.002	0.723 ± 0.003	0.295 ± 0.018	0.572 ± 0.095
	7	0.272 ± 0.009	0.129 ± 0.004	0.603 ± 0.025	0.004 ± 0.000[a]
	10	0.299 ± 0.012	0.112 ± 0.005	0.751 ± 0.068	0.004 ± 0.000[a]
P1D1A2	2	0.119 ± 0.005	0.612 ± 0.006	0.353 ± 0.017	0.250 ± 0.024
	7	0.308 ± 0.013	0.124 ± 0.005	0.581 ± 0.018	0.006 ± 0.000[a]
	10	0.358 ± 0.017	0.074 ± 0.004	0.683 ± 0.021	0.003 ± 0.000[a]
P1D2A1	2	0.083 ± 0.007	0.661 ± 0.009	0.311 ± 0.046	0.289 ± 0.097
	7	0.242 ± 0.013	0.156 ± 0.007	0.611 ± 0.033	0.004 ± 0.000[a]
	10	0.305 ± 0.014	0.096 ± 0.005	0.671 ± 0.024	0.003 ± 0.000[a]
P1D2A2	2	0.138 ± 0.007	0.391 ± 0.006	0.364 ± 0.025	0.030 ± 0.003
	7	0.296 ± 0.015	0.116 ± 0.005	0.680 ± 0.043	0.004 ± 0.000[a]
	10	0.347 ± 0.017	0.080 ± 0.005	0.704 ± 0.025	0.003 ± 0.000[a]
P2D1A1	2	0.094 ± 0.002	0.691 ± 0.003	0.376 ± 0.022	0.508 ± 0.070
	7	0.239 ± 0.015	0.234 ± 0.009	0.726 ± 0.082	0.018 ± 0.002
	10	0.284 ± 0.015	0.167 ± 0.007	0.714 ± 0.058	0.012 ± 0.001
P2D1A2	2	0.128 ± 0.006	0.612 ± 0.007	0.562 ± 0.070	0.198 ± 0.042
	7	0.270 ± 0.014	0.204 ± 0.007	0.674 ± 0.041	0.014 ± 0.001
	10	0.297 ± 0.021	0.167 ± 0.009	0.791 ± 0.050	0.013 ± 0.001
P2D2A1	2	0.106 ± 0.004	0.608 ± 0.005	0.341 ± 0.023	0.281 ± 0.040
	7	0.203 ± 0.014	0.235 ± 0.009	0.572 ± 0.039	0.011 ± 0.001
	10	0.259 ± 0.013	0.185 ± 0.007	0.629 ± 0.032	0.011 ± 0.001
P2D2A2	2	0.114 ± 0.003	0.777 ± 0.005	0.468 ± 0.066	0.279 ± 0.076
	7	0.231 ± 0.014	0.244 ± 0.008	0.650 ± 0.038	0.014 ± 0.001
	10	0.299 ± 0.017	0.162 ± 0.008	0.773 ± 0.056	0.012 ± 0.001
P2D2	2	0.271 ± 0.006	0.433 ± 0.005	0.458 ± 0.044	0.220 ± 0.029
	7	0.295 ± 0.013	0.248 ± 0.013	0.923 ± 0.062	0.027 ± 0.002
	10	0.162 ± 0.019	0.460 ± 0.035	0.602 ± 0.034	0.072 ± 0.005

a. Standard deviation (SD) lower than 0.001

An intermediate state between diffusion and relaxation occurs when $0.5 < n < 1$ [121-123]. However, all hydrogels showed $n<0.5$, which indicates a pseudo-Fickian behavior. This mechanism is observed when the diffusion coefficient changes with the time, consequently, the hydrogels never reach the swelling equilibrium[124, 125]. This can be explained by inhomogeneity of the hydrogels. The skin and bulk of the sample could differ in morphology and composition. Then, the diffusion process that occurs either on the surface or in the bulk of the hydrogel may be driven by a Fickian transport but its combination may not be Fickian. Moreover, as the bulk increases, the influence of skin on the swelling decreases. This explains the time-dependency of the coefficient diffusion[126, 127]. For hydrogels with AAc, both n and d values increase by increasing the pH, indicating a pH-dependent water transport mechanism.

The parameter k from power law (Eq. (4)) and the swelling rate constant (k_W) from (Eq. (5)) are related, respectively, to the diffusion coefficient and velocity at which the hydrogel achieves the equilibrium. In Table 3 it is observed for all samples that k and k_W are higher at pH 2 than at any other pH studied. This means that the hydrogels achieve the equilibrium more quickly in the acidic medium. Furthermore, there was no significant difference on both k and k_W at pH 7.0 and pH 10.0. These observations suggest that the water absorption barely changes at pH $\geq$ 7, in spite of the water transport mechanism showing more marked changes in both the acidic and the basic media.

4.5. Hydrogel morphology

Figure 21 shows the SEM micrographs of fractured frozen P1D1A1 and P2D1A1 hydrogels lyophilized after reaching the swelling equilibrium at different pH. For pH 7.0 and 10 (Figure 21B, 21C, 21E and 21F), porous morphology was observed in any part of the fractured samples. This means that there are pores on and within the matrix. This attribute makes these hydrogels attractive as polymer carriers, because their porous structures allow the drug to diffuse into, through and from the 3D polymer network. On the other hand, at pH 2 (Figure 21A and 21D), the hydrogels degraded after swelling, showing less defined shapes. This morphological characteristic results of the cleavage of ester bonds of the ^{GMA}PEG chains deconstructing the hydrogel networks.
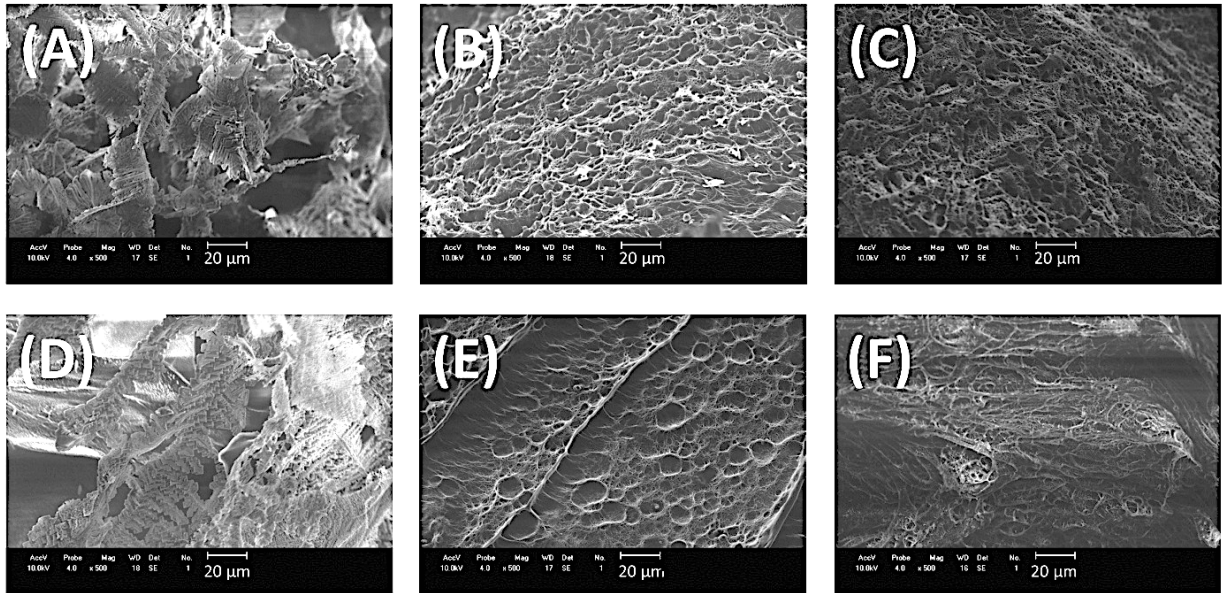
Figure 21. SEM images of fractured frozen ^{GMA}PEG-based hydrogels after reaching the swelling equilibrium at pH 2, 7 and 10. (A) P1D1A1-pH2, (B) P1D1A1-pH7, (C) P1D1A1-pH10, (D) P2D1A1-pH2, (E) P2D1A1-pH7, and (F) P2D1A1-pH10.

4.6. Mechanical behavior of the hydrogels

The correlation of stress and strain indicates an elastic deformation when the hydrogel undergoes a mechanical compression. In such a case, the strain is recovered by removing the applied stress. From a physical-chemical point of view, it is said that the strain is accommodated by the rearrangement of the polymer chains within the hydrogel. As a consequence, retractive elastic forces concomitantly develop in those polymer chains owing to their tendency to return to original configuration.

The modulus of elasticity (E) gives relevant information for development of hydrogels with excellent quality and stability to be applied in the biological environments. E was obtained from linear slope of the stress-strain curves (Figure 22) and the data adjusted to Eq. (2) were summarized in Table 4.
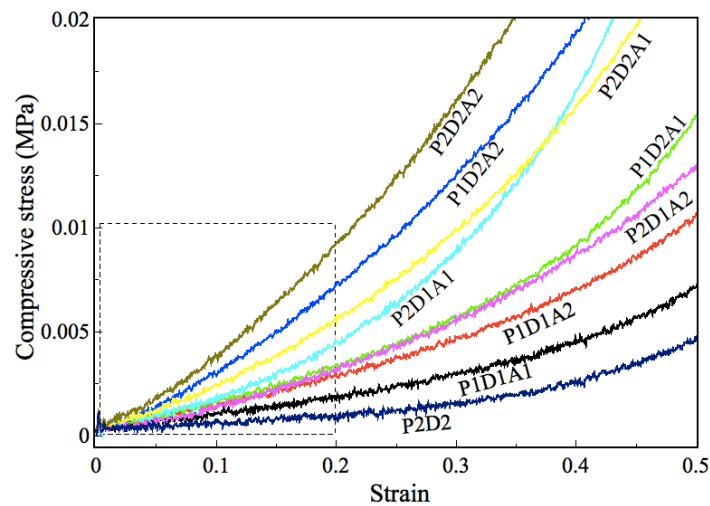
Figure 22. Applied stress versus the strain curves of hydrogels with different compositions. Highlighted box: Elastic deformation corresponding to the linear part of the stress-strain measurements.

The shape and characteristics of the stress-strain curves were affected by changing the amount of ^{GMA}PEG, AAc or DMAAm in the hydrogel. The E values increased when larger amounts of those reactants were used. In such a case, the hydrogel becomes less soft; therefore, a loader is necessary to compress it to 1 mm.

The P1D1A1 hydrogel showed an E value of 9.58 but this value increased to 19.13 in the P2D1A1 hydrogel. With addition of more ^{GMA}PEG, the hydrogel becomes more cross-linked and thus less soft. This finding may be associated with SW values of those hydrogels. The P2D1A1 hydrogel is a less efficient water absorber than the P1D1A1 hydrogel, because it has a less flexible, tighter polymer network that prevents its expansion in the liquid. The effect of acrylate groups on E (P1D2A1 and P2D2A1 hydrogels) is comparable to that of the PEG chains. On the other hand, it is important to highlight that the influence of the repulsion forces among the COO$^-$ groups on the swelling degree of those samples, which are richer in AAc, was more important than the cross-linking density.

Table 4. Moduli of elasticity of hydrogels with different polymer compositions.

Hydrogel	E (kPa)
P1D1A1	9.58 ± 0.06
P1D1A2	14.46 ± 0.06
P1D2A1	16.53 ± 0.06
P1D2A2	31.88 ± 0.11
P2D1A1	19.13 ± 0.11
P2D1A2	15.20 ± 0.06
P2D2A1	25.10 ± 0.09
P2D2A2	40.08 ± 0.16
P2D2	5.10 ± 0.06

4.7. Cytotoxicity research

In vitro cytotoxicity assay was performed to evaluate the pharmacological potential of the hydrogels (Figure 23). This approach is an excellent tool in the evaluation of biocompatibility and toxicity of new materials prior to *in vivo* tests. The cytotoxic concentrations for 50% of VERO cells (CC_{50}) were determined as the concentration necessary to reduce the cell viability by 50%. The hydrogels had different effects on the cells. Values for CC_{50} were higher than 150 µg mL^{-1}, indicating that the hydrogels do not have any toxic, destructive constituents for living cells[128, 129]. It is reasonable to say that the proposed hydrogels have acceptable biocompatibility and an appropriate level of security for use in the biological environments.
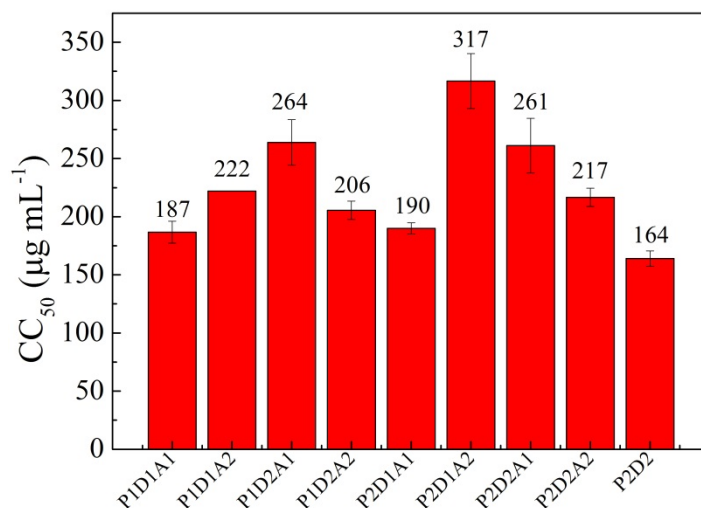
Figure 23. Evaluation of cytotoxicity for ^{GMA}PEG hydrogels in Vero cells after 72 h of incubation at 37°C and 5% CO_2 by the MTT assay.

5. Conclusions

We developed a pH-responsive hydrogel in which PEG is the key constituent in the polymer network that undergoes degradation by acid catalyzed hydrolysis. PEG was chemically modified with GMA and the reaction product was able to undergo radical cross-linking/polymerization with SA and DMAAm. The breakage of the PEG chains in the acidic solutions crumbled the hydrogel structure. This behavior was attributed to acid catalyzed hydrolysis. All hydrogels showed a pseudo-Fickian behavior, a transport mechanism that occurs when the diffusion coefficient changes with the time and the swelling equilibrium is never fully reached. This characteristic may be important in drug release systems. The PEG-richer hydrogels are less deformable when subjected to compressive stress. With addition of larger amounts of modified PEG, the material became more cross-linked and thus less soft. Results from cytotoxicity showed that the proposed hydrogels may have a great pharmacological potential for use in biological environments. This study offers important information on the synthesis and water transport mechanism of water-swellable networks, being relevant for the development of polymer carriers, although many technological challenges remain ahead.

PARTE I – CAPÍTULO 2

Synthesis and characterization of a multi-responsive poly(ethylene glycol)-based hydrogels: Effects of pH and magnetic field in Prednisolone release

1- Introduction

Prednisolone is a corticosteroid drug used to treat a variety of inflammatory and autoimmune conditions (i.e. asthma, rheumatoid arthritis, ulcers, and multiple sclerosis), and for improving the treatment- and desease-related symptoms in patients with cancer[130-134].

Depending on the type of disease, this drug can be administered either by oral or by intravenous route. However, the conventional formulation of prednisolone can be considered low in terms of efficacy, mainly due to their failure in maintaining the effective therapeutic drug levels[135]. In addition, it has been reported that the corticosteroid derivatives have several side effects, specially, when used in high concentrations. Furthermore, prednisolone is poorly-soluble in water which difficult its administration[136].

In order to overcome these drawbacks several researches have proposed new strategies for controlling the release of prednisolone which includes the use of PEGylated liposomes[137], tablets of chitosan and cellulose acetate phthalate[138], PVP microspheres[132], and also hydrogels[6].

Hydrogels (HGs) are polymers with three-dimensional network structure which are able to swell, absorbing a huge amount of either water or biological fluids[10, 11]. The HGs have received considerable attention, specially due to their ability to swell, without being dissolved, allowing nutrients diffusion which, in turn, makes HGs very similar to natural tissues. This characteristic makes the HG important for wide range applications, including controlled release of drug, and tissue engineering[14]. In addition, the possibility of using magnetic field, and/or pH stimuli to control the swelling of a hydrogel is considered to be highly advantageous for their future exploitation in the biomedical field[57].

Herein, the main goal of this work is given to synthesis and characterization of PEG-based hydrogels with multi-responsive properties (pH- and magnetic-responsive) for applying, as a polymeric carrier, in controlled release of prednisolone. The polymeric systems based on poly(ethylene glycol) (PEG) are among the most widely studied in the biomedical applications, owing to their biocompatibility and low toxicity. In addition, the PEG was approved by the U.S. Food and Drug Administration (FDA) for a variety of clinical uses[26]. PEG can be easily converted in a macromere (or cross-linking agent) by reacting its two hydroxyl-end groups with to others reactive groups, such as, methyloxyl, carboxyl, amine, thiol, azide, vinyl sulfone, azide, acrylate, and so on[21]. Here, before gelation, PEG was vinyl-modified (GMAPEG) with glycidyl methacrylate (GMA). The HG with magnetic- and pH-responsiveness were obtained after the cross-linking of GMAPEG with sodium acrylate (SA) and *N,N'*-dimethyl acrylamide (DMAAm) in presence of iron oxide nanoparticles dispersed under ultrasound. The drug release profile as well as the swelling behavior of the hydrogels under magnetic field were studied by the modeling of the release kinetics of prednisolone. The magnetic field-responsive release of prednisolone from the PEG-based hydrogels into a buffer solution of pH 1.2 (simulated gastric fluid) and pH 7.4 (simulated intestinal fluid) was also evaluated. The cytotoxicity measurements indicated that the PEG-based hydrogel is suitable for biomedical applications.

2- Experimental

2.1. Materials

Poly(ethylene glycol) (PEG) M_n 950-1050 g mol^{-1}, glycidyl methacrylate (GMA), sodium persulfate ($Na_2S_2O_8$), *N,N'*-dimethyl acrylamide (DMAAm), acrylic acid (AAc), and iron(II, III) oxide nanopowder (Fe_3O_4 − average size of 150 nm) were purchased from Sigma-Aldrich. Acetone and sodium hydroxide (NaOH) in pellets were supplied by Fmaia. All chemicals were of analytical grades and used without further purification.

2.2. Preparation of sodium acrylate (SA) from acrylic acid (AAc)

In the hydrogel-forming solutions, AAc was introduced as the acrylate salt form to prevent overheating over gelation at 70 °C owing to $Na_2S_2O_8$ (initiator). In a common example of neutralization, 50 mL of AAc were added to acetone at room

temperature while stirring. Next, 28.6 g (0.71 mol) of NaOH were slowly added to the stirred solution. After five hours, the clear solution turned to a whitish suspension, as a result of the salt precipitation. The precipitate was filtered under vacuum and left to dry in a ventilated oven at 35°C for 48 h.

2.3. Synthesis of macromere based on GMA-modified PEG (^{GMA}PEG)

Before hydrogel synthesis the poly(ethylene glycol) was modified with GMA in order to obtain a vinyl-modified cross-linking agent. The experimental conditions for PEG modification as well as for hydrogel synthesis were chosen according to our previous work[21]. Briefly, 16 g of PEG (16 mmol) were added to 80 mL of water at 50°C while stirring. The pH of the mixture was adjusted to pH 10.5 with addition of NaOH pellets. Afterwards, 4.8 mL of GMA (32.4 mmol) were introduced, causing a spontaneous decrease in pH to *ca.* 7. The solution of PEG with GMA was left to react for 6 h under mild stirring. Then, this solution containing ^{GMA}PEG (0.2 g mL^{-1}) was used for preparing the hydrogels.

2.4. Synthesis of hydrogels based on ^{GMA}PEG

PEG-based hydrogels were synthesized following the general procedure reported by Lima-Tenório et *al.*[5] with some adaptations. Briefly, 5mL of ^{GMA}PEG solutions were diluted in 5 mL of distilled water. Then, a desired amount of DMAAm, SA, and Fe_3O_4 were added into ^{GMA}PEG solution. Table 5 summarizes the hydrogel compositions. The as-prepared solution was subjected to ultrasonic irradiation with the use of a probe of ultrasonic oscillation (Cole Parmer$^{®}$ 500, model EW-04711-40) by applying a frequency of 20 kHz for 3 min. Then, 0.03 g of $Na_2S_2O_8$ were added to stirred solution, which was kept under ultrasound until a stiff material (gelation) be formed. The thus obtained hydrogels was washed with distilled water and stored at 15°C before swelling experiments.

Table 5. Amounts of DMAAm, SA, and Fe_3O_4 used for gelation[*].

Sample Name	DMAAm (g)	SA (g)	Fe_3O_4 (g)
A1	0.5	0.6	-----
A1_1	0.5	0.6	0.001
A1_3	0.5	0.6	0.003
A2	0.5	1.2	-----
A2_1	0.5	1.2	0.001
A2_3	0.5	1.2	0.003

* volume of solvent: 5 mL of [GMA]PEG solution with 5 mL of distilled water.

2.5. Swelling measurements

Swelling measurement of the hydrogels were investigated by immersing the 1 cm^3 of known hydrogel mass into buffer solutions of pH 1.2, 3.5, 5, and 7.4, in dependence on time at 36.5 °C either with or without magnetic field. The hydrogels were withdrawn from the solution buffers, the excess water droplets on the surface were wiped off carefully, and the samples were weighed at each new time-step. This procedure was done until to achieve the swelling equilibrium. The swelling measurements were repeated two times for checking the reproducibility. The relative mass of the hydrogels (m/m_0) was obtained by relating m which is the mass of the swollen hydrogel at certain time with the initial hydrogel mass (m_0). The graphs were obtained by plotting relative mass (m/m_0) against time (t).

2.6. Release of prednisolone from hydrogels under magnetic field

In this work, prednisolone was used as drug model. Prior to gelation, prednisolone was introduced to the hydrogel-forming solution to be loaded during the hydrogel synthesis. The amount of prednisolone corresponded to 10% (w/w) of the reactants used in the feed solutions. The general procedure for synthesizing prednisolone-loaded hydrogels was exactly the same as described in *section 2.4*.

A known weight of prednisolone-loaded hydrogel was immersed in a glass reactor containing 500 mL of either simulated intestinal fluid (pH 7.4) or simulated gastric fluid (pH 1.2). In order to avoid the gradient concentration, the homogenization of these

solutions was achieved by a peristaltic pump (with flow of 60 mL min^{-1}) which is coupled in a flow cuvette (pathlength of 1 cm) as illustrated in Figure 24.
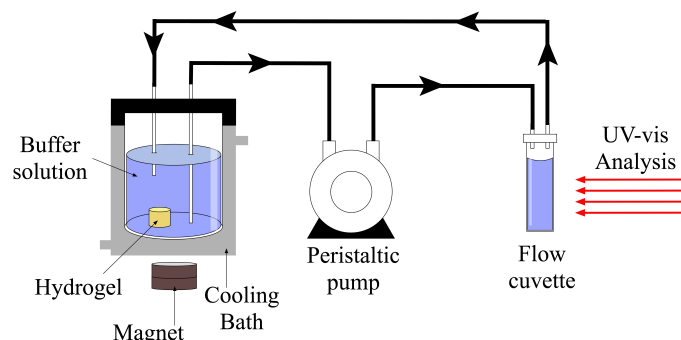
Figure 24. Scheme illustrating the experimental apparatus used for investigating the prednisolone release.

The absorption readings were done at the specified times by means of an UV–vis spectrophotometer (Thermo Scientific Genesys™ 10s). The absorption readings were made at 242 nm or 247 nm which is the wavelength for the maximum absorption of prednisolone at pH 1.2 and pH 7.4, respectively[6, 139].

The concentration of prednisolone released from the hydrogels were determined from analytical curves (see supplementary information) which correlates the absorption to the concentration of prednisolone. The measures of release were performed applying a constant magnetic field of intensity 48MGOe.

3- Characterizations

3.1. Scanning Electron Microscopy (SEM)

The hydrogels were swollen to equilibrium in phosphate buffer solutions (pH 1.2 and 7.4) prior to SEM imaging. They were withdrawn from water and immediately frozen by immersion in liquid nitrogen before being lyophilized for 24 h. Under these conditions, it is supposed that the morphology of the swollen hydrogels is maintained. The samples were fractured and sputter-coated with a thin layer of gold and the SEM images were obtained in a scanning electron microscope (Shimadzu, model SS550 Superscan) by applying an acceleration voltage of 15 kV and a current intensity of 30 μA.

3.2. Fourier Transform Infrared Spectroscopy (FTIR)

The FTIR spectra were recorded in a Bruker spectrometer model Vertex-70V. Powdered samples were prepared into pellets with KBr. The scan range varied from 400 to 4000 cm^{-1}, and 128 scans were run for each spectrum to reach the resolution of 4 cm^{-1}.

3.3. Cytotoxicity Measurement

Normal kidney epithelial cells originated from African green monkey (VERO cells – ATCC CCL81) and epithelial colorectal adenocarcinoma cells obtained from *Homo sapiens* (HT-29) were maintained in DMEM (Dulbecco´s Modified Eagle's Medium), supplemented with fetal bovine serum 10% (FCS) and incubated at 37 °C and 5% CO_2 tension, during 96 h. J774.A1 macrophages were maintained in RPMI 1640 (Roswell Park Memorial Institute medium - Sigma, St Louis, MO, USA), pH 7.6, supplemented with 10% FBS at 37 °C, 5% CO_2 atmosphere. 5.0 x 10^5 macrophages, 2.5x10^5 VERO and HT-29 cells were placed in 96-wells microplate after trypsinization. Cells adhered during 24 h and, next, different concentrations of the compounds were dispensed over the cells and the microplate was incubated at the same conditions described above. Cellular viability was determined after 72 h by using MTT method (3-(4,5-Dimethylthiazol-2-yl)-2,5-Diphenyltetrazolium Bromide - Amresco®). Briefly, MTT solution in PBS was prepared at 2 mg mL^{-1} and 50 μL were placed in each well. Microplates were incubated during 4 h, in the absence of the light and, next, formazan crystals were soluble with DMSO. Purple color generated from mitochondrial enzymatic metabolism of viable cells was measured on spectrophotometer microplate reader, at 570 nm wavelength. In addition, neutral red method was also used to measure cell viability. Briefly, neutral red solution (40 μg mL^{-1}) was added in each well and incubated for 3 h at 37 °C. Next, fixing solution (1% $CaCl_2$ and 2% formaldehyde in PBS) was added for less than 5 min. The dye was solubilized with ethanol/water 50% and glacial acetic acid 1% and the cell viability was measured on spectrophotometer microplate reader, at 540 nm wavelength. CC$_{50}$ index was calculated as the enough concentration to kill 50% of the cells when compared to control (Amphotericin B).

4- Results and Discussion

4.1. FTIR analysis

Figure 25 shows the FTIR spectra of ^{GMA}PEG, and sample A1_3 in the spectral range of 2000 cm^{-1} to 400 cm^{-1}. The spectra of ^{GMA}PEG showed characteristics signals from PEG and glycidyl methacrylate. For example, the bands at 1720 cm^{-1} and 1640 cm^{-1} in the spectra of ^{GMA}PEG were attributed to stretching vibrations of carbonyl groups (νC=O) and vinyl groups (C=C), respectively[103, 104]. These signals correspond to conjugated esters derived from GMA moieties. In addition, bending vibrations corresponding to =C-H could be observed at 840 cm^{-1}. Furthermore, in the same spectrum, the bands at 910 cm^{-1} and 860 cm^{-1}, owing to ν_{as}C-C and νC-O of the epoxy ring from GMA, respectively, were not observed[45]. Indicating that PEG reacted with GMA by an epoxide ring-opening mechanism.
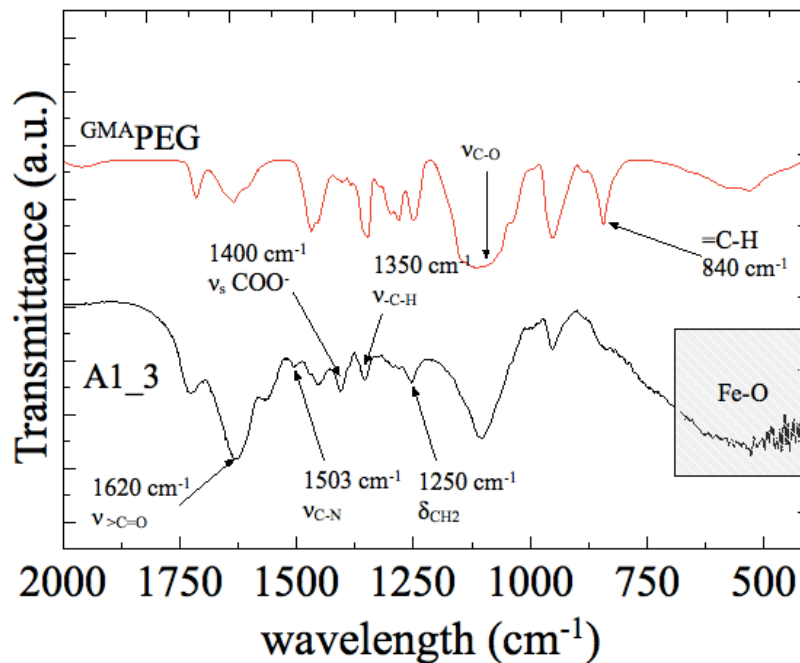
Figure 25. FTIR spectra of ^{GMA}PEG and hydrogel A1_3 in the spectral range of 2000 cm^{-1} to 400 cm^{-1}.

The signal at 1620 cm^{-1}, in the A1_3 spectra, corresponds to >C=O asymmetric stretching vibration of carbonyl groups from both DMAAm and acrylate group[140, 141]. Moreover, the signal corresponding to ν_sCOO$^-$ owing to acrylate group was observed at 1400 cm^{-1} [142].

In the same spectra, the high intensity band near 570 cm^{-1} was ascribed to Fe-O stretching vibration[143]; the peaks at 1503 cm^{-1} and 1250 cm^{-1} were attributed ν_{C-N} and δ_{CH2}, respectively.

4.2. Hydrogel morphology

Figure 26 shows SEM micrographs of fractured A2_3 hydrogels swollen at pH 1.2 and pH 7.4 with and without magnetic field (MF). This experiment was performed to investigate the influence of the MF in the porous morphology during swelling experiments, where the response of sample A2_3 (containing the highest concentration of Fe$_3$O$_4$) was evaluated. The porous morphology plays an important role during drug diffusion because these structures allow the drug to diffuse into, through, and from the 3D polymer network. For this reason, the hydrogels have been considered an attractive as polymer carriers. Comparing samples swollen under MF and without MF, at the same pH, any remarkable difference in the final porous morphology was observed. This result indicates that the iron oxide particle does not play any role on the porous morphology.
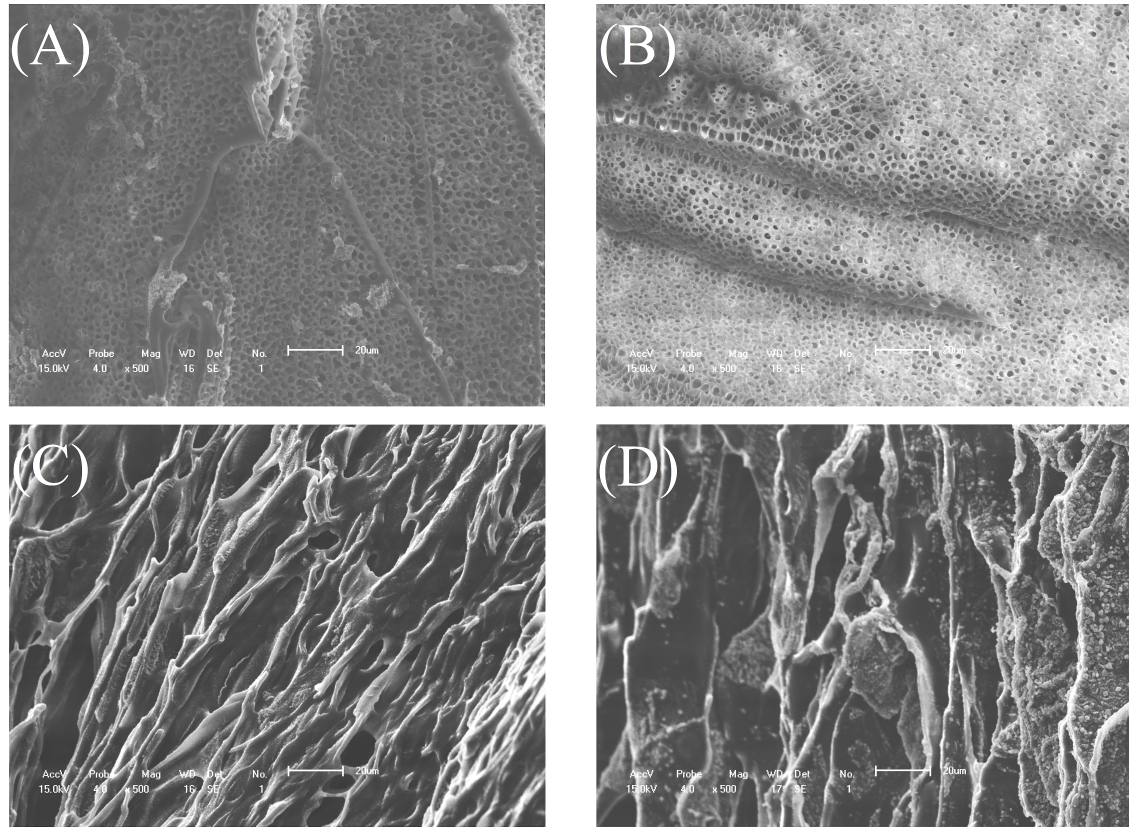
Figure 26. SEM images of fractured frozen A2_3 hydrogels after reaching the swelling equilibrium: (A) pH 1.2 with magnetic field, (B) pH 1.2 without magnetic field, (C) pH 7.4 with magnetic field, and (D) pH 7.4 without magnetic field. Scale bars of images are 20 μm.

In addition, it is important to highlight that at pH 7.4 porous size changed significantly when compared to those observed in acidic pH. This result can be considered as an indicative that the PEG-based hydrogels are pH-responsive. Furthermore, is expected that in acid pH the porous with low size may hinder the drug diffusion.

4.3. Swelling measurements

Swelling measurements were performed to investigate the influence of both the magnetic field and the pH in the water transport profiles through the hydrogels matrix; the results are shown in Figure 27.
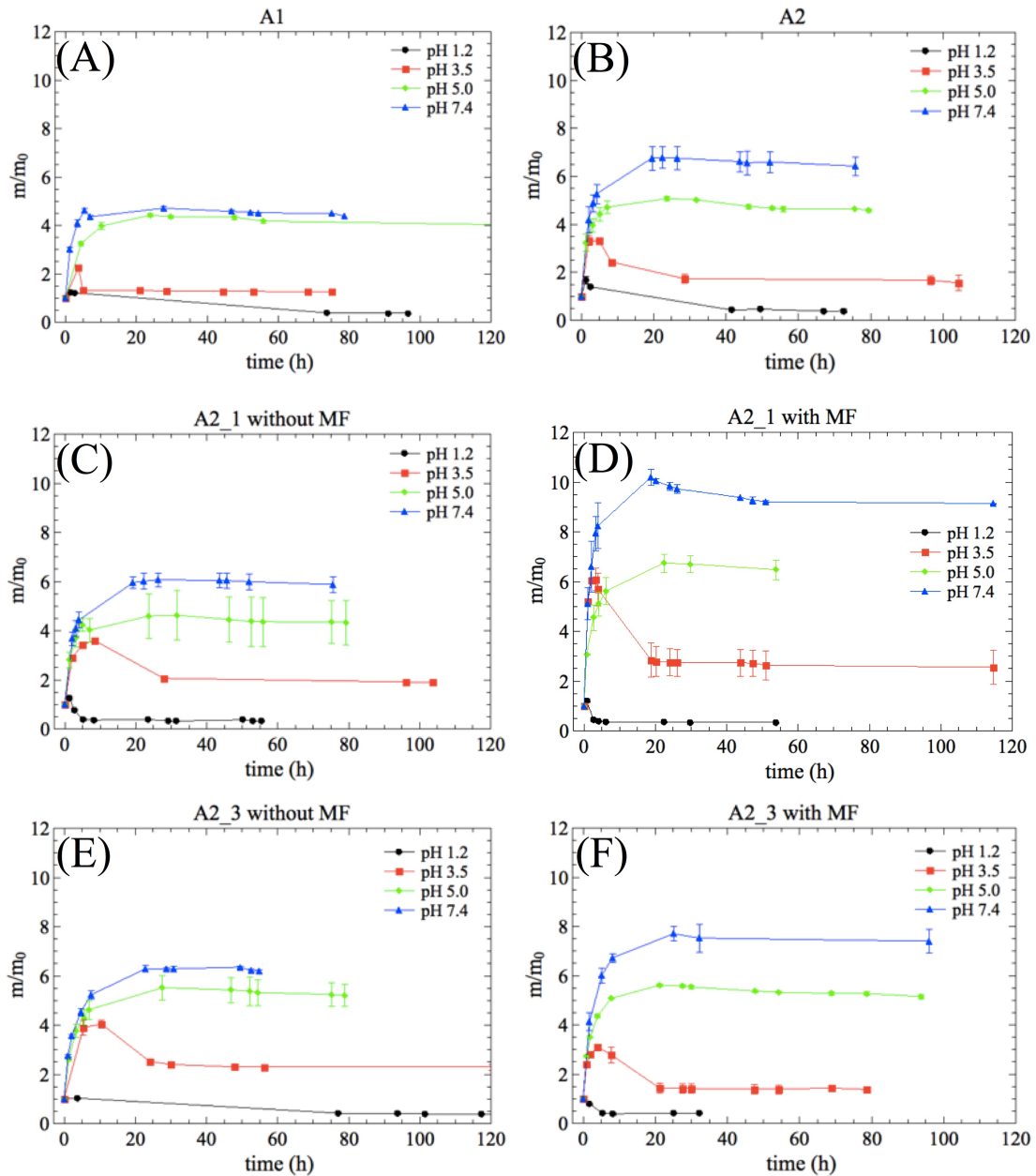
Figure 27. Time-dependent swelling curves at the indicated pH at temperature of 36.5°C: (A) A1 without MF, (B) A2 without MF, (C) A2_1 without MF, (D) A2_1 with MF, (E) A2_3 without MF, and (F) A2_3 with MF.

All samples shown a pH-dependent swelling profile. The water absorption was higher when the pH was increased. Moreover, it is important to highlight when the swelling was performed below pH 5.0 all the samples exhibited a decreasing in their m/m_0 ratio after absorbing some amount of solvent. This behavior may be associated with two main factors: *i)* erosion of the hydrogel network and/or *ii)* increase of cross-linking density by hydrogen bonds from carboxylic groups. The erosion is a result of either the

burst of vesicular structure (due to high osmotic pressure during the swelling) or the degradation of polymer networks. Moreover, in a work published earlier, we have demonstrated that ester groups from ^{GMA}PEG structure may be cleaved, specially, in acid media contributing to the erosion mechanism[21]. However, in this work, the crumbling of hydrogels as well as the degradation of polymer networks could not be visualized (see SEM images) indicating that the *ii*) has the widest effect in reducing the *m/m$_0$* ratio.

The presence of polyacrylic acid in hydrogel-network structure plays a predominant role on swelling profile. The pK$_a$ of polyacrylic acid is 4.5 [144]. When the pH < pK$_a$ the -COOH groups are predominantly undissociated favoring the interaction, by hydrogen bonds, between the polymer chains (hydrophilicity reduction). As a consequence, the water inside hydrogel is ejected decreasing the *m/m$_0$* ratio. On the other hand, when the pH > pK$_a$ the carboxylic groups are predominantly dissociated, generating electrostatic repulsion forces among the polymer chains. As a result, the hydrogel affinity for water increases. These observations are in accordance to those observed in SEM images.

The influence of the magnetic particles as well as the magnetic field on swelling behavior for samples containing iron oxide was also investigated. In absence of magnetic field, the swelling profile for all samples were kept almost unchanged (Figure 27C and 27E). In fact, only a little decrease in swelling equilibrium at pH 7.4 for samples A2_1 and A2_3 was observed. This is usually due to the influence of nanoparticles which act as physical barriers to hindering the diffusion of the water molecules (tortuosity effect)[145]. Under MF, only samples containing the highest concentration of acrylate groups (A2_1, and A2_3) shown a magnetic-responsive swelling profile. At pH > pK$_a$, the swelling ratio for both samples A2_1 and A2_3 (Figure 27D and Figure 27F) were higher than sample A2 (Figure 27B). This suggests a synergistic effect between the acrylate groups and iron oxide particles when exposed under MF. However, the magnetic field did not affect the swelling behavior for samples A1_1 and A1_3 (see supplementary information).

4.4. Cytotoxicity measurements

The cytotoxicity study was performed in order to evaluate the pharmaceutical potential of the hydrogels. The CC_{50} was defined as the dose required to inhibit the cell growth by 50%, considering a cut-off of 1000 µg mL^{-1}.

None of the hydrogels significantly inhibited the cell growth, indicating that CC_{50} should be higher than the concentration studied (1000 µg mL^{-1}). To give more precise information on how much the hydrogels inhibited at 1000 µg mL^{-1}, the results were expressed in terms of % growth inhibition (GI) (Figure 28). It may be observed that the values of GI were much lower than 50%, indicating nontoxicity and acceptable biocompatibility.
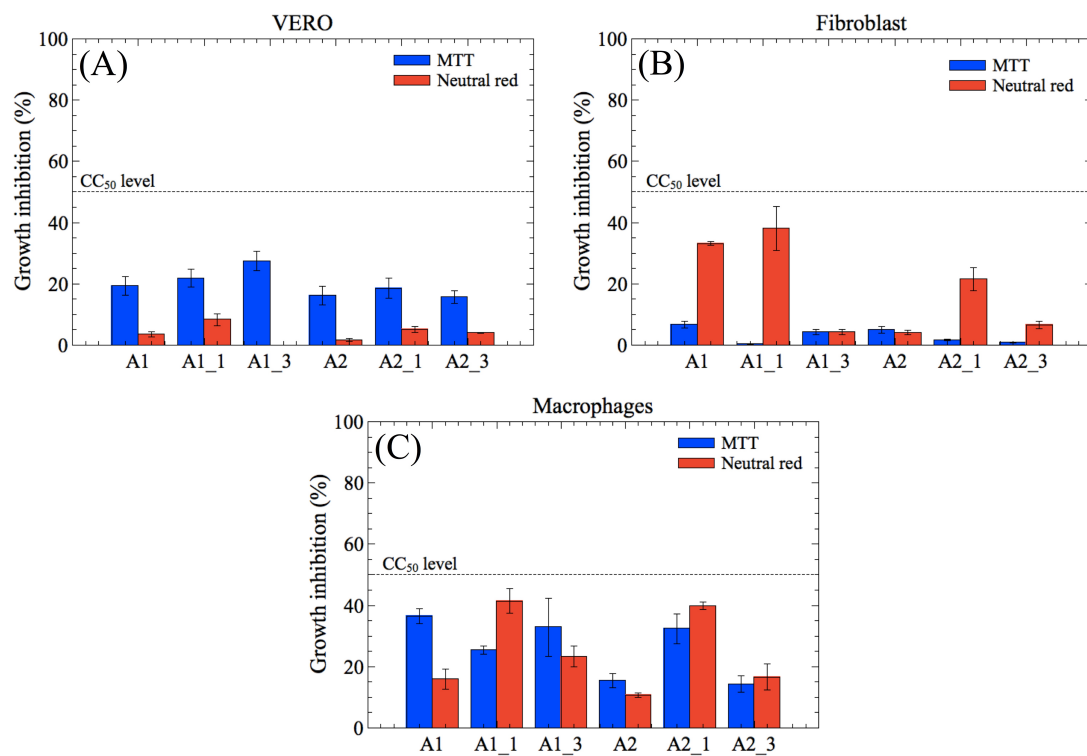
Figure 28. *In vitro* cytotoxicity results of PEG-based hydrogels nanocomposites. Data presented are the mean ± SD (*n=3*).

As a general trend, sample A2 and its derivative (A2 containing iron oxide) showed reduced GI values if compared with A1 samples. In addition, for VERO cells and, specially, for Fibroblasts, the GI shown the lowest values. Since the fibroblast (HT-29) cell line is used as an *in-vitro* model to study absorption, transport, and secretion by intestinal cells, these results demonstrate that the proposed hydrogels has a potential to be applied as drug carrier focusing drug release in the GI tract.

4.5. Drug release

Figure 29 shows the time-dependent fractional release curves of prednisolone from the hydrogels nanocomposites. In this study, samples A2 and A2_1 were chosen according to the previous results obtained from the cytotoxicity assays and the swelling measurements. For example, if compared with A1 and its derivatives, both A2 and A2_1 have low cytotoxicity. Moreover, the A2_1 shown an interesting magnetic-responsive swelling profile. Thus, for prednisolone release, the hydrogel without magnetic particle was used as reference while for the hydrogel nanocomposite the release experiments were analyzed in under magnetic field.

In this work, t_{50} and t_{90} was defined as the time where 50% and 90% of prednisolone was released. Although the swelling behavior for sample A2 at pH 1.2 is outwardly different than that one at pH 7.4, the release of prednisolone was not significantly affected by pH changing (Figure 29A and 29B). Since t_{50} and t_{90} was almost the same, we can assume that the ratio of prednisolone release has remained constant. On the other hand, A2_1 hydrogels showed prominent changes in prednisolone release in response to applied magnetic field (Figure 29C and 29D). The t_{90} increased from 19 h to 75 h and 18 h to 34 h at pH 1.2 and 7.4, respectively. This means that the MF could be used as trigger for sustained and controlled release of prednisolone.
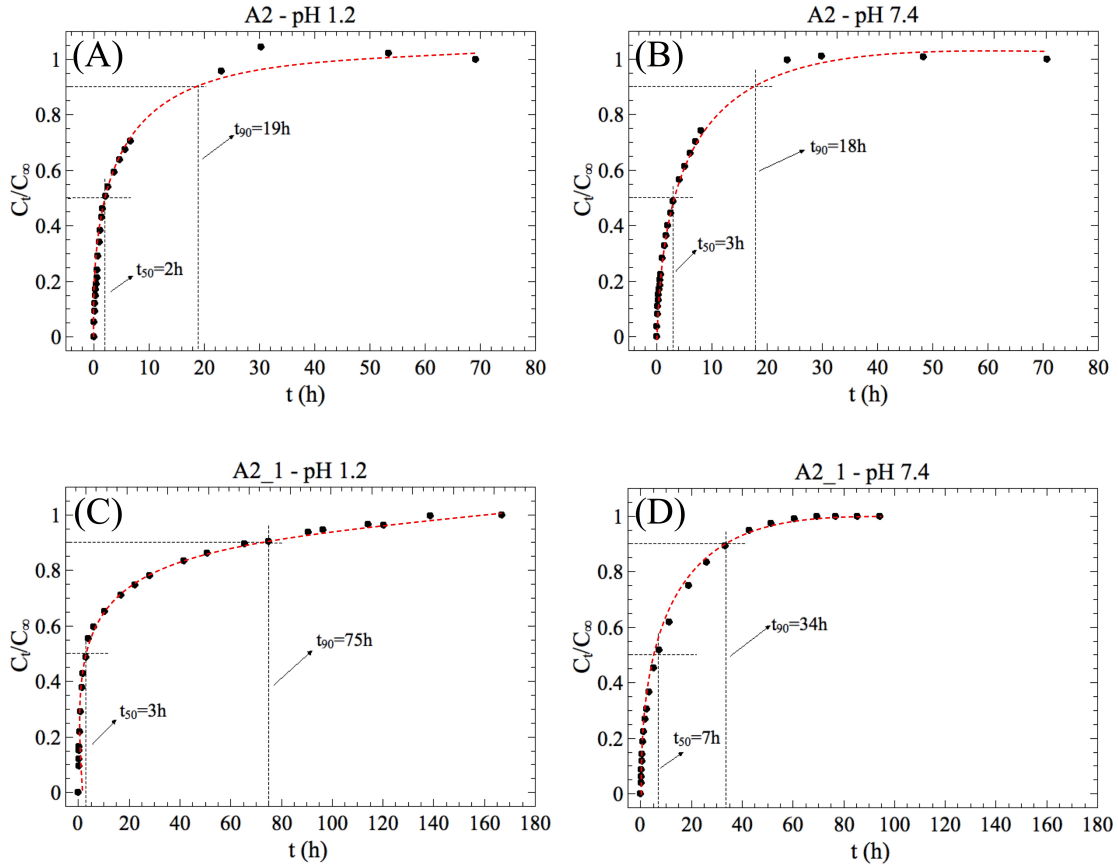
Figure 29. Time-dependent release curves of prednisolone from A2 (reference), and A2_1 hydrogels nanocomposites in different pH at a temperature of 37 °C. For sample A2_1, the experiments were carried out using an applied magnetic field of 48MGOe.

The experimental data were also adjusted by applying the more general version of the power law equation, described in Eq. (6). This is the most comprehensive mathematical model used to determine the release performance of drug from a polymer matrix[146, 147]:

$$\frac{C_t}{C_\infty} = kt^n \tag{6}$$

where C_t and C_∞ are the cumulative concentrations of solute released from the hydrogel at a specified time and at equilibrium, respectively, k is a constant and n is a parameter used to interpret the release mechanism. Furthermore, the conceptual meanings of n is dependent of the sample shape (i.e. cylinder, thin film, and sphere) as summarized in Table 6.

Table 6. Values of diffusional expoent (n) for the hydrogel matrix with different shapes[148].

Diffusional exponent (n)			Transport mechanism
Thin film	Cylinder	Sphere	
0.50	0.45	0.43	Fickian diffusion
$0.50 < n < 1.00$	$0.45 < n < 0.89$	$0.43 < n < 0.85$	Anomalous transport
1.00	0.89	0.85	Macromolecular relaxation

The values of n and k were obtained from slopes of the logarithmical curves of C_t/C_∞ as a function of time for the hydrogels A2 and A2_1 (Table 7). In addition, it is important to mention that the Eq. (6) is restricted to the first 60% of the released drug (linear part). The hydrogels used during drug release experiments had cylindrical shapes.

Independently of the pH changing, both samples A2 and A2_1 exhibited a n values between 0.49 to 0.73 indicating that the release is controlled by anomalous transport mechanism. However, after addition of magnetic particles, in the hydrogel matrix, the anomalous mechanism trended to the Fickian diffusion. As explained in *section 4.3* this variation in n may be attributed to the tortuosity effect which become more evident under MF.

Table 7. Fitting parameters (*n* and *k*) of Eq. (1) to experimental release data of prednisolone from the hydrogels A2 and A2_1 at pH 1.2 and 7.4 with an applied magnetic field.

Sample name		n	k ($h^{-1/2}$)
A2[*]	pH 1.2	0.73 ± 0.01	0.332 ± 0.003
	pH 7.4	0.66 ± 0.02	0.253 ± 0.005
A2_1[**]	pH 1.2	0.49 ± 0.02	0.303 ± 0.005
	pH 7.4	0.58 ± 0.02	0.185 ± 0.002

* without MF; ** under MF

The parameter k is a constant characteristic of the hydrogel and may be correlated with the diffusion coefficient (D)[149]. Moreover, the k results could be correlated with only t_{50} since the Eq. (6) is restricted to the first 60% of the release profile. Comparing sample A2 with A2_1, at pH 1.2, the k remained almost unchanged explaining the fact that the observed t_{50} values for both samples were approximately the same. On the other hand, the magnetic field has played an important role in reducing the k value specially at pH 7.4. For example, when the pH was changed from 1.2 to 7.4 the sample A2_1 had its k value reduced from 0.303 ± 0.005 to 0.185 ± 0.002. A decrease in the parameter k (which is proportional to a decrease in D) must implicate an increase in the time for releasing 50% of the drug which, in fact, was observed when the t_{50} increased from 3h to 7h (Figure 29C and 29D). This result indicates that the magnetic particle, dispersed in the hydrogel matrix, could control the prednisolone release by changing the releasing mechanism as well as its diffusion coefficient.

5- Conclusions

The hydrogel nanocomposite was prepared using vinylated PEG together with DMAAm, acrylic acid, and iron oxide nanoparticles via an ultrasound-assisted radical cross-linking/polymerization reaction. The swelling measurements and the SEM images showed that the HGs have a pH- and magnetic-responsive properties. Furthermore, in the hydrogel without magnetic particles, the prednisolone release was driven by an anomalous transport, which is defined as the sum of the contributions from macromolecular relaxation and Fickian diffusion. For hydrogels containing iron oxide, the release tended towards the Fickian transport, minimizing the influence of the macromolecular relaxation. The *in vitro* cytotoxicity results indicated that the obtained hydrogels have a great pharmacological potential for use this hydrogel as drug carriers in biological environments.

Supplementary data
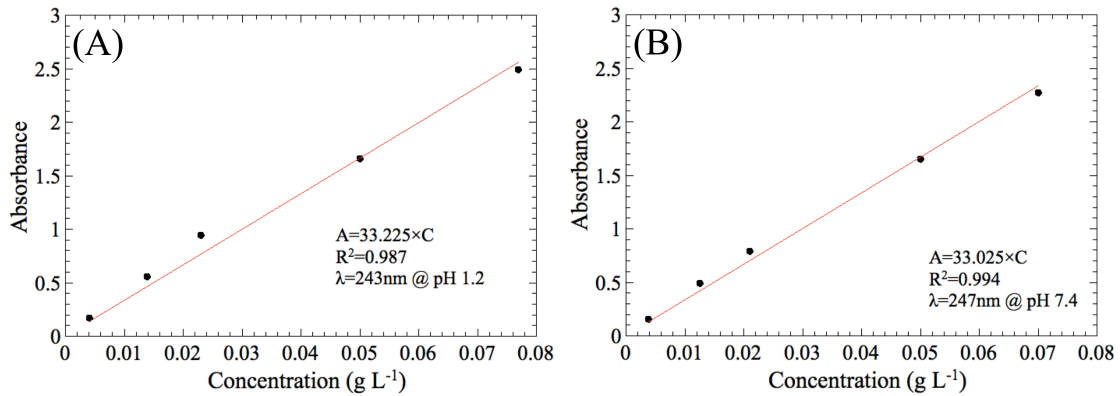
Figure S1. Analytical calibration curve of prednisolone in different buffer solutions: (A) pH 1.2, and (B) pH 7.4.
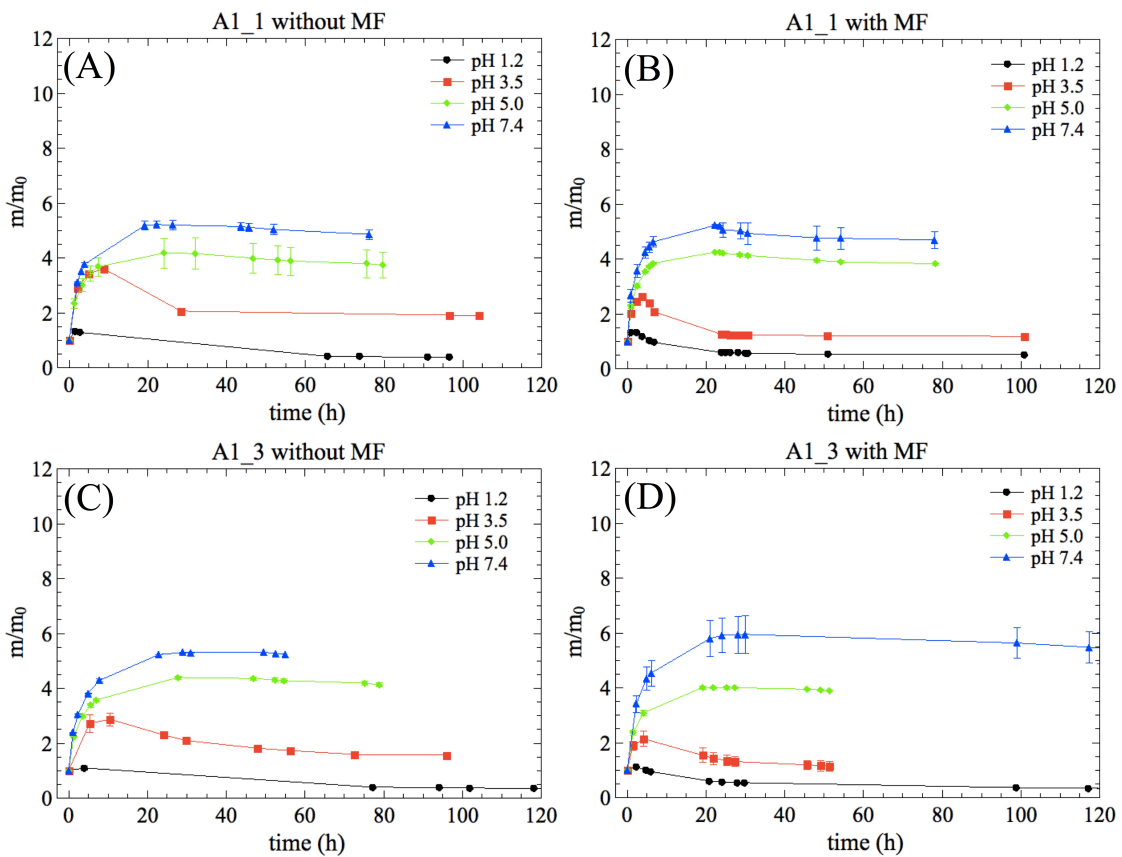
Figure S2. Time-dependent swelling curves at the indicated pH at temperature of 36.5°C: (A) A1_1 without MF, (B) A1_1 with MF, (C) A1_3 without MF, (D) A1_3 with MF. Note: Observe that the swelling behavior was not affected by the MF.
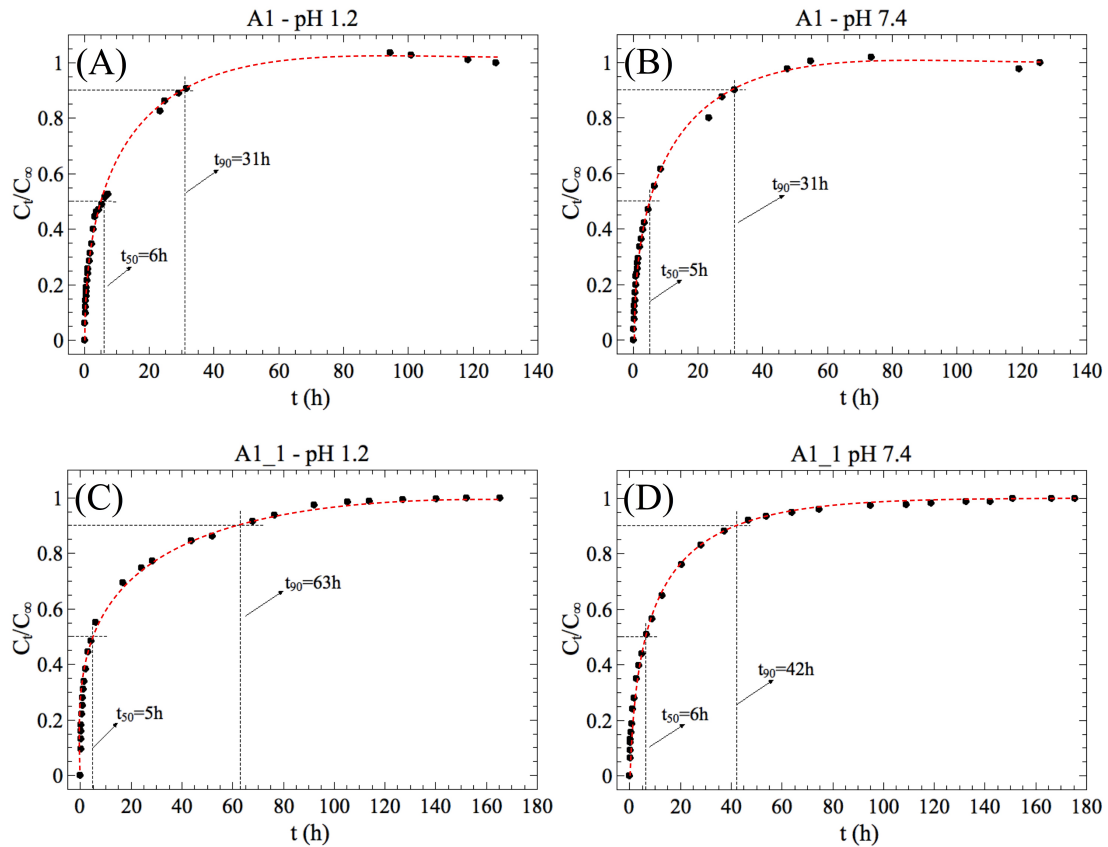
Figure S3.Time-dependent release curves of prednisolone from A1, and A1_1 hydrogels nanocomposites in different pH at a temperature of 37 °C. For sample A1_1, the experiments were carried out using an applied magnetic field of 48MGOe.

Table S1. Fitting parameters (n and k) of Eq. (1) to experimental release data of prednisolone from the hydrogels A1 and A1_1 at pH 1.2 and 7.4 with an applied magnetic field.

Sample name		n	k ($h^{-1/2}$)
A1	pH 1.2	0.52 ± 0.01	0.244 ± 0.002
	pH 7.4	0.58 ± 0.02	0.221 ± 0.004
A1_1	pH 1.2	0.42 ± 0.01	0.286 ± 0.003
	pH 7.4	0.46 ± 0.01	0.219 ± 0.002

PARTE II – *SÍNTESE E CARACTERIZAÇÃO DE PARTÍCULAS HÍBRIDAS MAGNÉTICAS EM TAMANHO SUBMICROMÉTRICO PARA APLICAÇÃO EM BIOSSENSORES*

RESUMO - PARTE II

Partículas magnéticas são de grande interesse na área biomédica. Por exemplo, partículas coloidais têm sido utilizadas para purificação e extração de ácidos nucléicos, para captura de amostras biológicas, absorção/dessorção de proteínas e detecção de antígenos específicos. Nesse contexto, a síntese de materiais híbridos do tipo "*core-shell*" torna-se muito importante na área biomédica. Para a aplicação em biossensores, a função do shell (casca) é proteger a parte magnética (core), reduzir a toxicidade além de conferir ao material obtido funcionalidade específica afim de imobilizar biomoléculas. As propriedades de partículas com tamanho nano/submicron são dependentes do tamanho e forma. Por este motivo, é muito importante desenvolver um processo que controle a morfologia final do material obtido.

Além da morfologia "*core-shell*", partículas Janus (que possuem formas anisotrópicas) oferecem grandes possibilidades em termos de estrutura e propriedades. O exemplo mais simples de partículas Janus é encontrado em materiais com dois hemisférios distintos (uma parte hidrofóbica e a outra hidrofílica, por exemplo). Materiais com esta morfologia possuem grande importância na área biomédica, especialmente em biossensores.

A combinação de propriedades magnéticas com as elétricas é de extrema importância, principalmente, quando um processo simultâneo de captura e detecção de um analito são desejadas. Neste sentido, a aplicação de partículas magnéticas combinadas com polímeros condutores vêm sendo investigados. Diferentes técnicas têm sido descritas para preparar látex de nanopartículas magnéticas. Estas, são baseadas nos métodos clássicos de polimerização (emulsão, miniemulsão, dispersão e etc.).

Assim sendo, no capítulo I da parte II desta tese, investigou-se inicialmente as melhores condições experimentais para a obtenção de um latéx magnético com morfologia específica. A técnica polimerização em emulsão com nucleação semeada foi escolhida por produzir materiais com alto teor de óxido de ferro. A polimerização foi realizada utilizando o estireno (St) como monômero e o divinilbenzeno (DVB) como agente reticulante. Como semente, utilizou-se uma emulsão magnética preparada previamente pelo grupo de pesquisa do *Laboratoire d'Automatique et de Génie des Procédés* (LAGEP) em Lyon na França. Neste capítulo, foram investigados a influência

da composição da mistura de St e DVB no tamanho de partícula, morfologia e propriedades magnéticas das amostras obtidas. E os resultados obtidos foram publicados na "*Polymers for Advanced Technologies*, **2015**, *26, 1102-1108.*

A partir dos resultados obtidos no capítulo I (descritos acima) estabeleceu-se uma rota de síntese para a obtenção nanopartículas híbridas com propriedades elétricas e magnéticas. Objetivando a aplicação em biossensores, verificou-se que a emulsão magnética sintetizada no laboratório era polidispersa se comparada com uma amostra comercial. Além disso, observou-se que para obter-se amostras do tipo *core-shell* com grupos funcionais específicos era necessário, em alguns casos, utilizar *co*-monômeros de modo a regular as interações do tipo hidrofílicas e hidrofóbicas presente nas gotas da fase óleo durante uma polimerização em emulsão semeada.

Utilizando as informações obtidas a partir dos primeiros ensaios com St e DVB, no capítulo II da parte II desta tese, sintetizou-se as desejadas nanopartículas híbridas do tipo *core-shell* com propriedades elétricas e magnéticas. Para conferir propriedades elétricas e grupos carboxílicos à partícula magnética, utilizou-se os monômeros pirrol e ácido pirrol-2-carboxílico. Os resultados desse trabalho foram publicados *Materials Science and Engineering C,* **2016**, 61, 688-694. Além disso, essas partículas foram aplicadas com sucesso na detecção de sulfapiridina (dados não apresentados nesta tese), no qual, o manuscrito encontra-se em fase de submissão. A parte II desta tese foi desenvolvida durante o doutorado sanduíche no exterior (09/2014 à 08/2015) sob orientação dos pesquisadores Dr. Abdelhamid Elaissari e Dr. Hatem Fessi no *Laboratoire d'Automatique et de Génie des Procédés* – LAGEP."

REVISÃO BIBLIOGRÁFICA

Magnetic particles: From preparation to lab-on-a-chip, biosensors, microsystems and microfluidics applications

1. Introduction

In the last decade, a great attention has been paid to the unique feature of magnetic nanoparticles (super-paramagnetism), which makes them easily guided by an external magnetic field. This unique property has been exploited in fast separation and particularly for *in vitro* biomedical diagnostic domain[150]. Therefore, the development of reactive magnetic nanoparticles for immobilization and fast magnetic separation of biomolecules (e.g. antibodies, proteins, enzymes, etc.) is of great importance nowadays, especially, for fast diagnostic applications providing early detection of diseases. This in turn helps us to get optimal results in therapy and consequently management and treatment of diseases at early stages of infection. Moreover, magnetic colloidal particles have also been tried in various *in vivo* diagnostic and therapeutic applications such as in Magnetic Resonance Imaging (MRI)[151] as contrast agents, drug delivery, and hyperthermia.

Among magnetic nanoparticles, iron oxides and in particular magnetite (Fe_3O_4) and its oxidized form maghemite (γ-Fe_2O_3) have attracted much attention due to their biocompatibility, low toxicity, and ease of preparation at low cost[152]. More interestingly, the specific optical (fluorescent) or magnetic feature of magnetic nanoparticles are sometimes exploited and integrated in microsystems in order to elaborate medical devices. This provides fast analysis with high sensitivity for low volume analyte, similar to that existing in large-scale analysis equipment. Such systems are called micro-Total Analysis Systems (μ-TAS)[153] in which all steps are concentrated in one device (e.g. lab-on-a-chip systems (LOC), biosensors, microfluidic systems, etc). These devices and systems (with highly automated operations) are characterized by their small size and robust mechanics. Hence, are important for routine applications and can also be developed as easy-to-use portable devices. In addition, they are not only cost effective but also have low running costs. These are the features that are very much required in biomedical diagnosis, clinical analysis, and nanomedicine. Hence, attracting significant attention from various research groups.

However, in order to be conveniently used in bio-related applications, the control of surface chemistry of superparamagnetic iron oxide nanoparticles (SIONPs) is required. Generally, the pristine SIONPs tend to aggregate into large clusters due to their large surface area-to-volume ratio and dipole-dipole interaction. As a result, this leads to reduction in their intrinsic superparamagnetic properties. Therefore, surface modification of SIONPs is of a paramount importance not only to prevent aggregation of SIONPs, leading to colloidal stability, but also to enhance their water solubility, bio- compatibility, bioconjugation, and nonspecific adsorption to cells. Surface modification, therefore, provides them an edge over the other separation techniques (e.g. filtration, centrifugation and sedimentation) that are laborious as well as time consuming. For instance, the coupling of biomolecules (e.g. proteins, enzymes, antibodies, antigens, etc.) to magnetic nanoparticles has been used to achieve simple, fast, inexpensive and highly efficient separation of targeted biomolecules under the effect of an external magnetic field.

Magnetic colloidal particles are commonly used as solid supports (carriers) for the immobilization of biomolecules such as oligonucleotides, peptides, ligands, proteins or antibodies in order to prevent nonspecific adsorption to cell and so enhance the specific capture of the targeted biomolecules (e.g. bacteria, viruses, etc.). Furthermore, the ideal magnetic nanoparticles should have high magnetic properties, sufficient small size with narrow distribution, high surface functionality and well defined morphology[154]. These characteristics can be achieved by optimizing the synthesis process of SIONPs in order to prepare structured magnetic nanoparticles bearing a reactive shell with well-defined properties[155]. In this regard, several approaches for preparation and modification of SIONPs have been investigated using various materials starting from low molecular weight compounds (e.g. ligands, surfactants, etc) to the use of high molecular weight compounds (e.g. synthetic polymers, synthetic and natural biopolymers like proteins, polysaccharides, polyethylene oxide, dextran, etc.)[156]. The coating or encapsulation of SIONPs with polymers has several advantages in that, they enhance biocompatibility, colloidal stability in aqueous and physiological media, and provide mechanical and chemical stability for SIONPs. More interestingly, they impart functionality to SIONPs to form conjugates with various biomolecules (e.g. enzymes, proteins, antibody, antigen, DNA, RNA, etc), which is highly needed for biomedical applications[157]. Recently, there is a great research attempts to use SIONPs in theranostic applications (diagnostic and therapeutic purposes at the same time)[158].

2. Magnetic nanoparticles: from preparation to encapsulation

2.1. Magnetic particles preparation

Main approaches for the preparation of SIONPs include thermal decomposition of iron precursors in organic (or water) media and co-precipitation of iron salts from their aqueous solutions. The latter is attracting much interest due to high yield as well as effectiveness in controlling nanoparticle size and water-in-oil (w/o) microemulsion. Chemical co-precipitation method depends on the type of iron salt as well as pH and ionic strength of precipitating solution. This can be done by either partial oxidation of ferrous hydroxide by different oxidizing agents or by the addition of alkali to an aqueous solution containing mixture of ferrous (Fe^{2+}) and ferric (Fe^{3+}) ions. Iron oxide particles obtained by this way are often not stable and hence are stabilized by using low molecular weight polymers, surfactants or functionalized polymers. In addition, magnetic nanoparticles are coated with carboxylate surfactants e.g. oleic acid ($C_{18}H_{34}O_2$) during co-precipitation reaction followed by dispersion in organic medium e.g. octane. The obtained magnetic ferrofluids can be used as a template for further encapsulation with various types of polymers.

Surface modification of hydrophilic inorganic nanoparticles has been performed via two main processes namely, physical encapsulation and chemical encapsulation. Physical encapsulation of SIONPs includes direct modification of magnetic nanoparticles with surfactant adsorption, or via layer-by-layer (LBL) electrostatic adsorption or self-assembly of preformed polymers. LBL assembly method involves controlled synthesis of novel nanocomposites core-shell materials and hollow capsules. By using this strategy, magnetic colloidal particles have been coated with alternating layers of polyelectrolyte, nanoparticles, and proteins that can be utilized for various biomedical applications.

Chemical encapsulation of SIONPs includes surface functionalization or modification of magnetic nanoparticles via specific grafting, surface initiated controlled polymerization, inorganic silica/polymer hybridization, or by heterogeneous polymerization in dispersion media. Inorganic silica/polymer hybridization involves the encapsulation of SIONPs by a cross-linked silica shell through hydrolysis/condensation reactions with the hydroxyl groups on the surface of iron oxide nanoparticles. Heterogeneous polymerization is used to prepare well-defined SIONPs-embedded magnetic spheres as well as cross-linked microgels and nanogels. For *in vitro* diagnostic

applications, the seeded emulsion polymerization technique has been extensively used[159].

3. Magnetic particles as a solid support and as a carrier

Although, polymer and hybrid particles have been used for numerous biomedical applications but magnetic colloidal particles[160] have advantage over them because they can be used as solid supports for biomolecules in order to enhance the specific capture of the targeted biomolecules (e.g. bacteria, viruses, etc.), specific RNA recognition[161], separation of DNA from probiotic dairy products[162], and as potential solid support for recyclable biocatalysts[151].

3.1. Magnetic carrier for sample preparation and generic capture

Magnetic latexes are combination of colloidal polymer particles and magnetic materials i.e., iron oxide nanoparticles. The iron oxide in the polymer particles imparts the magnetic properties to composite latexes. Magnetic latexes are widely utilized in biomedical field as a solid support, in molecular biology, immunoassays, cell sorting, and isolation of both viruses and bacteria[163]. The magnetic property enables the separation through the use of single magnetic and particle guidance in microsystems. Additionally, the magnetic property also enhances the sensitivity of biomedical diagnostic by enhancing the concentration of biomedical samples. Due to the possible elaboration of well-defined magnetic latexes, several biological tests are automated leading to quick and high sensitivity of biomolecules analysis.

3.2. Magnetic particles for detection

Basically, magnetic colloidal particles are mainly used as solid supports for biomolecules in order to enhance the specific capture of the targeted biomolecules. For instance, the individual magnetic nanoparticles were examined in specific capture and isolation of bacteria[163]. In this context, iron oxide nanoparticles were first chemically modified with a specific reactive shell by introducing commonly used functionalized compounds such as carboxylic acid, amines or thiols[164]. Then, the selected antibody (e.g. anti-bacteria) was chemically grafted onto the magnetic nanoparticles. These sensitive nanoparticles were then mixed with bacteria containing sample under given buffer conditions (i.e. pH, salinity). The recognized bacteria were then easily extracted using a permanent magnetic field, whereas, the individual magnetic nanoparticles were

less sensitive to the applied field, and consequently remained in the supernatant. The extracted bacteria obtained thus can be used for extracting nucleic acid after the bacteria-growing step[165].

Recently, Salmonella in milk were captured by antibody-conjugated magnetic nanoparticles (MNPs) and separated from analyte samples by applying an external magnetic field[166]. The MNP–Salmonella complexes were re-dispersed in a buffer solution followed by their exposure to antibody-immobilized TiO_2 nanocrystals (TNs), which absorb UV light. The assay exhibited high sensitivity toward low concentrations of Salmonella bacteria as shown in Figure 30. The detection limit of Salmonella in milk was found to be more than 100 cfu mL^{-1}.
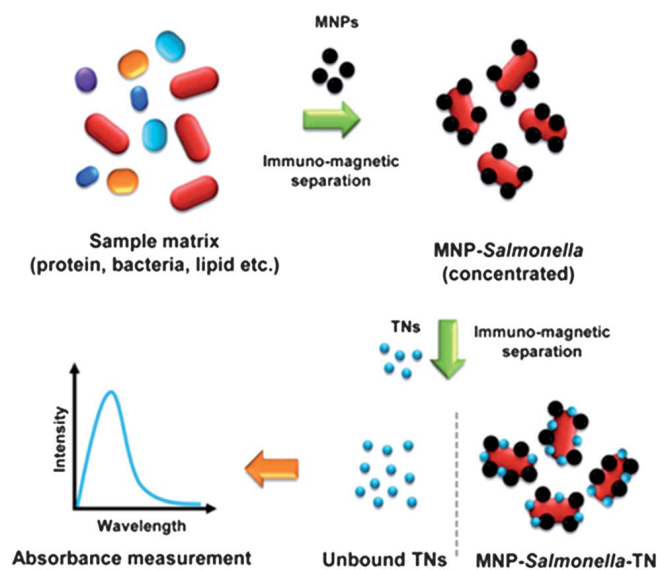
Figure 30. Schematic illustration for detection of the pathogenic bacteria in milk using magnetic nanoparticles and optical nanoprobes[166].

4. Magnetic particles in Microsystems

4.1. Magnetic particles in microfluidics

Regarding biology of human body, the molecular processes play an important role in biomedical diagnosis[167] that can be performed in specific laboratories with the help of different biological tests. These tests require multi-step and complex processes, including sample collection, preparation, and specific identification of biomolecules necessitating both labor and time[168]. However, more and more biological tests can be performed at the point of care[169] i.e. close to the patient allowing smooth testing in the

area of medicament. In this regard, a new method was developed, dealing with miniaturization and combination of molecular-level biological tests into high-performance and ultrafine systems called Lab- on-a chip[170]. To facilitate the biological tests, magnetic hybrid particles were integrated in these systems in order to facilitate capturing, transportation, labeling and detection of biological molecules from physiological samples[171-173]. In lab-on-chip systems, magnetic separation occurs by binding specific biomolecule to a magnetic particle and then separating it from surrounding matrix by use of magnetic field for manipulating of biological cells or molecules. Magnetic particles, called superparamagnetic particles, are often used for such separations. These particles retain no residual magnetism after the field is removed.

Bioseparation in microfluidic channel occurs with help of these magnetic particles. In bioseparation, first specific antibody is immobilized onto magnetic particles in microfluidic system. The anti-body magnetic particles are then incubated with solution consisting of cells, proteins etc. By collecting the magnetic particles, biomolecules then can be collected in a magnetic field. Magnetic particle-based bioseparation in microfluidic channel is shown in Figure 31.
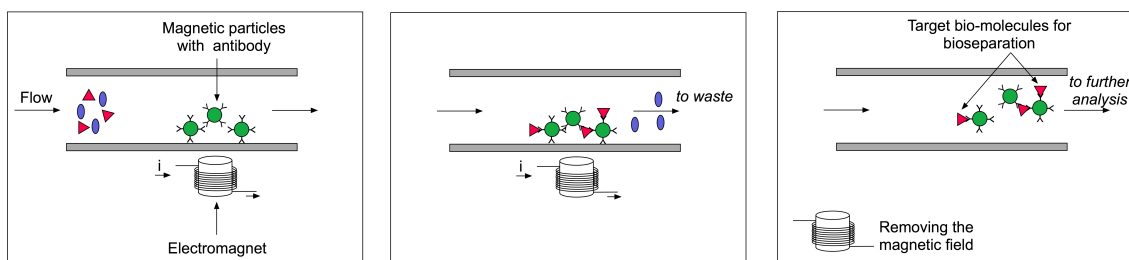
Figure 31. Magnetic particle-based bioseparation in microfluidic channel.

Microfluidic technology has been rapidly developed in recent years and found various interesting applications in pharmaceutical industry, life science and chemical researches. Based on microelectromechanical technology, microfluidic technology integrates and miniaturizes the separating reaction and mixing devices in general laboratories onto a very tiny chip. This microfluidic chip is also called lab-on-a-chip[174].

The use of microfluidic devices with magnetic particles manipulation efficiently implements bioanalytical steps in miniaturized systems[175-177]. In addition, magnetic particles in microfluidic devices provides new possibilities of manipulating molecules in small volume[178]. This can be used as solid support for mRNA isolation[153],

immunoassay[179], DNA hybridization[180], protein analysis[181] and retaining of magnetic labeled cells[182].

Polymer or silica nanoparticles with embedded iron oxide nanoparticles are most commonly used as magnetic objects inside the microfluidic devices[183]. Different forms of biological applications can be recognized by using magnetic particles in microfluidic systems. These applications include sample purification, solid substrate to sample, sample manipulation, labeling, transport, separation and protein-interaction which have been found in recent years[182, 184, 185]. Nano and microparticles present large specific surface for chemical binding when applied in microfluidic channel.

Another type of microfluidic device which consists on micro channels, micro valves and micro pillars was produced for specific capture and sorting of cancer cells as shown in Figure 32[186].
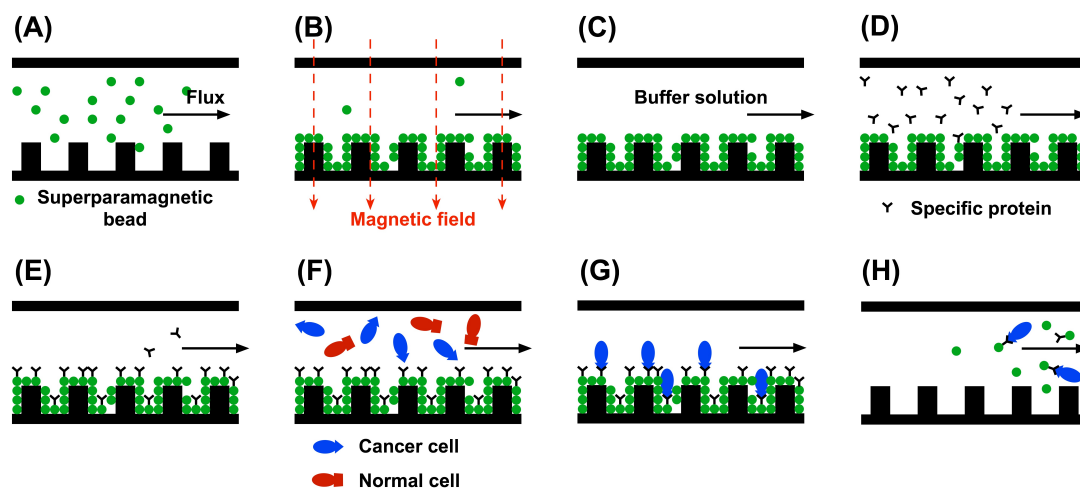
Figure 32. Schematic representation of the experimental protocol for cell capture and sorting. (A) The channel was initially filled with a suspension of superparamagnetic beads. (B)The external magnetic field was applied and the beads were trapped by the Ni micro pillars. (C) Flow of buffer solution which activates carboxyl groups on the surface of the beads and washes out any untrapped beads simultaneously. (D) Protein solution was then introduced into the flow stream. (E) Proteins were attached to the beads, and any unbound protein was washed out of the channel. (F) Cells were introduced into the channel. (G) Cancer cells were captured by specific protein-functionalized beads anchored to the nickel micro pillars. (H) The cancer cells captured by the beads were eluted from the channel, when the external magnetic field was removed.

Initially, channel was filled with a suspension of superparamagnetic beads and then, beads were biofunctionalized *in situ* by covalent attachment of specific proteins directly to their surface. This figure demonstrates how the *in situ* functionalized superparamagnetic beads in micro channel and to capture A549 cancer cells (human lung carcinoma cell line) from a flow is performed. Due to specific interaction between wheat germ agglutinin and N-acetyl glucosamine on the cell membrane, A549 cancer cells were successfully captured on magnetic particles.

In bioanalytical procedure (nucleic acid assays), magnetic particles play an important role. In macroscopic lab-bench protocols, magnetic particles are used as mobile substrate for capturing and extraction of nucleic acids[187, 188]. Different steps followed in an assay, where magnetic particles are applied with different purposes and at different phases of the assay are represented in Figure 33.
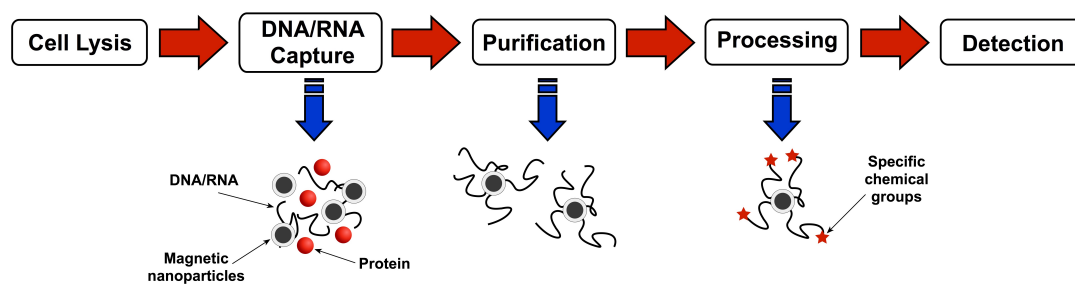
Figure 33. Different-steps of an on-chip magnetic nucleic acid assay through magnetic particles.

Purification and capturing of molecules are an important task while performing on-chip nucleic acid analysis. By the use of magnetic microparticles in a microfluidic system, nucleic acid can be brought into contact with particle surface through different means. A preferred solution is the incubation of activated magnetic particles with the sample in a reservoir[189]. Here, purification is done by introducing magnetic field to separate magnetic particles from the sample and nucleic acid capturing is driven by diffusion. However, some solutions used relative velocity between sample and magnetic particles by immobilizing the latter. Mostly, it is based on immobilization of magnetic particles inside a microchannel before or after capture step[177, 190]. Magnetic particles are herewith held against a flow through a magnetic field perpendicular to channel, while

source of magnetic field occurs by integrating electromagnetic element into the chip[177] or by placing permanent magnet at the bottom of the system[189].

Proteolysis is the direct degradation of proteins through cellular enzymes called proteases. Magnetic particles in conjunction with microfluidics can also be used for developing micro reactors for proteomic applications[191]. Proteolyzation of the proteins occurs through porous magnetic plug when magnetic particles are grafted with enzyme. Magnetic particles when grafted with specific enzymes can very efficiently proteolyzed the protein of interest. This can be done by flowing the protein through the porous magnetic plug.

An important advantage of microfluidic magnetic particle based digestion system is the replacement of magnetic matrix by flushing out the old beads and loading new beads into same channel. Another advantage of such system is the reduced cost and better reproducibility due to the fact that grafting on particles can be done ex situ in large quantities[174]. Protein digestion inside a microfluidic channel occurs by grafting trypsin on magnetic beads while maintaining self-assembled magnetic particles chain in a microchannel to digest several types of protein samples from flow for subsequent analysis[192].

5. Conclusion

Paramagnetic or superparamagnetic particles, which can respond to an external magnetic field, provide an efficient method for separating samples linked to the magnetic particles from the liquid suspension. Various efficient synthetic approaches have been used for the preparation of uniform and monodisperse SIONPs in order to be used in biomedical applications. Magnetic particles have been widely used as a universal separation tool to purify nucleic acids (i.e., DNA and RNA), proteins & peptides cells and other biologically active compounds from crude samples.

Micro and nano-sized magnetic particles provide a new technology for their applications in microfluidics, which includes lab-on-a-chip systems, biosensors, and microfluidic systems. Biomolecules labeled with magnetic nanoparticles will be magnetically driven to retain a surface. By combination with precisely engineered microfluidic, flow patterns on-chip will allow to develop and to remove non-specifically adsorbed particle on surface. The use of catalyst immobilized on magnetic nanoparticles for catalytic and separation processes will also be interesting development in

microfluidics, especially for chemical and pharmaceutical industries. Numerous of sensitive magnetic field detection devices have been developed to be suitable for biosensing applications.

TGA & magnetization measurements for determination of composition and polymer conversion of magnetic hybrid particles

1. Introduction

At the end of last century, inorganic nanoparticles (e.g. gold, silver, iron oxides, quantum dots, second harmonic generation nanoparticles (SHG), etc) have been widely used in various technological and biomedical applications due to their catchy features emanating from their nano-size and structure, as compared to their bulk counterparts. These features include nonlinear optical properties, superparamagnetic properties, as well as some biological and catalytic activities.[193] Superparamagnetic properties of magnetic iron oxide nanoparticles and in particular magnetite (Fe_3O_4) and maghemite (γ-Fe_2O_3), which render them easily affected by even low external magnetic field, have attracted much attention, as reported in literature.[194] In addition, their biocompatibility, low toxicity, and ease of preparation at low cost make them suitable candidates for many promising applications in various technological and more particularly in biomedical diagnostic and therapeutic domains.[195-197]

In addition, magnetic iron oxide nanoparticles cover a broad spectrum of industrial and technological applications such as ferrofluids, magnetic seals in motors, magnetic inks for bank cheques, magnetic recording media, organic and biochemical syntheses, and industrial water treatment.[195]

In the biomedical domain, the ideal magnetic nanoparticles should have high magnetic properties, sufficient small size with narrow distribution, high surface functionality, and well defined morphology.[198, 199] Generally, the pristine superparamagnetic iron oxide nanoparticles (SIONPs) tend to make aggregates due to their large surface area-to-volume ratio and dipole-dipole interaction, leading to the reduction in their intrinsic superparamagnetic properties.

Therefore, surface modification of SIONPs is of paramount importance to enhance their water solubility, biocompatibility and colloidal stability in aqueous and physiological media, and to provide mechanical and chemical stability for SIONPs. In this regard, several approaches for modification or encapsulation of SIONPs have been investigated through physical or chemical processes using various materials starting from low molecular weight compounds (e.g. ligands and surfactants) to the use of high molecular weight compounds (e.g. synthetic and natural polymers).[200-203] More

importantly, the polymer coat induces reactive chemical functions capable for immobilizing biological species via chemical interaction (e.g. enzymes, proteins, antibody, antigen, DNA, RNA, etc), which is highly needed for biomedical applications[162, 204, 205].

For any application of magnetic nanoparticles, magnetic properties (saturation magnetization), which mainly depend on particle size, chemical nature of the used magnetic material and magnetic content are considered as the key factors affecting their successful use. Recently, various techniques have been used for colloidal and physical chemistry characterization of such complex particles, including Transmission Electron Microscopy (TEM), Fourier Transform Infrared spectroscopy (FTIR), Powder X-ray Diffraction (XRD) Technique, Atomic Absorption Spectroscopy (AAS), Gel Permeation Chromatography (GPC), Differential Scanning Calorimetric (DSC), Thermogravimetric Analysis (TGA), and Electrical Conductivity Measurement[206].

However, due to the presence of magnetic iron oxide some techniques are automatically discarded (e.g. NMR) which needs to use new roots. Therefore, the most efficient techniques which are now widely used for their characterization include magnetization measurements and thermal gravimetric analysis.

Then, the main objective of this review is to demonstrate that the combination of TGA and magnetization, as complementary techniques, is good to characterize magnetic latex particles which cannot be performed by conventional techniques.

2. Description of TGA

According to the International Union of Pure and Applied Chemistry (IUPAC), thermogravimetry (TG) can be classified as a technique in which the mass of a substance (and/or its reaction product(s)) is measured as a function of temperature whilst the substance is subjected to a controlled temperature program[207].

The development of thermogravimetric analysis expands its scope beyond simply confirming gravimetric techniques. Currently, studies in the fields of kinetics, thermodynamics, metallurgy, corrosion, and polymers can be performed using TGA technique[208].

Figure 34 shows a simplified diagram describing the thermogravimetric system which basically constituted by a balance, thermocouple, gas flow system, and an oven.
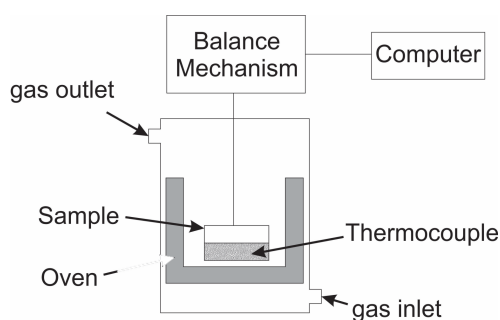
Figure 34. A simplified scheme of the thermobalance used for TG analysis.

Nowadays, thermal gravimetric analysis is a versatile technique used for studying the effect of heat on decomposition characteristics of organic materials and more particularly for polymers. Moreover, this technique may be used for polymer characterization, especially on kinetic studies, lifetime prediction, water absorption, and more particularly for thermal stability which considered as a basic requirement for some important applications[209-211].

For polymer composites containing inorganic particles (e.g. magnetic polymer hybrids), TGA technique is widely used for estimation of the chemical composition (i.e. polymer amount and consequently magnetic content) of the composite. Furthermore, in polymer blends, each polymer shows a characteristic decomposition profile which may be attributed to different ways of chemical degradation, such as, main-chain scission, side group scission, elimination, and depolymerization[212]. This in turn helps in distinguishing qualitatively one polymer from another, especially in polymer mixtures, using only few milligrams of material. The results of quantitative analysis can be improved if the TGA is coupled with another device, such as, gas chromatograph, Fourier-transform infrared spectroscopy, and mass spectrometry[213, 214].

For quantitative analysis, the thermogravimetric curves provide information about the decomposition mechanisms for various materials, since, change in sample mass during analysis could be observed[215]. If TGA curves do not overlap each other, the mass loss profile of a mixture of materials may be considered as the sum of individual profiles of each of its components providing, easily, quantitative results. Figure 35 shows an example of the thermal behavior of pure polymers and their physical mixtures.
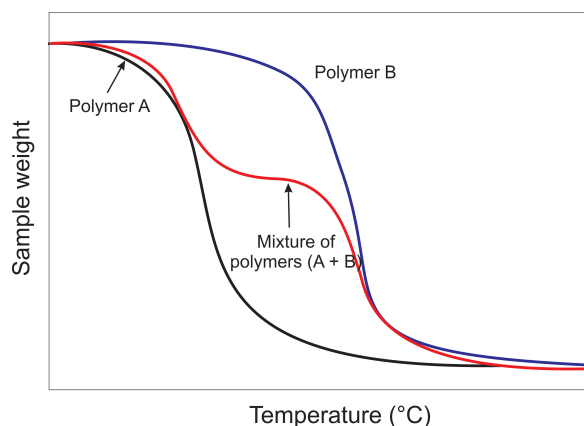
Figure 35. Schematic illustration of TGA curves for hypothetical pure polymers and its physical mixtures (blends).

However, when the degradation events from different polymers overlap each other, the simple graph observation for obtaining quantitative results is not possible. In order to overcome this drawback, the TG graphics can be differentiated. Then, the derivative of TG curves (DTG) is sometimes used for determining inflection points on the TG curve. Moreover, DTG is useful in revealing extra details, for example, a hide degradation event, which would not have been seen on the TG curve itself [216]. An example for such overlapping can be observed in Figure 36.
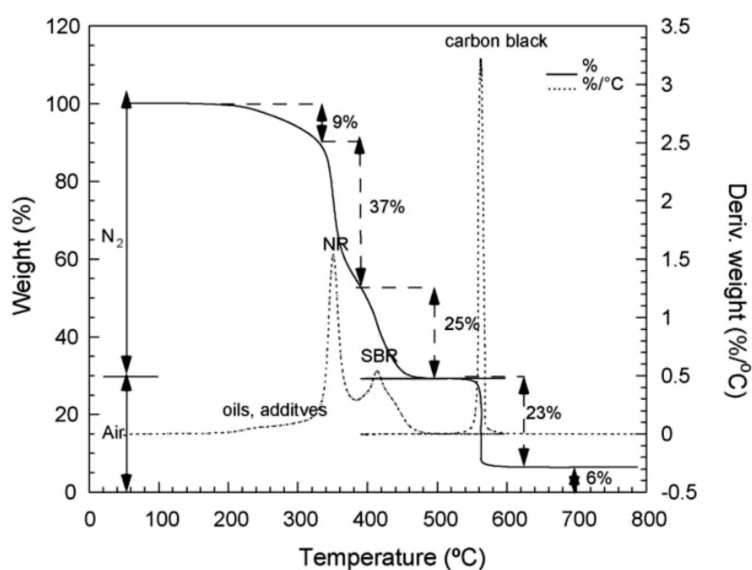
Figure 36. TGA and DTG curves of sample containing natural rubber (NR) 40% (w/w) and styrene-butadiene rubber (SBR) 60 % (w/w) vulcanizates[215]. Reproduced with permission. Copyright © 2006 Elsevier.

In general, the derivative weight loss curve (DTG) is more sensitive to subtle difference in weight loss than TG curves[217]. Moreover, by DTG, it is possible to distinguish in which temperature a specific degradation event starts and finish. Besides identification of an event, the DTG curves may be used to estimate the ratio (%) of polymers in blends. One way consists in plotting a calibration curve, which can be done through the correlation of peak heights of desired event against a specific temperature or composition[217]. In order to obtain good consistence on TG experimental, it is important to be careful on the experimental details. The way in which the sample is packed, amount of sample mass analyzed, heating rate, and gas flow rate are some factors which can affect the reproducibility.

3. Description of Magnetization

Various organic and inorganic materials exhibit magnetic properties which may interest to be explored for well-defined applications. In the last decade, various magnetic materials have been prepared and examined in terms of magnetic properties. Ferrite based materials and more particularly metallic particles such as iron oxide based particles have been extensively studied due to their easy chemical preparation (mainly via coprecipitation process) at low cost and the possibility to control their magnetic properties and magnetization[218]. In order to point out the existence of this property, it is urgent to study their behavior when they are subjected to an external magnetic field. In this regards, vibrating sample magnetometer (VSM) was used.

3.1. Vibrating sample magnetometer

Vibrating sample magnetometer (VSM) is an instrument that measures the magnetization of a small sample of magnetic material placed in an external magnetizing field by converting the dipole field of the sample into an electrical signal. VSM is based on Faraday's law, which states that an electromagnetic force is generated in a coil when there is a change in flux linking the coil[218]. In the measurement setup, a magnetic sample is moved in the proximity of two pickup coils as indicated in Figure 37. The oscillator provides a sinusoidal signal that is translated by the transducer assembly into vertical vibration. The sample, which is fixed to the sample rod, vibrates with a given frequency and amplitude (60 Hz and 1 mm). It is centered between the two pole pieces

of an electromagnet that generates a magnetic field H_0 of high homogeneity. Field strengths of several Tesla are commonly possible with laboratory VSM systems. Stationary pickup coils are mounted on the poles of the electromagnet. Their symmetry center coincides with the magnetic center of the sample. Hence, the change in magnetic flux originating from the vertical movement of the magnetized sample induces a voltage U_{ind} in the coils. H_0 being constant, has no effect on the voltage but is necessary only for magnetizing the sample. By measuring in the field of an external electromagnet, it is possible to obtain the hysteresis curve of a material.

The measurement setup is sensitive even to very low magnetic moments. Today's vibrating sample magnetometers are able to detect magnetic moments down to the u emu range, which corresponds to approximately 10^{-9} g of iron[219].
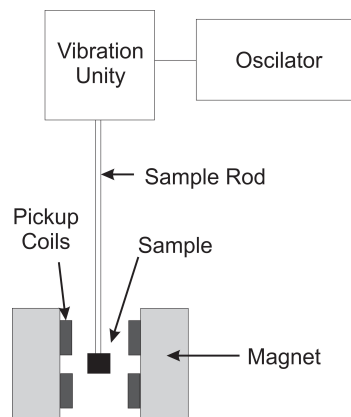
Figure 37. Vibrating Sample Magnetometer set up.

3.2. Magnetic behavior of iron oxide nanoparticles

Iron atom has a strong magnetic moment due to the four unpaired electrons in its 3d orbitals[195]. As shown in Figure 38, when crystals are formed from iron atoms, four different magnetic states can arise; Paramagnetic (or Diamagnetic), Ferromagnetic, Ferrimagnetic, and Antiferromagnetic state. In the Paramagnetic or Diamagnetic state; the individual atomic magnetic moments are randomly aligned with respect to each other, and the crystal has a zero net magnetic moment. If this crystal is subjected to an external magnetic field, some of these moments will align, and the crystal will attain a small net magnetic moment. In case of Paramagnetic crystal, the moments will align in the same direction of the magnetic field while in the Diamagnetic state, the moments will align against the magnetic field. In Ferromagnetic state; all the individual moments in the

crystal are aligned even without an external magnetic field (e.g. permanent magnet). In Ferrimagnetic state; the crystal has a net magnetic moment arising from two types of atoms with moments of different strengths that are arranged in an antiparallel fashion. While, in Antiferromagnetic state; magnetic moments are antiparallel and have the same magnitude, then the crystal has no (zero) net magnetic moment.
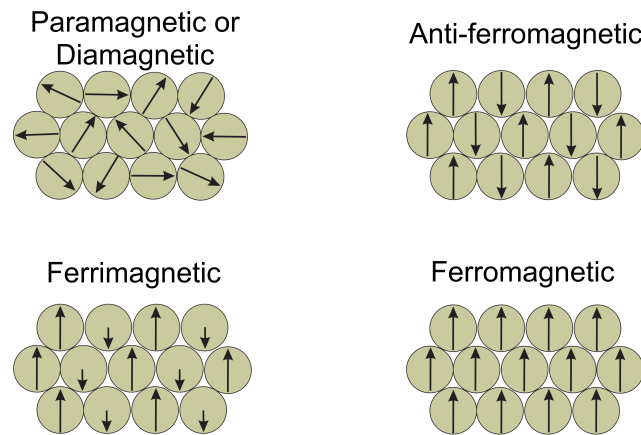
Figure 38. Alignment of individual atomic magnetic moments in different types of materials.

In the bulk ferromagnetic material, the magnetization M is the vector sum of all the magnetic moments of the atoms per unit volume of the material. The magnitude of M is generally less than its value when all atomic moments are perfectly aligned, because the bulk material consists of domains (Figure 39). Each domain has its own magnetization vector arising from the alignment of atomic magnetic moments within the domain. The regions separating magnetic domains are called domain walls where the magnetization rotates coherently from the direction in one domain to that in the next domain. Thus, the magnetization vectors of all domains in the material may not be aligned in the same direction, leading to a decrease in the overall magnetization.
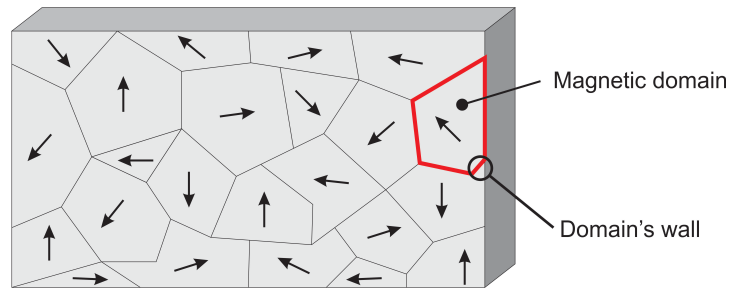
Figure 39. Magnetic domains in a bulk ferromagnetic material.

If an external magnetic field of strength H is applied to a ferromagnetic material of magnetic strength M (Figure 40A), the magnetization curve is obtained (Figure 40B, blue line) showing that M increases with H until a saturation magnetization value M_S is reached. The magnetization curve displays a hysteresis loop, because all domains do not return to their original orientations when the magnetic field is removed *(H=0)*. Thus, the material will attain a remnant (residual) magnetization M_R, which can only be removed by applying a coercive field H_C in the opposite direction to the initially applied field.

When the size of the material goes down to the submicron or the nanoscale, the number of domains decreases until there is a single domain where the characteristic size of the material is below a critical size (D_c) (Figure 40C). This single domain describes a region within a magnetic material which has uniform magnetization, and has no hysteresis loop (Figure 40B, red line) and is said to be superparamagnetic. In this case, the individual magnetic nanoparticles have large constant magnetic moment and behave like a giant paramagnetic atom with a fast response to the applied magnetic field without remnant magnetization M_R. It was found that iron oxide nanoparticles smaller than 20 nm often display superparamagnetic behavior at room temperature[220, 221].
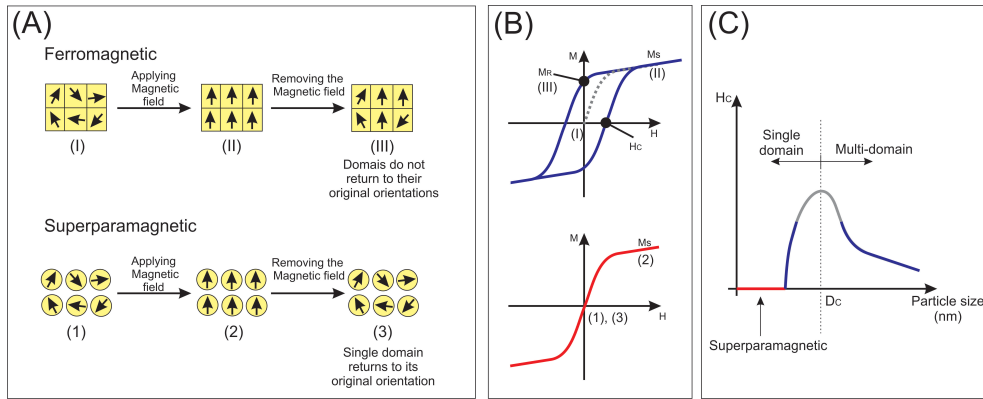
Figure 40. Magnetic properties of ferromagnetic materials as a function of particle size (A and C), and their magnetization curve (hysteresis loop) (B).

3.3. Hybrid magnetic particles

The preparation of magnetic latex particles is incontestably based on the use of magnetic iron oxide nanoparticles. In this direction, modified superparamagnetic iron oxide nanoparticles prepared via co-precipitation process are used (Figure 41A)[222]. The iron oxide nanoparticles are first coated with low water solubility surfactant in order to be dispersible in organic phase such as alkane solvent (organic ferrofluid)[223]. Then, the use of this organic ferrofluid in well appropriate surfactant aqueous solution leads to the formation of oil in water (o/w) emulsion by using high shearing process or even ultra sound. The obtained o/w magnetic emulsion can then be used as such to perform mini-emulsion polymerization when the organic solvent is replaced by monomer such as styrene, but the final magnetic latex particles exhibit low magnetic content and then low particles separation under any applied magnetic field. In order to overcome this problem, the prepared magnetic emulsion (Figure 41B) was used as such and as seed in radical emulsion polymerization after avoiding the presence of free micelles in the aqueous phase leading generally to secondary nucleation[224]. The well prepared and characterized magnetic emulsion can then be encapsulated using various hydrophobic and/or hydrophilic monomers (mainly styrene monomer or mixture of styrene and functional monomer like glycidyl methacrylate (GMA) in presence of divinylbenzene (DVB) as a crosslinker (Figure 41C)[225]. The polymer shell surrounding the magnetic core can also be further functionalized using acrylamide derivative leading to stimuli-responsive highly magnetic submicron latex particles (Figure 41D)[226].
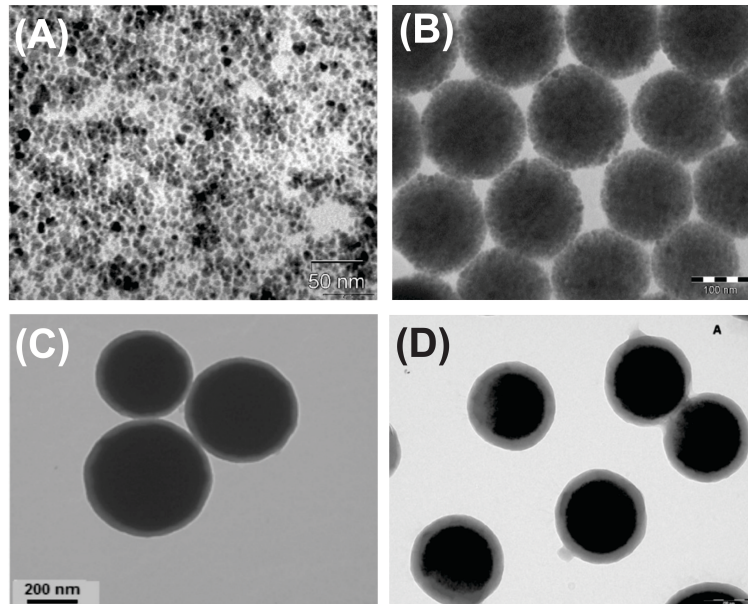
Figure 41. TEM analysis of iron oxide nanoparticles (A)[221], magnetic emulsion (B)[224], magnetic poly(divinylbenzene-*co*-glycidyl methacrylate) colloidal particles (C) [225],and temperature sensitive poly(NIPAM) coated magnetic particles (D)[222]. Photos A, C and D are reproduced with permissions. Copyright © Elsevier. Photo B is reproduced with permissions. Copyright © 2006 American Scientific Publishers.

4. Chemical composition measurements

4.1. Chemical composition by TGA

Thermogravimetric analysis (TGA) may be an interesting tool for characterization of magnetic latex particles with different morphologies (e.g. core-shell, Janus, and polymeric matrix). In general, inorganic oxides do not degrade completely in TG experiment. Based on this fact, it is possible to measure the amount of both organic and inorganic part.

For estimating the inorganic content, it is important to point out the importance on choosing either inert (e.g. nitrogen) or reactive atmosphere (e.g. air). Since the gas employed on TGA measurements can affect the behavior of thermogravimetric curves. For example, in nitrogen (N_2) flow, magnetite (Fe_3O_4) usually is stable up to 600°C and the TGA data can be used for estimating directly the total amount of Fe_3O_4 in the sample[199, 227, 228]. Moreover, it is well known that FeO is thermodynamically stable above 570°C; for this reason phase transition from Fe_3O_4 to FeO may be formed when temperature is between 600°C and 800°C. Furthermore, when T > 800°C the deoxidation

of FeO may be observed[199, 229]. On the other hand, when TGA curve is obtained under air flow, magnetite is totally converted to Fe_2O_3 in a temperature range between 200°C and 300°C[230, 231]. In such case, the Fe_3O_4 content in the hybrid particles may be estimated by the following chemical equation:

$$2\,Fe_3O_4 + {}^1\!/_2\,O_2 \rightarrow 3\,Fe_2O_3 \tag{7}$$
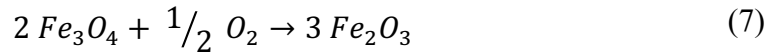
An interesting example on applying the TGA measurement under air flow was reported by Xu and co-workers[231]. They estimated the amount of Fe_3O_4 polyacrylamide-coated magnetic particles using the Eq. (7). In addition, they could correlate, with reasonable precision, the amount of magnetite with saturation magnetization for all samples studied.

In the case of hybrid based magnetic nanoparticles, TGA under N_2 flow was used to determine the weight percentage of Fe_3O_4 in the Fe_3O_4/chitosan-PAA composite microspheres, as shown in Figure 42[232]. As clearly seen from the TGA curve (a) of bare Fe_3O_4 nanoparticles, the weight loss is about 3% for the whole temperature range. This might be due to the evaporation of absorbed or crystalline water in the sample. On the other hand, for Fe_3O_4/chitosan-PAA composites (TGA curve (b)), below 200°C, the weight loss of all the nanocomposites is quite small (7%) due to removal of the absorbed physical and chemical water. Then, the principal chains of chitosan-PAA begin to degrade at about 230 °C and the temperature of final decomposition is at around 500 °C, reaching to a weight loss of 68%. In addition, there is no a significant weight change from 500 to 900 °C was observed, implying the presence of only iron oxide. Calculation results showed that the magnetic content of composite microspheres is about 41.3 wt%.

These results are very close to and in conformity with those obtained by magnetization measurements, as can be seen in the coming *section (4.2)*.
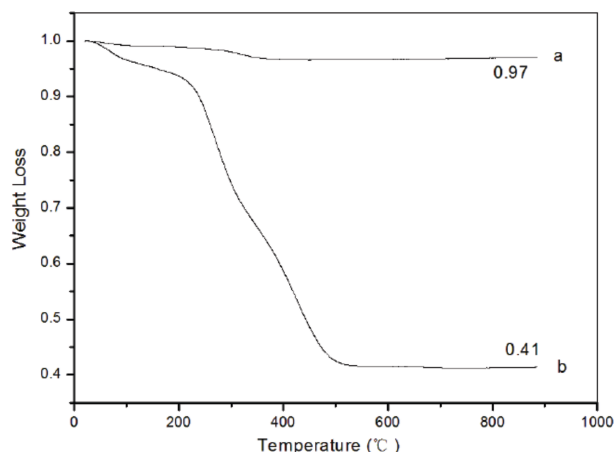
Figure 42. Weight loss curves of (a) bare Fe_3O_4 and (b) Fe_3O_4/chitosan-PAA magnetic microspheres[226]. Reproduced from © 2010; licensee MDPI, Basel, Switzerland. Distributed under the terms and conditions of the Creative Commons Attribution license (http://creativecommons.org/licenses/by/3.0/).

Moreover, TGA was not only used for basic hybrid particles, but also for more complex ones and principally for quantitative aspect in order to have more information about polymerization conversion. For instance, the amount of inorganic magnetic core of the prepared P(NIPAM/MBA/AEMH) coated magnetic particles (Figure 43) was easily estimated from the weight loss % of the organic part (Figure 44).
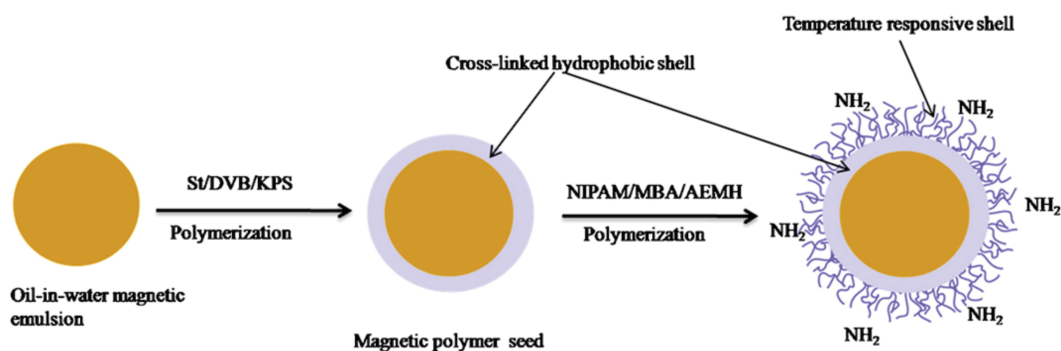
Figure 43. Schematic representation for the preparation of temperature sensitive amine containing magnetic poly(DVB)/poly(NIPAM-AEMH) colloidal particles. The starting material is oil-in-water magnetic emulsion, which consisted of oleic acid-coated iron oxide nanoparticles emulsified in aqueous surfactant solution[222]. Reproduced with permission. Copyright © 2011 Elsevier. AEMH: aminoethyl methacrylate hydrochloride (AEMH), MBA: N,N-methylenebisacrylamide, DVB: divinylbenzene.

As clearly seen, the major weight loss occurred in the range of 350–450°C and reached a plateau after 500° C. As expected, the amount of residual mass (mostly magnetic content and little amount of ash) about 60% in cross-linked magnetic seed particles is lower than that of magnetic emulsion (82%). This was attributed to the incorporation of polymers on the magnetic seed particles, which lowers magnetic content in the final particles[226]. Furthermore, the authors also could estimate the percentage of temperature-sensitive polymer brushes coated onto magnetic polymer seed by comparing the plateau of the magnetic polymer seed with samples (MP2, MP3, and MP4) after further and successive polymerization. From these observations it was possible to identify that the sample MP4 showed the highest encapsulation efficiency. Moreover, their TGA results were in a good agreement with TEM observations (Figure 41).
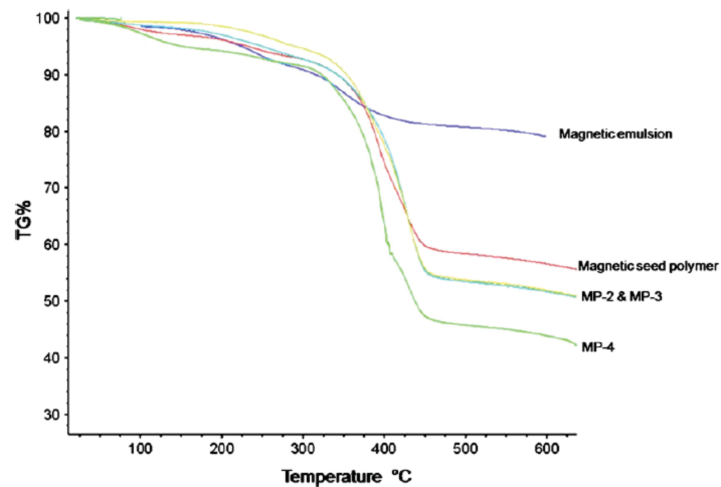
Figure 44. Thermogravimetric curve of magnetic emulsion, magnetic cross-linked polydivinyl benzene particles seed, and magnetic PDVB/P(NIPAM/AEMH/MBA) hybrid composite particles at various seed/monomer ratios (MP-2, MP-3 and MP-4)[222]. Reproduced with permission. Copyright © 2011 Elsevier.

4.2. Chemical composition by magnetization

Chemical structure, physical properties and the amount of inorganic ''magnetic'' material in the final particle are the key parameters which control their physical separation in a magnetic field[223]. In order to determine the chemical composition of magnetic latex particles via magnetization measurement, it is necessary to know the chemical nature of the used magnetic material, which can be examined by X-ray diffraction (XRD)

technique and/or Mössbauer spectra. Thereafter, the quantitative analysis (magnetic content) can be performed by using TGA, as above mentioned, or by magnetization measurements using vibrating sample magnetometer.

Generally, saturation magnetization (M_S) of the magnetic particles is highly dependent on the magnetic content and also on the chemical nature of the used magnetic material[199, 231]. Then, this property can be exploited to determine the amount of magnetic part in the final particles using magnetization measurements at room temperature. More intensely, this technique is considered as a non-destructive analytical tool as compared with TGA analysis.

Based on the value of M_S of the used initial magnetic nanoparticles and that of dry prepared magnetic hybrid particles, then the magnetic content in the final particles can be measured according to the following equation:

$$Magnetic\ Content\ (wt\%) = \frac{M_S}{M_{S_0}} \times 100 \tag{8}$$

Where M_S is the saturation magnetization of dry magnetic latex particles, and Ms_0 is saturation magnetization of initial magnetic nanoparticles.

In almost cases, this technique is complementary and consistent with TGA analysis for determination of magnetic content in the final particles, as previously reported[232].

For instance, the magnetization curves of bare Fe_3O_4 particles and Fe_3O_4/chitosan-Polyacrylic acid (PAA) composite microspheres recorded with VSM are illustrated in Figure 45A and 45B, respectively[232]. As shown in Figure 45, the magnetization of the samples would approach the saturation values when the applied magnetic field increases to 10,000 Oe. The M_S of bare Fe_3O_4 nanoparticles is 72.5 emu g^{-1}. For the Fe_3O_4/chitosan-PAA composite microspheres, M_S was about 29.1 emu g^{-1}, which was much less than that of bulk magnetite (84 emu g^{-1})[233]. The lower value of the measured M_S of bulk Fe_3O_4 nanoparticles was attributed to the presence of the smaller size of maghemite nanoparticles[234]. In addition, the low saturation magnetization of Fe_3O_4/chitosan-PAA composite microspheres may be attributed to the incorporation of Fe_3O_4 nanoparticles into chitosan-PAA spheres which added mass of the thick polymer layer on the magnetite nanoparticles. When the magnetic component size of the particles is smaller than critical size, the particles will exhibit superparamagnetism. A narrow hysteresis loop can be seen

in Figure 45 indicating to a small remnant magnetization. It might be that some of the particles are magnetically blocked.

By applying Eq. (8), polymer content could be calculated to be 40.1% and consequently polymer or organic content is 59.9%. These values are consistent with those obtained by TGA measurements, as above mentioned (Figure 42).
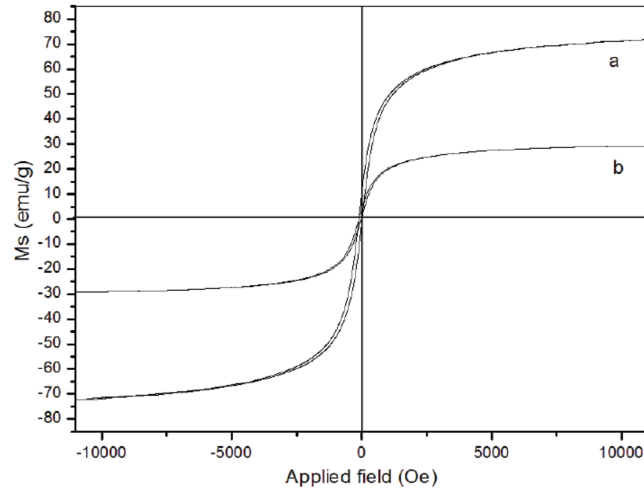
Figure 45. Magnetization curves obtained by vibrating sample magnetometer (VSM) at room temperature: (a) naked Fe_3O_4; (b) Fe_3O_4/chitosan-PAA magnetic microspheres[226]. Reproduced with permission. Copyright © 2010 John Wiley and Sons.

Xu et al have used TGA to measure the magnetite content in magnetic Poly(St-DVB-GMA) microspheres (MPL)[235]. As shown in Figure 46A, the weight loss of the prepared latex was 50 wt % at 400–450°C, which implied that up to 50 wt % of the MPL consisted of magnetite nanoparticles. On the other hand, the magnetization curve of the prepared latex is plotted in Figure 46B. As shown, the saturation magnetization value was 30 emu g^{-1}. Neither remanence nor coercivity was observed, which indicated superparamagnetic property of the MPL we obtained. The magnetite content calculated from the ratio of the original saturation magnetization of Fe_3O_4 nanoparticles (about 60 emu g^{-1}) and that the synthesized MPL was 50 wt %; this was in agreement with the result of TGA measurements.
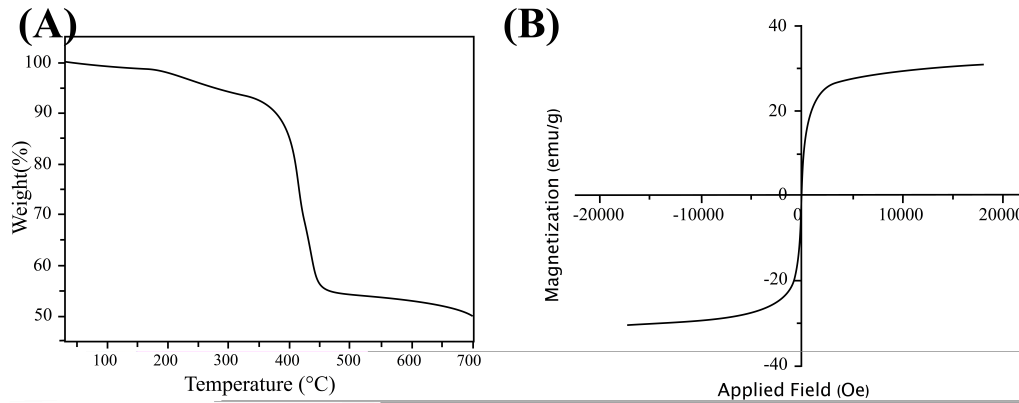
Figure 46. TGA diagram (a) and magnetization curve (b) of MPL of Latex.[38] Reproduced with permission. Copyright © 2010 John Wiley and Sons.

More complex systems have been deeply examined on washed magnetic latex particles after complete removal of any possible secondary nucleation[205]. As can be easily deduced from Figure 47, that the increase of polymer content in the particles, leads to decrease in magnetization. The chemical composition of the used magnetic seed was first determined by TGA and also by magnetization. After polymerization step, the amount of added polymer on the particles can then be determined by magnetization in comparison with the used seed. The obtained results are generally in agreement with the values obtained by TGA analysis[205].

As a result, we can say that the combination of TGA and magnetization (as complementary techniques) is good to characterize magnetic latex particles which can't be performed by other conventional techniques. If the magnetization of the used seed is well known, the polymerization conversion of monomers to polymer on particles can then be determined even in disperse media after subtracting the diamagnetic property of water only.
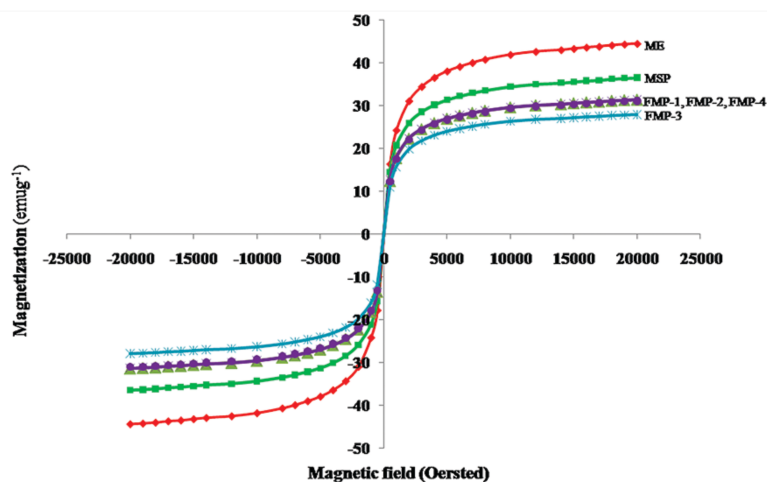
Figure 47. Magnetic hysteresis curve for the oil-in-water magnetic emulsion (ME), magnetic poly(divinylbenzene) seed (MPS) and magnetic@poly(divinylbenzene) @ poly(N-isopropyl acrylamide -co-acrylic acid) submicron particles at different AA content, FMP-1, FMP-2, FMP-3 and, FMP-4[162]. Reproduced with permission. Copyright © 2012 American Scientific Publishers.

5. Combination of TGA and Magnetization

Combining TGA and magnetization, it is possible to have access to the polymerization conversion. In fact, TGA gives the exact amount of organic and inorganic material while magnetization gives exact amount of magnetic and non-magnetic material. For instance, in our previous work,[225] saturation magnetization of magnetite emulsion (oleic acid-coated Fe_3O_4 nanoparticles) and their corresponding poly(divinylbenzene-co-glycidyl methacrylate) colloidal particles were measured to be 43.85 emu g^{-1} and 35.49 emu g^{-1}, respectively. By assuming that saturation magnetization of the magnetite nanoparticles is 60 emu g^{-1} [235] then the amount of magnetic material is 60 wt.%, with 40 wt.% organic material (oleic acid and surfactant from the seed emulsion, and polymer from the polymerization step). These results were very close to that obtained by TGA analysis[225].

Similarly, Nguyen and co-authors reported the synthesis of poly(methyl methacrylate)-coated magnetite nanoparticles. For characterizing the samples, TGA data was used for estimating both polymer contents and polymer-shell thickness. Then, the results were correlated with magnetization[236]. Another interesting work was reported by Chen and co-workers[237]. Zwitterionic polymer-coated core–shell magnetic

nanoparticles ($Fe_3O_4@SiO_2@PMSA$) were obtained for applying in specific capture of N-linked glycopeptides. For particles characterization, the authors used TGA for calculate both $Fe_3O_4@SiO_2$ and polymer amounts; then, the results could be correlated with magnetization data. Analogous correlations can be found elsewhere[238, 239].

Moreover, by performing such combined analysis, the amount of polymer induced by polymerization process can be easily deduced and consequently to polymerization conversion as below illustrated in Table 8 [240]. Firstly, it is interesting to notice that total polymerization conversions were observed leading to polymer formation on magnetic emulsion and polymer forming secondary nucleation. After subtracting the amount of organic material from the used seed magnetic dispersion and by determining the amount of organic material after polymerization (of washed dispersion), the polymerization conversion leading to polymer on particles can then be estimated and found to be 64% for MP-DVB(1) and 56% for MP-DVB(5).

Table 8. Estimation of magnetic content for dry magnetic emulsion (ME) and magnetic poly(divinylbenzene) latexes (MP-DVB), which prepared at various DVB content, based on magnetization and TGA data[230]. Reproduced with permission. Copyright© 2012, Springer Verlag.

Property	Magnetic emulsion	MP-DVB (1) (0.9 ml DVB)	MP-DVB (5) (1.2 ml DVB)
Specific saturation magnetization (emu g^{-1})	51.1	39.6	34.4
Polymer content (wt.%) by TGA	0.0	20.2	24.1
Iron oxide content (wt.%) by TGA	79.0	67.3	65.2
Iron oxide content (wt.%) by VSM	67.2	52.1	45.3
Polymerization conversion (%)	----	64	56

Conclusion

Colloids characterization is of great interest, since much information can be deduced such as colloidal properties, chemical composition, intrinsic properties and then the mechanism of particles formation or modification.

Regarding inorganic or organic particles, various methods are widely used for particles characterization and surface determination including Transmission Electron Microscopy (TEM), Scanning Electron Microscopy (SEM), Fourier Transform Infrared spectroscopy (FTIR), Powder X-ray Diffraction (XRD) Technique, Atomic Absorption Spectroscopy (AAS), Gel Permeation Chromatography (GPC), Differential Scanning Calorimetric (DSC), and Electrical Conductivity Measurement as largely reported in literature.

Regarding hybrid particles, its necessary to combine various complementary characterization techniques in order to get more information and various analytical tools can be used. In fact, the most problems are related to chemical composition and surface functional groups on the colloidal particles. But for some hybrid particles, the use of classical methods is not sufficient and in some cases these methods can't be used only. This is the case of hybrid magnetic latex particles which can't be analyzed by NMR for instance. Then the complete characterization of magnetic latex particles can be, for instance, performed using TGA and magnetization measurements. TGA is used for exact chemical composition by providing the ratio between organic and inorganic materials. The changes in organic composition between the used seed and the final particles lead to polymerization conversion. Regarding magnetization measurement, the amount of magnetic material can be exactly determined. Then, when the polymerization conversion increase, the amount of this magnetic material decreases and consequently, the polymerization conversion can be deduced.

PARTE II – CAPÍTULO 1

Preparation and characterization of submicron hybrid magnetic latex particles

1. Introduction

Colloidal particles are used as solid support in biomedical field which include immunoassay[151], cell sorting[241], and nucleic acid capturing and detection[161]. However, such applications require different tedious and time consuming separation processes, mainly when two kinds of separation processes are used i.e. a) filtration and b) centrifugation[242]. These processes lead to limit automation of biomedical diagnosis resulting in loss of time and delay in diagnosis[197]. Although magnetic latex particles are overcoming these methods, improving the process of automation while also decreases time delay and providing fast particles separation upon applying even low, magnetic field[154, 242]. Magnetic latex is a hybrid material consisting of polymer-encapsulated magnetic particles[243]. Purpose for the preparing of magnetic composite and latexes in biomedical area is to protect the inorganic part and to induce reactive chemical functionality, which is capable of immobilizing biomolecules through chemical reactions[244, 245]. Furthermore, it is important to mention that target in the preparation of magnetic latexes is the elaboration of superparamagnetic magnetic latex particles containing well defined amount of iron oxide, submicron in size and with narrowly size distribution[246, 247].

Different approaches have been reported for the preparation of magnetic latex particles for in vitro biomedical diagnostic applications. These approaches are based on classical polymerization in dispersed media such as emulsion[248], suspension[249], miniemulsion[250], dispersion[251], combination of various polymer-based process[252], and inverse emulsion[253, 254]. The pioneer work was described by Ugelstad et al.[255] by reporting not only the preparation of magnetic latexes (ML) but also their uses in invitro biomedical diagnosis. On the other hand, Elaissari et al.[154] has been reported the synthesis of magnetic latexes using a process called seeded emulsion polymerization. This process leads to submicron magnetic latex particles containing high

iron oxide amount. These prepared functional submicron highly magnetic latex particles have been used for nucleic acid extraction and purification[256], for capturing of biological samples[257], in controlling of protein adsorption and desorption[258], molecular imaging[259], and specific antigen detection[225].

However, the properties of nano/submicron particles are dependent of both size and shape. For this reason, the morphology controlling of the obtained material has a crucial role on its applications. Advantages of core-shell structures consist on enhance the chemical stability of the magnetic core, while the shell can be tuned improving its biocompatibility and/or decrease its toxicity. Moreover, its surface may be modified in order to obtain specific functionalities[260].

On the other hand, Janus microparticles, which have anisotropic morphology, offer more possibilities in terms of achievable structure and behavior. The simplest case of Janus particles is achieved by dividing in two distinct hemispheres, such as hydrophobic and hydrophilic parts[261, 262]. This characteristic gives to Janus particles important role in industry, since it could be applied as stabilizers in emulsions[263], as liposomes in biological sciences[264], as colloidal particles for generating surfaces with water-repellent properties[265], and so forth.

It is well known that the final morphology of the magnetic latex nanoparticles can be controlled by adjusting some factors, such as, i) monomer chemical nature, ii) type of initiator, iii) surfactant or stabilizer, iv) polymerization process, v) monomers/seed ratio, and vi) amount of internal oil phase of the used oil in water magnetic emulsion[240, 266].

In order to evaluate the influence of the main monomer concentrations and also for the purpose of obtaining desired morphology, the aim of this work was to synthesize submicron magnetic latex particles with magnetic core and homogeneous polymer shell bearing sulfate surface group by using styrene (St) monomer, divinylbenzene (DVB) crosslinker, potassium persulfate (KPS) as hydrophilic initiator and well controlled oil in water magnetic emulsion. In this study, special attention was dedicated to the influence of St/DVB weight ratio on the particle size, morphology, and magnetic properties of the obtained samples.

2. Materials and methods

2.1. Materials

Styrene (99%) and divinylbenzene (DVB) 80% were purchased from Sigma–

Aldrich and used after washing with 5% NaOH solution. Potassium persulfate (KPS) was purchased from Sigma-Aldrich and used without purification. Sodium dodecyl sulfate (SDS) was purchased from Sigma-Aldrich and used without purification. Deionized water was used in all experiments. Home-made magnetic emulsion were prepared according to our previous work[155, 222].

2.2. Methodology

Different types of morphologies were achieved by using oil in water magnetic emulsion as seed by using seed emulsion polymerization methodology for polymerization of Styrene (St) with cross-linker divinylbenzene (DVB) using Potassium persulfate (KPS) as initiator.

The polymerization was carried out in a 60 mL three necked double wall glass reactor made up of glass anchor type stirrer, a reflux condenser and a nitrogen inlet. The temperature was controlled at 70 °C by using a thermal bath. The home-made magnetic emulsion (approx. 50 mL of 4% solid content) was stabilized with 1 g L^{-1} (below critical micelle concentration - CMC) aqueous solution of SDS via serum replacement process performing only one time separation/dispersion cycle and introduced in the reactor. Then, the solution was purged with nitrogen for 1 h under stirring of 300 rpm for removal residual oxygen. The concentration of SDS solution was below the CMC because the excess of surfactants, during polymerization, could increase the amount of particles formed without magnetic seed due to second nucleation (SN).

After that, a total amount of monomers (1200 μL) at different St/DVB (volume/volume) rates were introduced at once into reactor and kept for 70 minutes under stirring. This time was necessary in order to favor monomers diffusion in the oil in water droplets. The polymerization temperature was rapidly increased up to 70°C and 2 wt. % of KPS (with respect to the weight of monomers) was added into the polymerization medium. The radical polymerization was then conducted at constant mechanical stirring (300 rpm) during 18 h.

3. Characterization

3.1. Transmission electron microscopy (TEM)

Transmission electron microscopy images were obtained by a (Phillips CM120, CMEABG, University of Claude Bernard Lyon I) to investigate the morphology and

microstructure of the magnetic polymer particles. Briefly, a drop of sample diluted in water was deposited on a carbon-coated copper grid and then left to dry at room temperature overnight before TEM imaging.

3.2. Particle size measurements

A Malvern Zetasizer (Nano ZS, Malvern Instruments limited, UK) was used to measure the average hydrodynamic size (Dh) of the magnetic polymer colloidal particles in 10^{-3} M NaCl solution. It was considered as result, the average of at less three measurements of 10 runs for each dispersion.

3.3. Zeta potential measurement

A Malvern Zetasizer (Nano ZS, Malvern Instruments limited, UK) was used to measure the electrophoretic mobility, which is converted to Smoluchowski's zeta potential[267]. The measurements were performed using highly diluted dispersion of the considered colloidal particles in 10^{-3} M NaCl solution at different pH. The pH was adjusted using NaOH or HCl. Each recorded value was the average of at less three measurements.

3.4. Thermal gravimetric analysis (TGA)

Thermo gravimetric analysis measurements were carried out on a thermogravimetry analyzer (NETZSCH -TG209F1 Iris$^{®}$ASC). The measurements were performed under a N_2 atmosphere from ambient temperature up to 700 °C at a heating rate of 10 °C min^{-1}. All samples were washed with water dried at 50 °C before analysis.

3.5. Fourier Transformed Infrared

The investigation of surface properties of the obtained sample was performed using Attenuated Total Reflexion-Fourier Transformed Infrared spectrophotometer (ATR-FTIR)-Shimadzu, Japan. All samples were clean and dry before analysis. The spectra were scanned over range 4000-400 cm^{-1}.

3.6. Magnetic properties

The saturation magnetization and magnetic behavior of the dried magnetic polymer latex were investigated using a vibrating sample magnetometer. This

measurement was carried out on the Automatic Bench of Magnetic Measurements (ABMM) at CNRS-IRC Lyon. The magnetization measurements were performed at room temperature.

4. Results and discussion

The seeded-emulsion polymerization was performed by varying St/DVB (volume/volume) ratio. The influence of St/DVB ratio was investigated in order to point out the relationship between the initial monomers composition and the final morphology of the obtained magnetic hybrid particles and the used initial chemical compositions are summarized in Table 9.

Table 9. Composition of monomers employed during seeded-emulsion polymerization experiments.

Sample name	St (% vol)	DVB (% vol)
ML1	0	100
ML2	10	90
ML3	20	80
ML4	40	60
ML5	60	40
ML6	80	20
ML7	90	10
ML8	100	0

*Total amount of monomers 1,200 μL, 50 mL at 70°C

4.1. Particle morphology analysis

Figure 48 shows TEM images of various magnetic hybrid particles prepared with different contents of styrene and DVB. According to the state of the art[154, 268], it is well known that the final morphology of magnetic latex nanoparticles may be controlled by adjusting various factors, such as, i) type of monomer, ii) type of initiator, iii)

surfactant, iv) polymerization time, v) monomers/seed ratio, and vi) amount of octane in the magnetic-seed emulsion[154, 257, 268]. In order to evaluate the influence of St concentration and St/DVB ratio on the final morphology of magnetic latex particles, various polymerizations changing St concentration were performed. The experimental conditions are reported in Table 9. Polymerizations were conducted using KPS as initiator, SDS as surfactant, and the magnetic seed containing a negligible amount of octane, which was found to be below 10 mg of octane/g of dried emulsion. Compared to what has been investigated and reported, the residual amount of octane, in used seed magnetic emulsion, was not considered as it should be. In fact, the presence of high octane amount in the used emulsion leads to non-core shell magnetic hybrid particles formation.
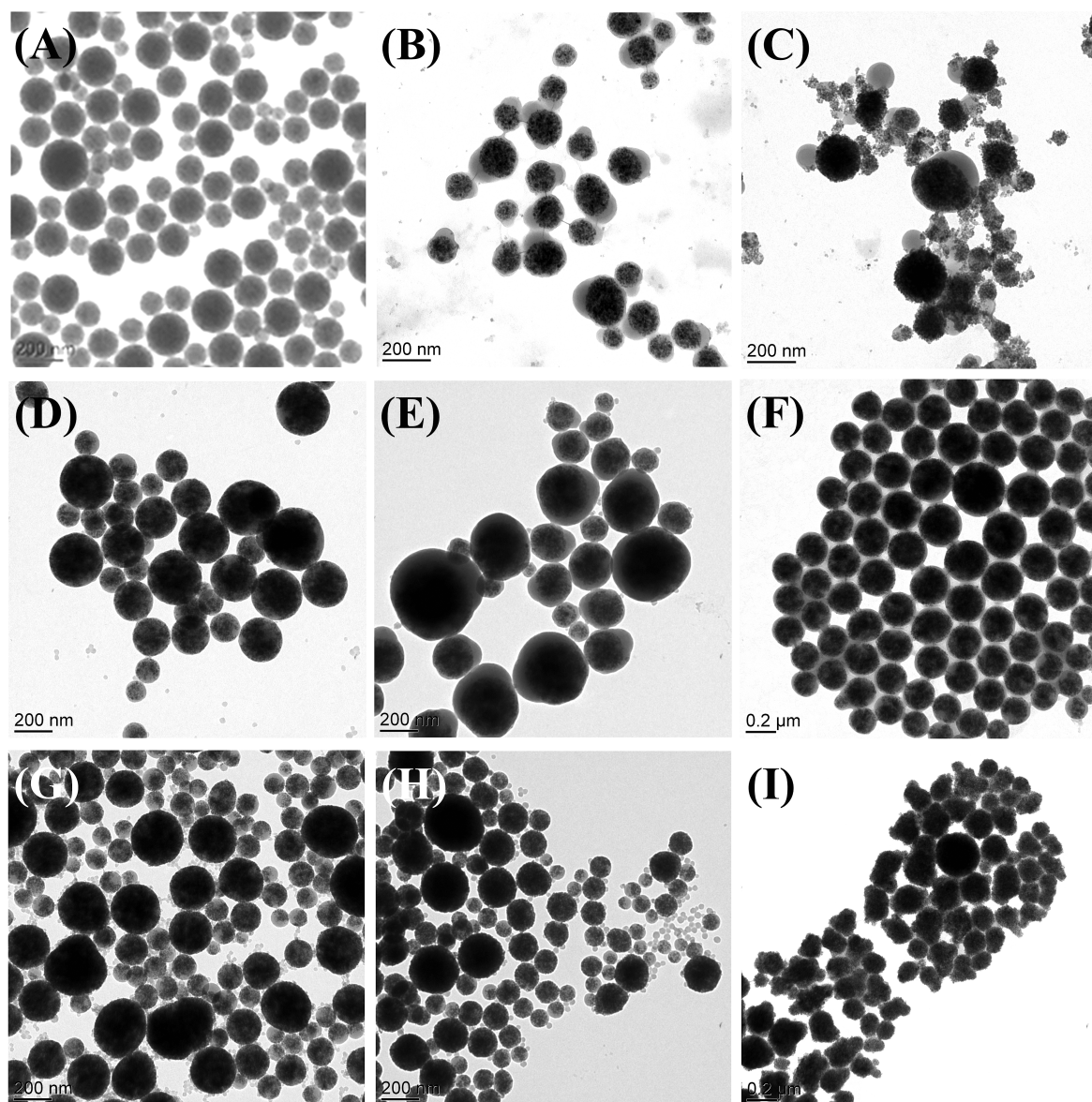
Figure 48. TEM images of samples (A) MES, (B) ML1, (C) ML2, (D) ML3, (E) ML4, (F) ML5, (G) ML6, (H) ML7, and (I) ML8. Bar charts of 200 nm.

It can be observed in Figure 48A that prepared magnetic emulsion (MES) showed a spherical shape with wide distribution size. When emulsion polymerization of DVB was carried out without St (Figure 48B), surprisingly, Janus nanoparticles were obtained. The formation of sub-microparticles with this morphology can be explained in terms of chain mobility. During early stage of polymerization, the cross-linked oligomeric DVB radicals which are into the oil droplet cannot diffuse very well. As a consequence, the monomers, that had not been reacted, move to near of the cross-linked oligomer DVB chains while the iron oxide moves to the opposite side occurring phase separation. Due

to this incompatibility, Janus particles were obtained. For sample which has approx. 10% of styrene on its composition, it was observed the appearance of some particles from second nucleation (SN) without any marked changes in the final morphology (Figure 48C). When styrene was added in the initial composition the monomers diffusion, into the oil droplet, was enhanced. Polystyrene oligomers have high chain mobility if compared with oligomers containing DVB. In this case, the styrene oligomer radicals, originating from the water phase, can either enter in a magnetic droplet/particle or undergo homogeneous nucleation which contributes to the growth of particles from SN[154, 240].

Increasing styrene content in the St/DVB ratio, the obtained sub-micron particles were becoming spherical-like and the secondary nucleation was reduced as can be seen in Figure 48D, 48E, and 48F. The high mobility of St monomer reduces, inside magnetic droplets, phase separation between formed polymer and iron oxide nanoparticles. In addition, polystyrene oligomers (or oligomers rich in styrene) have sulfate-end groups which in turn contribute to anchor the polymer chains on the particle surface. This effect is similar to the surfactant property (hydrophobic chain and hydrophilic end group). When St concentration increases up to 60% perfect-core shell morphology could be obtained as shown in Figure 48F.

When the amount of styrene was increased to between 80-90%, the influence of DVB on polystyrene oligomers mobility was drastically decreased. It can be seen in Figure 48G and 48H that the prepared samples exhibit a non-uniform size distribution. Furthermore, when the emulsion polymerization was performed using 100% of styrene, the obtained particles showed small nodules randomly distributed around the magnetic core as shown in Figure 48I. This morphology may be explained taking in account to the high specific surface developed by the presence of small polymer particles compared to large one. In the early stage of emulsion polymerization, the styrene monomer is initiated in water phase and not inside of oil droplet due to water-soluble used KPS[255]. Since the polymerization starts, in water phase, the oligomers chains increase (increasing polymerization degree). For this reason, the polystyrene oligomers become less and less water soluble. As a consequence, these oligomers are deposited on the magnetic-core surface. Based on these results, the following schematic morphology versus St/DVB ratio is bellow suggested (Figure 49).

[St]/[DVB]

| 0% St | 10-40% St | 60% St | 80-90% St | 100% St |
| Janus: Aglomeration of DVB chains in one side | Janus: Moon-like Decresing phase separation | Perfect core-shell | high mobility of St chains: Increasing the second nucleation | Aglomeration of polySt on the surface of seed |
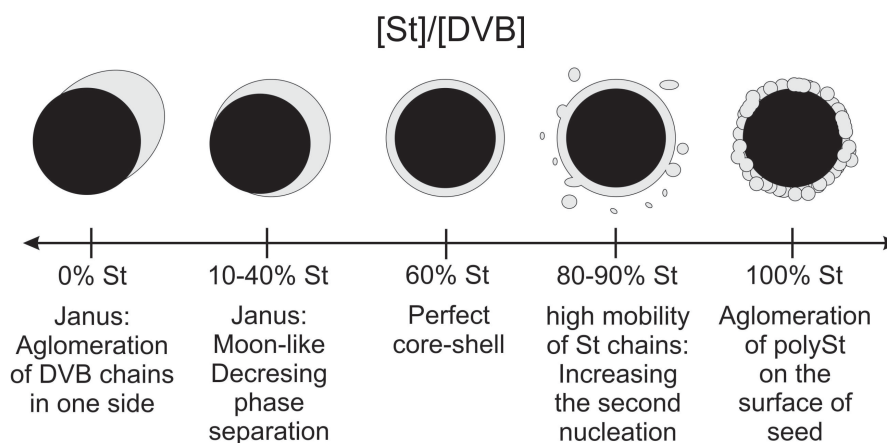
Figure 49. A schema suggesting for the morphology dependency with St/DVB ratio for iron oxide-seeded emulsion polymerization with low octane content (> 10 mg octane / g of dried emulsion).

4.2. Chemical composition and size determination

The chemical composition of the magnetic hybrid particles was investigated using thermo gravimetric analysis (TGA). Before analysis, the magnetic latexes were separated from the supernatant by applying permanent magnetic field. Then, washed with deionized water. This procedure was done three times, in order to remove the non-magnetic material such as surfactant and free polymer particles.

Figure 50A shows the thermogram of magnetic emulsion (MES) used as seed during polymerization. In this figure, it can be visualized that degradation of magnetic emulsion could be divided into three steps: i) 25°C-150°C, ii) 150°C-500°C, and iii) above 500°C which corresponds, respectively, to dehydration of physically adsorbed water (1.1%), degradation of organic part (16.6%), and residual inorganic part (82.3%). In the same figure, it can be seen observed in dTG graph that the organic content present in the MES showed three peaks, which overlaps each other. These peaks were assigned to free oleic acid, SDS and complexed oleic acid on magnetic nanoparticles degradation[244].

Figure 50B shows the thermograms of magnetic particles obtained after emulsion polymerization for samples with different morphologies ML1 (Janus), ML2 (Janus moon-like), ML5 (perfect core-shell), and ML8 (heterogeneous shape). As a general trend, all samples showed higher weight loss than the used seed magnetic emulsion. This is due to polymer induced during the polymerization process. However, the ML8 prepared using styrene only, showed lower polymer content than sample ML5 (perfect-core shell). The

difference of the residual mass can be attributed to the second nucleation favored in the case of ML8. In fact, TEM analysis of crude sample ML8 (data not shown) showed the presence of high amount of submicron polymer based particles. Then, the polymer partition between secondary nucleation and encapsulation of magnetic particles induced drastic decreases of polymer content in the washed ML8 sample.
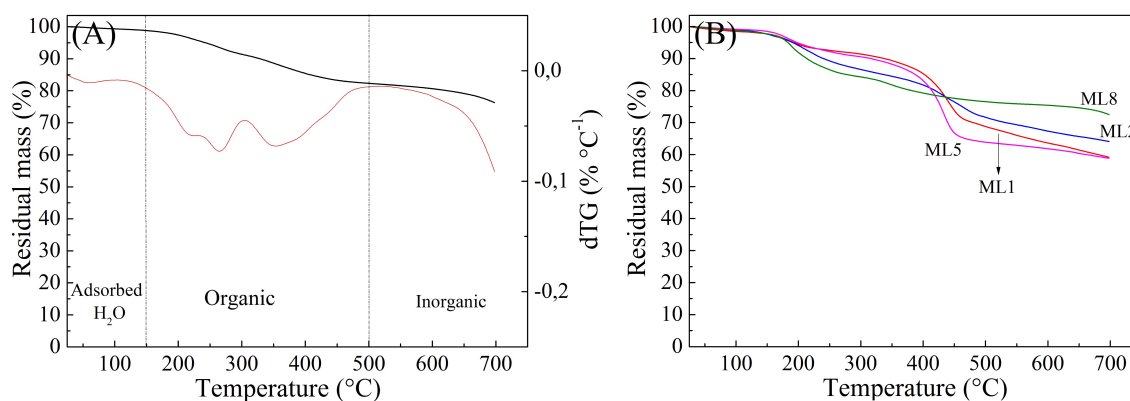
Figure 50. Thermogravimetric curves (TG and dTG) of samples analyzed in dried state. (A) magnetic emulsion seed (MES), and (B) magnetic latexes ML1 (Janus), ML2 (Janus moon-like), ML5 (perfect core-shell), and ML8 (surface PSt aggregated).

Table 10 shows the percentage of both polymer and iron contents in the prepared magnetic latex obtained at different St/DVB rates and the average particle size. In this study, residual mass at 500°C was attributed as percentage of iron oxide content for each sample. This consideration is reasonable, since there was no increase in weight resulting from oxidation of Fe_3O_4 to Fe_2O_3, because TGA experiment was carried out under nitrogen atmosphere[269, 270]. The polymer content was calculated by the difference between weights of organic and inorganic part taking in account the amount of organic surfactants (OS). In this work, it is important to mention that OS corresponds to 16.5% of iron oxide content as shown in Figure 50A (organic part).

It can be deduced from this study that both polymerization conversions (30-70%) and iron content (50-83%) were not directly correlated to St/DVB ratio. However, St/DVB ratio seems to have significant role in the particles morphology. Moreover, it was observed that all the synthesized magnetic latexes particles ML1 (Janus), ML2 (moon-like Janus), and ML5 (perfect core-shell) are submicron diameter, since the average particle size is between 257 and 300 nm with near narrow size distribution (see Fig. S1,

Supporting Information). It can be clearly seen at Table 10 that after polymerization the particle size of all the synthesized magnetic latexes particles with respect to magnetic seed (237 nm) increased irrespective of morphologies. The increase in particle size is due to the formation of organic polymer shell upon polymerization of monomers. In addition, the measured sizes and size distribution show that the obtained dispersions are not under aggregated state after polymerization process.

Table 10. Percentage of polymer and iron oxide contents in the magnetic latex obtained at different St/DVB rates.

Sample	Iron oxide content (wt%)[a]	Polymer content (wt%)[a]	yield (%)[b]	Particle size (nm)
MES	82.3	-----	-----	237
ML1	68.8	15.3	35	270
ML2	71.7	11.2	46	295
ML3	63.8	21.6	41	272
ML4	52.7	35.4	44	339
ML5	63.9	21.8	68	269
ML6	71.9	11.7	24	242
ML7	66.2	18.7	56	247
ML8	76.6	6.0	31	300

a. Determinated by TGA analysis.

b. The yield was calculated by gravimetric measurements taking into consideration only the magnetic particles coated with polymer.

Comparing the size of seed magnetic emulsion with the prepared magnetic latex (ML1 to ML8), it could be observed that the final particles size as well as the size distribution are not dramatically affected (since the secondary nucleation is discarded) by both low polymerization conversions and high polydispersity.

4.3. ATR-FTIR analysis

Figure 51 shows the FTIR spectra of magnetic emulsion seed (MES), and the

sample ML5 (60% St: 40% DVB) after polymerization. The polymer-containing sample was chosen due to its perfect core-shell morphology, as shown in TEM images. The bands at 763 and 698 cm^{-1} were attributed to out-of-plane C-H bending vibrations of styrene aromatic rings. The same vibration for DVB 1,4-disubstituted aromatic ring was observed at 796 cm^{-1}. Furthermore, in the same spectrum, it was observed the appearance of bands at 987 and 840 cm^{-1} which was ascribed to stretching vibrations of SO$_4^-$ and C-O-S respectively[271-273]. The presence of –SO$_4^-$ on the polymeric-nanoparticle surface was attributed to sulfate initiator linked to styrene (end-groups) of the polymer.
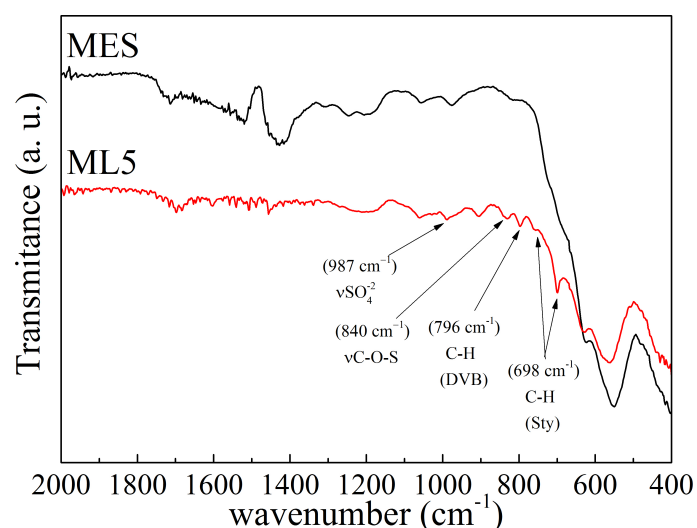
Figure 51. ATR-FTIR spectra of magnetic seed (MES), and sample ML5 (after polymerization) in the spectral range of 2000 cm^{-1} to 400 cm^{-1}.

4.4. Zeta Potential measurement

To study the electrokinetic properties of the prepared dispersions, zeta potential was deduced from the measured electrophoretic mobility as a function of pH and contact ionic strength and temperature and the obtained results are shown in Figure 52.
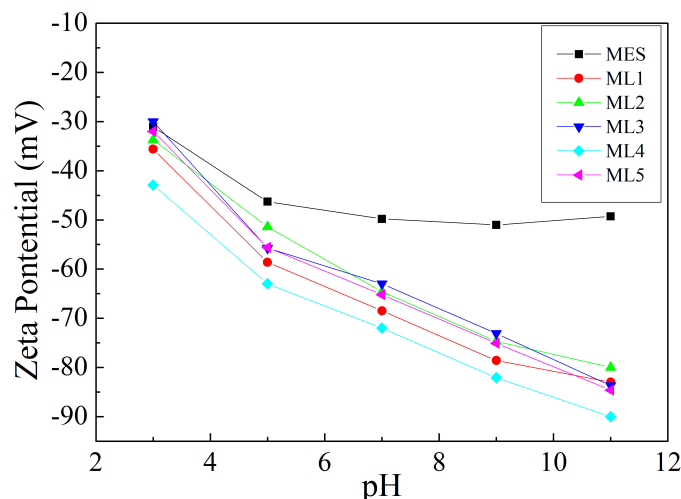
Figure 52. Zeta potential of magnetic emulsion (MES) and magnetic magnetic latex particles ML1 to ML5.

In order to point out the surface modification after encapsulation of magnetic seed, the zeta potential of all prepared magnetic latex particles (ML1 to ML5) was examined as a function of pH and in 1 mM NaCl solution. As can be clearly seen from Figure 52, magnetic emulsion and magnetic latex particles exhibit negative charges in the investigated pH range (from pH 3 to 11). Zeta potential values of seed magnetic emulsion was almost unchanged irrespective of pH of the aqueous medium. This behavior can be attributed due to the presence of the strong acid sulfate groups ($-SO_4^-$) emanating from SDS of the stabilizing agent (in case of magnetic emulsion), and also ($-SO_4^-$) groups originating from Potassium persulfate in case of magnetic latex particles. This indicates for both magnetic emulsion and all magnetic latex particles (ML1 to ML5) possess good colloidal stability over the pH range studied.

4.5. Magnetization study

The saturation magnetization and magnetic behavior of the dried magnetic polymer latex were investigated using a vibrating sample magnetometer. This study was carried out on the Automatic Bench of magnetic measurements using all dried particles by decreasing the magnetic field (H) from +20,000 to -1,000 Oersted at room temperature. This is performed to check the amount of inorganic magnetic material in final particles. Therefore, controlling magnetic properties before and after encapsulation is very important.

Figure 53 shows the magnetization curve for seed magnetic emulsion (MES) before and after polymerization (ML1 to ML5). From this figure, it can be clearly seen from magnetization (emu. g^{-1}) against magnetic field (Oe); saturation magnetization of the seed magnetic emulsion 28.3 emu g^{-1} decreased to 15.4 emu g^{-1} after polymerization in the case of perfect core shell (ML5). Others samples like ML1, ML2, ML3, and ML4 also showed decrease values respectively (14.5 emu g^{-1}, 5.6 emu g^{-1}, 19.8 emu g^{-1}, and 12.6 emu g^{-1}). The decrease in saturation magnetization after polymerization is attributed to increase of organic material and consequently decreases of magnetic amount. Importantly, at zero magnetic field (H=0) there is no marked residual magnetization reveling negligible remanence of all used magnetic particles. So this interesting result indicates that all of the magnetic particles before and after polymerization are superparamagnetic in nature[154]. The observed superparamagnetism was conserved after polymerization, indicating that the polymerization conditions had no effect on the intrinsic magnetic properties of the iron oxide nanoparticles used in the oil in water magnetic preparation.
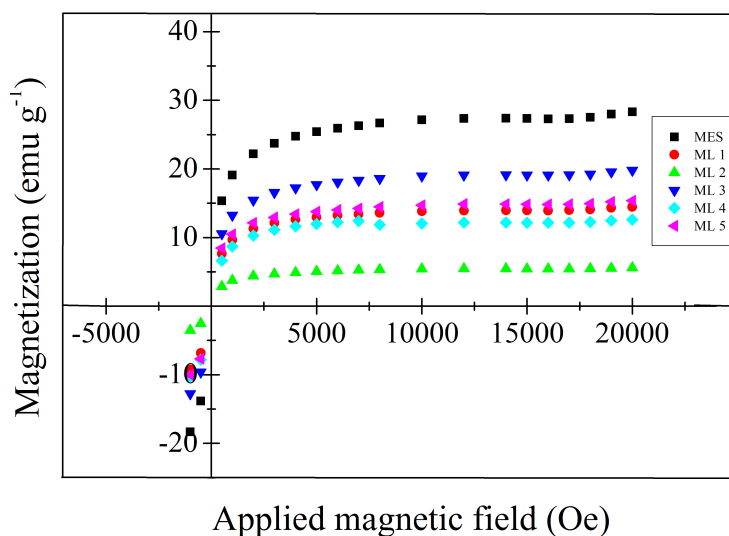
Figure 53. Magnetization curves for the magnetic emulsion, magnetic latexes ML1, ML2, ML3, ML4, and ML5. Measurements were performed at room temperature from samples in a dried state.

5. Conclusion

In order to prepare submicron magnetic latex particles bearing high magnetic properties, oil in water magnetic emulsion was first prepared. After oil phase of the magnetic emulsion evaporation, complete colloidal characterization of the resulting

magnetic dispersion was performed by examining size, size distribution, chemical composition and magnetic properties. Then the oil in water magnetic emulsion was used as seed of radical emulsion polymerization of Styrene (St), cross-linker divinylbenzene (DVB) in the presence of Potassium persulfate (KPS) as initiator

After performing various polymerizations as a function of styrene/ DVB ratio, three types of morphologies were observed; Janus, moon-like Janus towards desired perfect core-shell magnetic latex particles. Core-shell morphology of the magnetic latex nanoparticles is the most favorable for in vitro biomedical diagnostic field. In fact, such well-prepared magnetic core-polymer shell prevents the release of ferric, ferrous and magnetic pigment in the dispersion medium, which are not suitable in any molecular biology based process.

Anyway, the prepared magnetic latexes were characterized using various techniques such as TEM for morphology analysis, light scattering for particle size, TGA for chemical composition, magnetization for magnetic property, and zeta potential measurements as a function of pH for possible surface charge modification and surface charge density. Interestingly, two marked morphologies were obtained: (i) Janus like morphology obtained when 10% of styrene (90% DVB) was used and (ii) perfect core-shell magnetic latex particles was obtained using 60%/40 St/DVB with negligible secondary nucleation. In addition, the obtained core-shell magnetic particles contain a large amount of superparamagnetic iron oxide (approx. 63.9%). Such particles after functionalization step can be used as a solid support in microsystems, microfluidic and Lab-on-a-Chip in which submicron size and fast magnetic separation are necessary.

Supplementary Information
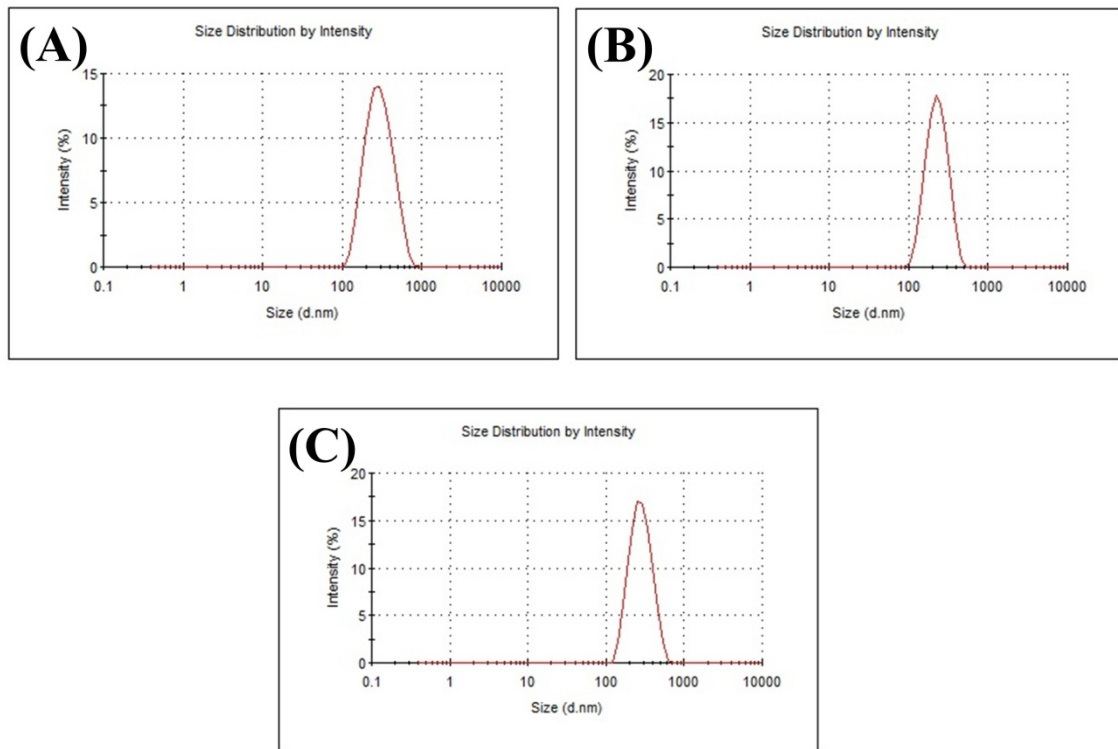
Fig. S1. DLS curves of the magnetic latexes synthesized from seeded-emulsion polymerization. (A) ML1 (Janus morphology), (B) ML2 (moon-like Janus), and (C) ML3 (perfect core-shell).

PARTE II – CAPÍTULO 2

Submicron magnetic core conducting polypyrrole polymer shell: Preparation and characterization

1. Introduction

Conducting polymers (CPs) are carbon-based molecules, which exhibit electrical, optical, and electronic properties analogous to metals. However, if compared to metals, CPs have advantages due to their polymer properties, such as, flexibility, low toxicity, low cost, and easy processing[274]. All these characteristics make CPs a potential material for applications in sensors, fuel cells, energy storage, and so forth[275]. In sensors, the charge transport properties of conducting polymers are changed when exposed to some analytes. This change in transport charge can be correlated directly to the concentration of target analyte[276].

Polyaniline (PANI), polypyrrole (PPy), polythiophene, and their derivatives are a class of CPs which are most studied specially due to their facile synthesis and flexibility in processing[275]. In addition, their conductivity ranges from 10^{-10} S cm^{-1} to 10^{-5} S cm^{-1} [277]. Among CPs, polypyrrole is one of the most extensively used in conducting polymers for the construction of bioanalytical sensors and supporting matrix in electrochemicals due to its good physical and electrical properties, high conductivity, chemical stability, and biocompatibility[278-280]. CPs containing specific functional groups can exhibit individual physicochemical properties if compared to the original polymer. For example, carboxylic acid-functionalized CPs can be used for DNA, proteins, and enzyme immobilization[281, 282].

Magnetic latex (ML) particles have attracted much attention due to their properties, especially superparamagnetism, which makes them responsive to an external magnetic field. This unique property has been exploited in fast separation applications and particularly the *in vitro* biomedical diagnostic domain. In this sense, superparamagnetic nanoparticles have been used in core–shell structures for improving chemical stability of the magnetic core, while the shell can be tuned providing functional groups for specific interactions and applications.

Combining both electrical and magnetic properties in one particle is of paramount importance in order to be used as a carrier and for detection in a sensor field or in any microsystem based on microfluidics. Different approaches have been described to prepare magnetic latex particles. These approaches are based on classical polymerization in dispersed media, such as, emulsion[283], suspension[249], miniemulsion[250], dispersion[251], combination of various polymer-based process[252], and inverse emulsion[254]. The pioneer work was reported by Ugelstad et al.[255] by performing micron magnetic particles in more than two steps. Two of the magnetic latex particles were prepared; 2.8 μm and 4.2 μm size with high sedimentation velocity. On the other hand, Elaissari et al.[154] have reported the synthesis of magnetic latexes using a process called seeded emulsion polymerization. This process leads to submicron ML particles containing high iron oxide content. These prepared functional, submicron, and highly magnetic particles have been used for nucleic acid extraction and purification[256], capturing of analyte in biological samples[257], controlling protein adsorption and desorption as a function of numerous parameters[258], *in vivo* molecular imaging[259], and in immunodiagnostics for specific antigen detection[225].

In order to take advantage of conductive properties from polypyrrole-coated latexes and to improve by that way the accuracy of the biosensing event, in this work, we describe the preparation, and characterization of polypyrrole-coated magnetic particles. To prepare such material, a seeded emulsion polymerization process was used. For obtaining magnetic responsive particles, magnetic emulsion (ME), containing superparamagnetic iron oxide nanoparticles, was used as the seed. In order to obtain acid-functionalized CPs on the particle surface, pyrrole (Py) was copolymerized with pyrrole-2-carboxylic acid (Py-2-COOH). The obtained core–shell magnetic particles were characterized in terms of particle size, size distribution, FTIR analysis, morphology, chemical composition, and finally, both magnetic and electric behaviors were studied. Moreover, the influence of monomer composition on the final morphology was also investigated.

2. Experimental

2.1. Materials

Pyrrole (Py) 98%, povidone (PVP), pyrrole-2-carboxylic acid (Py-2-COOH) 99%, and iron chloride hexahydrate 97% (FeCl$_3$.6H$_2$O) were purchased from Sigma-

Aldrich. The oil-in-water magnetic emulsion (ME) (total solid content 7.9%) consisted of magnetite nanoparticles stabilized with oleic acid, octane, and dodecyl sodium sulfate was acquired from Ademtech S. A. (lot E5 255b-2). Pyrrole was purified by passing through a column of activated basic alumina (Acros) before use. All other reagents were used without further purification and aqueous solutions were prepared with deionized water.

2.2. Synthesis of magnetic particle-coated Py/Py-2-COOH

The seeded-polymerization was carried out in a 25 mL glass reactor using a Teflon paddle stirrer. For each experiment, 1.52 g of magnetic emulsion (ME) (0.12 g dried extract) was weighed, and added into the reactor. Then, the supernatant was removed after 5 min of magnetic separation. After that, 10 mL of aqueous solution containing PVP (stabilizing agent) was added into the reactor and ME was re-dispersed under continuous stirring (300 rpm) for 4 h. Then, desired amounts of Py and Py-2-COOH (monomers) were added into the reactor (see Table 11) with 90 mg $FeCl_3.6H_2O$ (initiator). The reaction was kept under stirring during 12 h at room temperature.

Table 11. Compositions of monomers (Py and Py-2-COOH) and stabilizer (PVP) employed during seeded polymerization.

Sample Name	Py (mmol)	Py-2-COOH (mmol)	PVP (mg)
1600	16	00	20
1608	16	08	20
1616	16	16	20
1632	16	32	20
3232	32	32	20
1616-PVP0	16	16	00
1616-PVP5	16	16	05
1616-PVP10	16	16	10

* 90 mg $FeCl_3.6H_2O$, RT, 12h

3. Characterization

3.1. Transmission electron microscopy

Transmission Electron Microscopy, TEM, was performed with a Philips CM120 microscope at the "*Centre Technologique des Microstructures*" (CTμ) at the University of Lyon (Villeurbanne, France). Briefly, a drop of sample diluted in distilled water was deposited on a carbon-coated copper grid and then left to dry, at room temperature, overnight before TEM imaging.

3.2. Particle size measurements

A Malvern Zetasizer (Nano ZS, Malvern Instruments Limited, UK) was used to measure the average hydrodynamic size (Dh) of the magnetic polymer colloidal particles in 10^{-3} mol L^{-1} NaCl solution. The average of at least five measurements (10 runs for each colloidal dispersion) was taken into consideration.

3.3. Fourier transformed infrared (FTIR)

The investigation of surface properties of the obtained sample was performed using attenuated total reflection–Fourier transformed infrared spectrophotometer (ATR–FTIR) — Shimadzu, Japan. All samples were clean and dry before analysis. The spectra were scanned over range 4000–400 cm^{-1}.

3.4. Zeta potential measurements

Malvern Zetasizer (Nano ZS, Malvern Instruments limited, UK) was used to measure the electrophoretic mobility, which is converted to Smoluchowski's zeta potential. The measurements were performed using a highly diluted dispersion of the considered colloidal particles in 10^{-3} mol L^{-1} NaCl solution at different pH. The pH was adjusted using NaOH or HCl. Each recorded value was the average of three measurements.

3.5. Thermal gravimetric analysis (TGA)

Thermo-gravimetric analysis measurements were carried out on a thermogravimetry analyzer (NETZSCH-TG209F1 Iris®ASC). The measurements were performed under a N_2 atmosphere from ambient temperature up to 1000 °C at a heating rate of 10 °C min^{-1}. Before analysis, the magnetic core–shell particles were separated

from their supernatant by applying a permanent magnetic field and then washed with deionized water. This procedure was done in order to remove the non-magnetic material such as surfactant and free polymer particles. After that, the samples were dried at 40 °C for 24 h before analysis.

3.6. Magnetic properties

The saturation magnetization and magnetic behavior of the dried magnetic polymer latexes were investigated using a vibrating sample magnetometer. Magnetization measurements were carried out at room temperature on the automatic bench of magnetic measurements at CNRS-IRC Lyon.

3.7. Cyclic voltammetry (CV) and impedance measurements (EIS)

Electrochemical characterizations were carried out by using a VMP-3 potentiostat (Biologic CE-Lab VMP3). All measurements for CV and EIS analysis were made at room temperature (approx. 24 °C). The electrolyte for both CV and EIS measurements was made from a redox probe using ferro- and ferricyanide $K_3(Fe(CN)_6)/K_4(Fe(CN)_6)$ at 5 mM in PBS buffer (pH 7.4). Electrochemical measurements were made within a teflon cell in which the gold working electrode (WE) was sandwiched between the two parts of the electrochemical cell (see Supplementary data). Platinum wire was used as the counter electrode (CE) and a calomel saturated electrode was used as the reference electrode (RE). The gold area exposed to the electrolyte was approx. 3 mm in diameter. The volume of ferrocyanide buffer was affixed for all measurements at 1.3 mL.

4. Results and discussions

4.1. Influence of monomer composition on the morphology

Figure 54 shows TEM images of final magnetic particles prepared using different amounts of Py and Py-2-COOH. Polymerizations were conducted using magnetic emulsion (ME) as the seed. During polymerization, the monomers are oxidized under the action of Fe^{3+} ions. This leads to the formation of radical cations of Py/Py-2-COOH, which connect either to monomers/oligomers or polymer chains already synthesized[284].
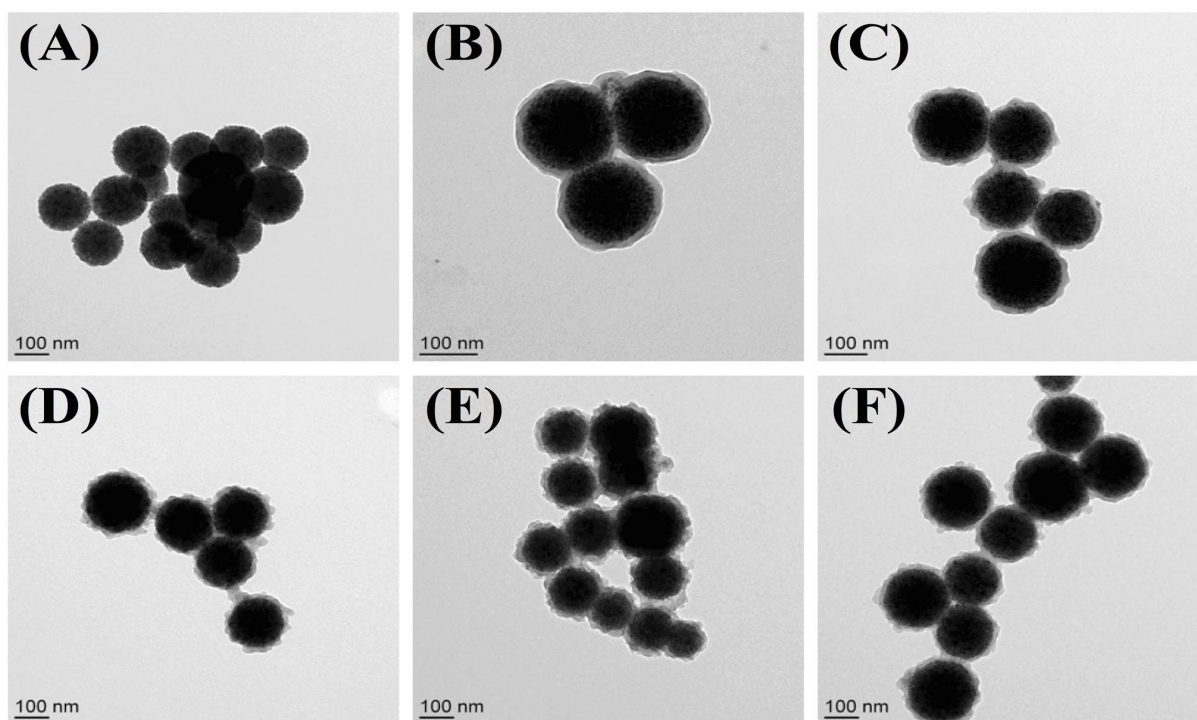
Figure 54. TEM images for samples obtained by seeded-polymerization changing the monomer composition: (A) Magnetic emulsion, (B) 1600, (C) 1608, (D) 1616, (E) 1632, and (F) 3232.

As shown in Figure 54A ME exhibits a spherical shape with a narrowed size distribution. After polymerization using pyrrole, sample 1600 (Figure 54B), a thin and smoothed layer of conducting polymer covering the ME surface was clearly evidenced. The effect of monomer composition on the morphology can be explained in terms of polymer solubility. Polypyrrole (PPy) exhibits poor solubility in water[279], for this reason, polypyrrole has more affinity to the ME surface (which is hydrophobic). During polymerization PPy spreads on the ME surface covering particle surface by a uniform way leading to a smoothed coating. However, when the Py-2-COOH was added to the formulation (Figure 54C to F), core–shells were obtained with a roughness surface. Py-2-COOH has carboxyl groups and when its amount is increased in the polymerization recipe, the formed polymer become more hydrophilic. Consequently, the efficiency on the covering ME surface decreases leading to a rough surface.

4.2. Influence of stabilizer on the morphology

The influence of the PVP amount on the final particle morphology was also investigated. For performing these experiments, sample 1616 was chosen for the comparison rate related to Py and Py-2-COOH. Figure 55A shows the TEM images of sample 1616 synthesized without a stabilizer. It can be seen in this figure that a perfect homogeneous shell could be obtained, but all prepared particles were aggregated and could not be redispersed even using ultrasound. When 5 mg of stabilizer was added to the sample composition, the cluster amount decreased. The same behavior was observed when the PVP amount was 10 mg. However, good dispersion was only obtained when the PVP amount reached 20 mg (see Figure 54D).
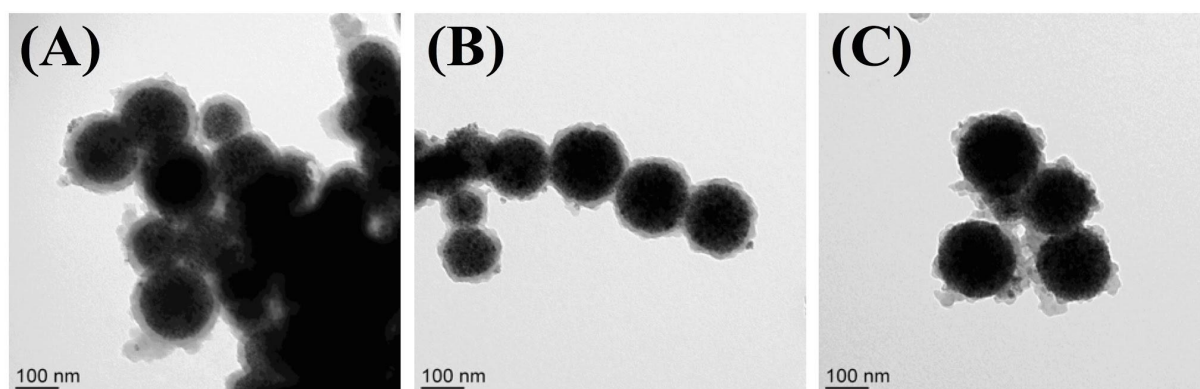
Figure 55. TEM images for samples obtained by seeded-polymerization changing the amount of stabilizer: (A) 1616-PVP0, (B) 1616-PVP5, and (C) 1616-PVP10.

4.3. FTIR results

Figure 56 shows the FTIR spectra of magnetic emulsion (ME), 1600, and 1632 in the spectral range of 2000 cm^{-1} to 800 cm^{-1}. ME was prepared by emulsification of ferrofluid (oil phase) in water solution containing surfactant. Besides that, in the oil phase, iron oxide particles are stabilized with oleic acid (OA). In ME spectra, it could be observed as an absorption band near 1700 cm^{-1} which is ascribed to C=O stretching of free OA[227, 285]. However, for sample 1600, the same one was shifted near 1660 cm^{-1} probably due to interactions between free oleic acid with polypyrrole chains.
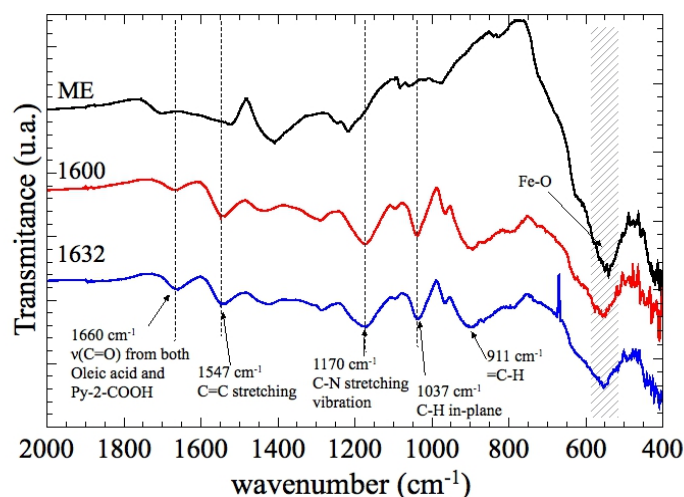
Figure 56. FTIR spectra of magnetic emulsion (ME), sample 1600 and 1632 in the spectral range of 2000 cm^{-1} to 800 cm^{-1}.

On the other hand, for sample 1632, the peak near 1660 cm^{-1} could also be attributed to C=O stretching ($\nu_{C=O}$) from Py-2-COOH segments. The reduction of carbonyl stretching frequencies is associated with two factors: i) The molecule of Pyrrole-2-carboxylic acid has unsaturation in the α,β-position which is conjugated with carboxylic groups. ii) Due interaction by hydrogen bonds, dimers can be formed[142]. Dubis et al. have investigated vibrational models of Py-2-COOH by FTIR and Raman[286]. They found that the Py-2-COOH molecule contains O–H, C=O, and N–H groups which may generate different types of hydrogen-bonded dimers linked either through R–C=O···H–O–R′ or R–C=O···H–N–R′ groups. Thus, the absorption band of C=O stretching of Py-2-COOH can be found between 1685 cm^{-1} and 1660 cm^{-1} overlapping the same $\nu_{C=O}$ absorption band of OA.

The high-intensity band near 570 cm^{-1}, corresponding to Fe–O stretching vibration, was observed in all samples indicating the presence of the magnetic phase in polymer particles[278, 284]. In addition, peaks at 1547 cm^{-1} and 1037 cm^{-1} were attributed, respectively, to C=C stretching and =C–H in plane bending vibration from poly(pyrrole-co-pyrrole-2-carboxylic acid) rings; the peak at 1170 cm^{-1} was ascribed to C–N stretching vibration[275, 287]. While the signal at 911 cm^{-1} was attributed to =C–H out-of-plane bending vibration[288].

4.4. Thermogravimetric analysis

Figure 57A shows the thermogram of ME used as the seed during polymerization. These experiments were carried out under N_2 atmosphere. In this figure, it can be visualized that degradation of magnetic emulsion could be divided into three steps: (i) 25–500 °C, (ii) 501–850 °C, and (iii) above 850 °C. The first step is associated with degradation of the organic part (approx. 20%), which corresponds to the used oleic acid surfactants in ME preparation. The second step is attributed to the phase transition from Fe_3O_4 to FeO (weight loss approx. 2.5%), because FeO is thermodynamically stable above 570 °C [199]. The third one is attributed to reduction of FeO. In this case, FeO is totally converted to Fe^0 when the temperature is higher than 850 °C [199, 229].
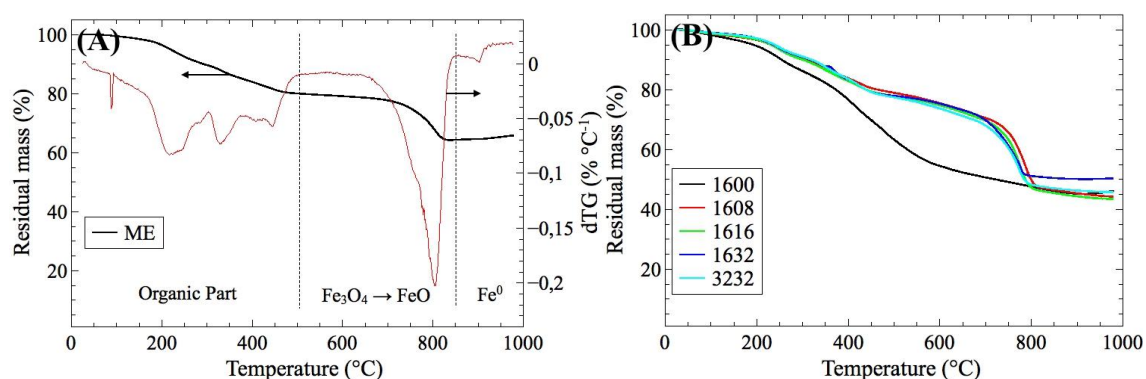
Figure 57. Thermogravimetric curves of dried samples. (A) TGA and dTG of magnetic emulsion seed, (B) TGA of magnetic latexes.

Figure 57B shows the TGA results of magnetic latexes. In this figure, it could be observed that degradation steps up to 800 °C overlapping each other, then it was difficult to estimate the exact polymer contents. In addition, it is important to point out the presence of a new degradation step (between 400–760 °C) for samples 1608, 1616, 1632, and 3232. This difference on the degradation step may be associated with the presence of Py-2-COOH copolymerized on the particle shell. The same thermal behavior is observed for samples 1616-PVP0, 1616-PVP5, and 1616-PVP10 (see Supplementary data).

When degradation temperature is higher than 850 °C the residual mass became constant indicating that organic parts (oleic acid, polymers, and surfactants) were completely removed and the iron content on each sample could be estimated, as shown in Table 12. For all samples, the percentages in weight (wt.%) were between 45–52%.

These values are very close; indicating that the percentage of iron encapsulated was not affected by the used recipe.

Table 12. Particle size, iron oxide content, and magnetic content of the obtained particles.

Sample name	Particle size (nm)	Iron content (% wt)[a]	Magnetic content (% wt)[c]
ME	193 ± 5	65.8	ND
1600	276 ± 25	45.0	72.1
1608	294 ± 24	45.3	95.1
1616	277 ± 33	44.3	92.7
1632	672 ± 125[b]	50.1	86.3
3232	283 ± 9	46.2	82.3
1616-PVP0	583 ± 217[b]	50.0	ND
1616-PVP5	404 ± 48[b]	50.6	ND
1616-PVP10	327 ± 37[b]	51.1	ND

a. Determined by TGA; b. Particle agglomeration; c. Determined by magnetization; ND. Not Determined.

4.5. Magnetic properties

Magnetic curves for the dried latexes obtained by seeded polymerization are presented in Figure 58. According to the results, all the samples showed superparamagnetic characteristics at room temperature. The saturation magnetization (SM) for magnetic emulsion was 41.54 emu g^{-1} while, for all samples, SM values were between 29 emu g^{-1} and 36 emu g^{-1}. Magnetic content was calculated by the following equation:

$$Magnetic\ content = \frac{MS}{MS_0} \times 100 \tag{9}$$

where MS is the saturation magnetization of dry magnetic latex particles, and MS_0 is the saturation magnetization of dry magnetic emulsion[2]. The results are shown in Table 12. The samples showed magnetic contents higher than 80 wt.% (except for sample 1600).

However, both the magnetic properties and the magnetic contents were not dependent of the experimental conditions.

According to papers published elsewhere, saturation magnetization (SM) of iron oxide can be found between 60 emu g^{-1} and 80 emu g^{-1} depending on the predominant crystalline phase[225, 257, 289]. In our work, oil in water magnetic emulsion (ME) was used. The magnetic emulsion is obtained dispersing iron oxide in octane followed by dispersion in water using surfactants (i.e. SDS). Therefore, magnetic emulsion has a significant percentage of non-magnetic material on its composition, which, in turn, contributes to decrease saturation magnetization to 41.54 emu g^{-1}. In this work, magnetic emulsion was used as the seed during polymerization. Thus its saturation magnetization value was used as reference. For core–shell particles, the percentage of non-magnetic material was increased after coating magnetic emulsion with poly(pyrrole-*co*-pyrrole-2-carboxylic acid). As a consequence, saturation magnetization of core–shell particles decreases as can be observed in Figure 58. However, if compared to the reference sample, saturation magnetization values of core–shell particles decreased slightly indicating the presence of a thin polymeric external layer with a huge amount of magnetic material in their core.
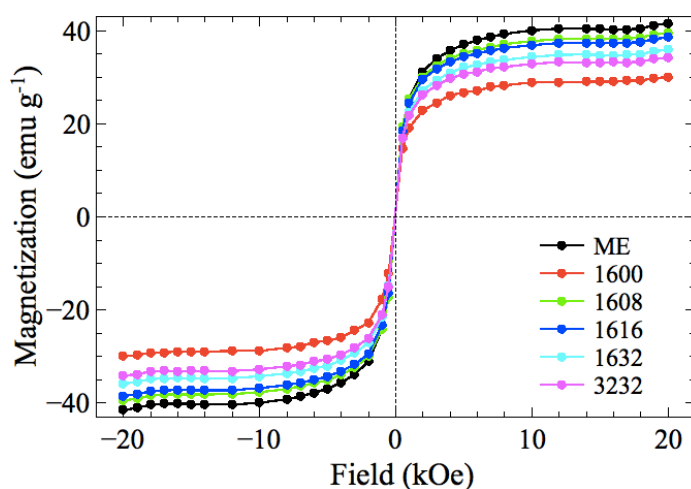
Figure 58. Magnetization curves of superparamagnetic polymeric particles obtained by seeded polymerization with different Py and Py-2-COOH contents.

4.6. Particle size

For samples 1600, 1608, 1616, and 3232 the average size was between 270–295 nm. However, when the amount of Py-2-COOH was increase two times, if compared

to 1616, sample 1632 showed an average size of 672 nm. The reason of this high value in size may be associated with particle agglomeration during the earlier stages of polymerization. The carbonyl groups from Py-2-COOH present on the Fe_3O_4 surface may interact with other iron oxide particles favoring particle agglomeration.

The effect of PVP (stabilizer) on the particle size was also investigated. It can be seen in Table 12 that final particle size decreased from 583 nm to 277 nm when the amount of PVP was increased from 0 to 20 mg evidencing the role of stabilizer during the synthesis.

4.7. Cyclic voltammetry (CV)

In order to have an insight about the sample conductivity, the core–shell particles were electrochemically deposited on gold substrate using CV technique. For each sample of magnetic dispersion, a new gold working electrode was used. The window of potential for electrodeposition was from − 0.4 V to 0.6 V with a scan rate of 100 mV s^{-1}. While CV technique was applied from − 0.3 to 0.5 V with a scan rate of 100 mV s^{-1}.

Figure 59 shows the CV characterization of conducting magnetic particles (CMP) obtained after electrodeposition on bare gold (BG). Electrodes containing particles showed a single electron oxidation-process similar to the bare gold. Cathodic and anodic peaks were respectively 0.1 and 0.3 V vs SCE. It can be seen in Figure 59A that the peak current of BG containing magnetic particles changed with monomer composition. As shown in Figure 59A, the peak current increased with the increase of pyrrole concentration (samples 1600, 1608, and 1616). However, a contrary effect was observed when the amount of Py-2-COOH increased. This behavior may be associated with the influence of carboxylic amount on the particle surface. In fact, when Py-2-COOH was used in high concentrations, electron transfer was hindered. This hypothesis is also supported by analyzing the difference in potential (ΔE) between the anodic and cathodic peaks. The samples 1600, 1608, and 1616 showed ΔE near to +0.2V while samples 1632 and 3232 showed ΔE near to +0.3V indicating that the electron-transfer potential increased when the Py-2-COOH concentration increased.

Figure 59B shows cyclic voltammetry characterization of BG after electrodeposition of conducting magnetic particles changing PVP amount. In this case, except for sample 1616-PVP5, no significant variation in the peak current by addition of PVP during particle preparation was observed.
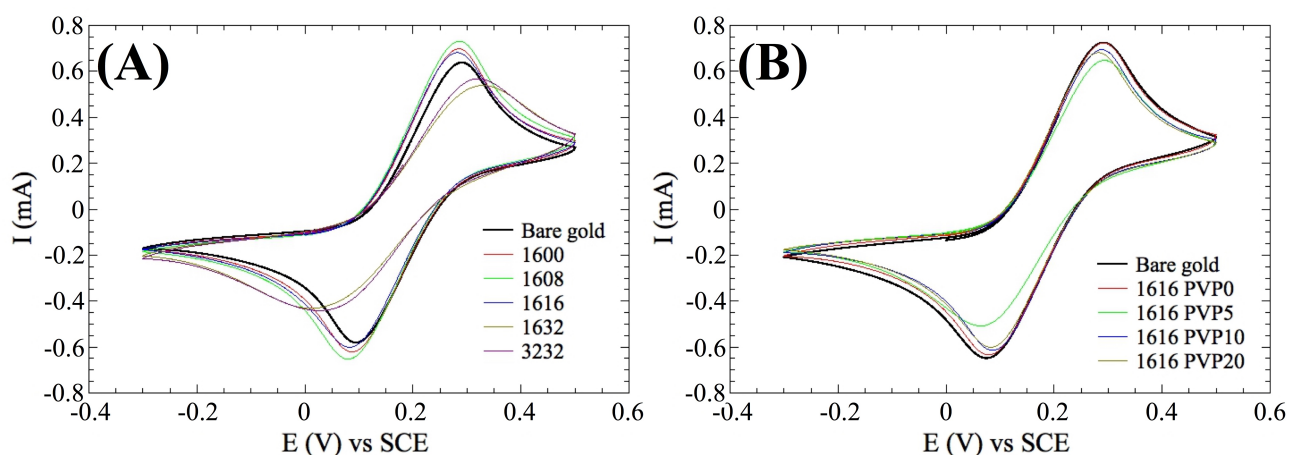
Figure 59. CV characterization after electrodeposition of conducting magnetic particles: (A) Changing monomers composition, and (B) changing PVP amount.

4.8. Impedance spectroscopy

Impedance spectroscopy analyses (Figure 60) were performed after each electrodeposition of different samples. The applied potential at the WE was 0.228 V within a window of frequency from 100 mHZ to 200 kHz. As it was mentioned in the cyclic voltammetry part, the conductivity of the WE surface has increased (decrease of impedance) after MNP deposition for samples: 1600, 1608 and 1616, which can be correlated to the high conductivity of PPy. By increasing the Py-2-COOH concentration (sample 1632), the impedance has increased thus highlighting a deposition of an insulating layer onto the WE surface, which is in agreement with CV characterization after MNP electrodeposition. The same behavior of impedance was also seen for sample 3232 even when the concentration of Ppy was increased from 16 mmol (sample 1632) to 32 mmol (sample 3232). This was due to the high concentration of carboxylic acid amount, which may affect the polymerization of Ppy during the synthesis process of MNP, thus allowing a decrease of the electrical signal of WE after magnetic particle deposition.
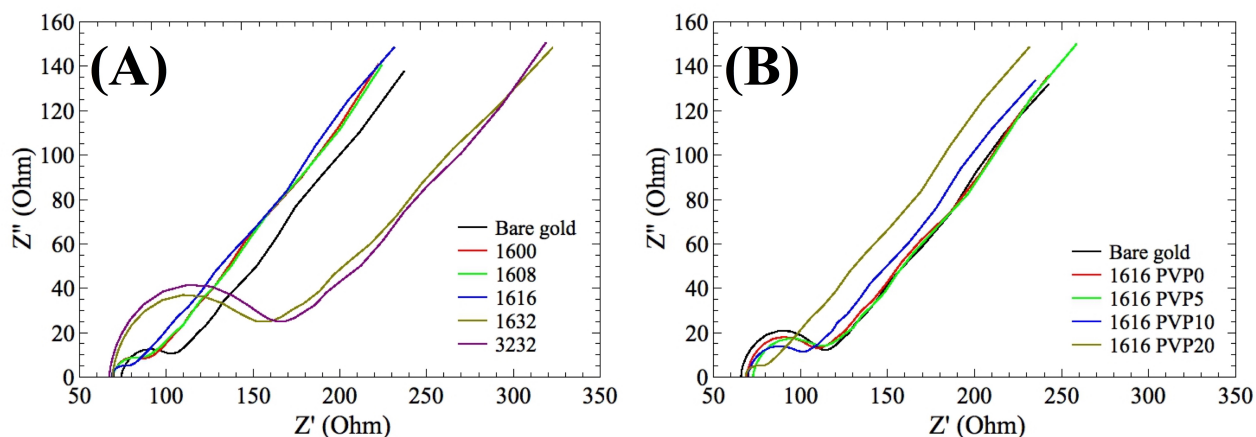
Figure 60. Impedance spectroscopy analysis before and after electrodeposition of modified MNP for different sample composition: (A) Changing monomers composition, and (B) changing PVP amount.

5. Conclusions

Conducting magnetic particles were successfully synthesized by a simple chemical route. The resulting magnetic core-conducting polymer shell has both ferromagnetic and electric properties as shown by magnetization, cyclic voltammetry and impedance spectroscopy analysis results. Properties of the obtained material can be adjusted by changing Py-2-COOH initial concentration during polymerization. Neither final morphology nor electric properties were changed by the presence of a stabilizing agent (PVP). However, the use of PVP during the synthesis is important to control the colloidal stability and also the shell morphology as shown via size measurements and TEM analysis. The prepared magnetic particles showed conducting property and superparamagnetic behavior, which is important for fast separation under magnetic field when used for sample preparation for instance. In addition, due to the presence of Py-2-COOH in the polymer shell, covalent coupling of amine containing biomolecules (oligonucleotides, proteins, and antibodies, specific ligands) will be possible and for sensors and lab-on-a-chip, microsystems, and microfluidic use.

Supplementary Information
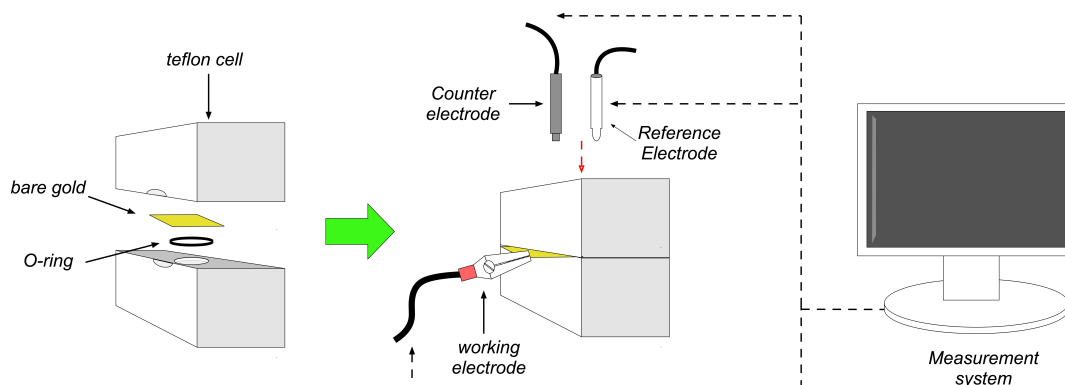
Figure S1. Experimental apparatus for performing cyclic voltammetry and impedance spectroscopy measurements.
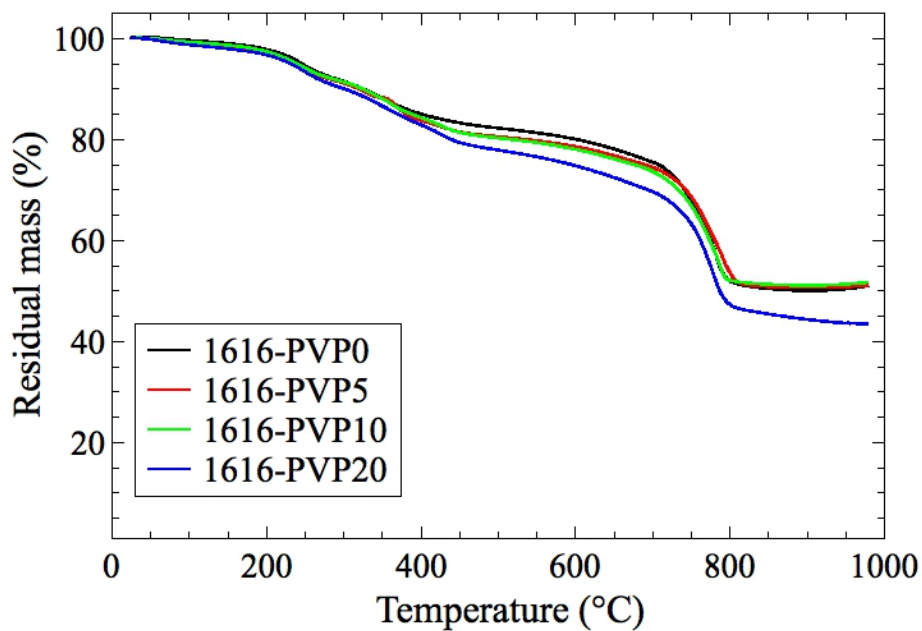
Figure S2. Thermogravimetric curves of dried samples containing different amount of stabilizer (PVP).
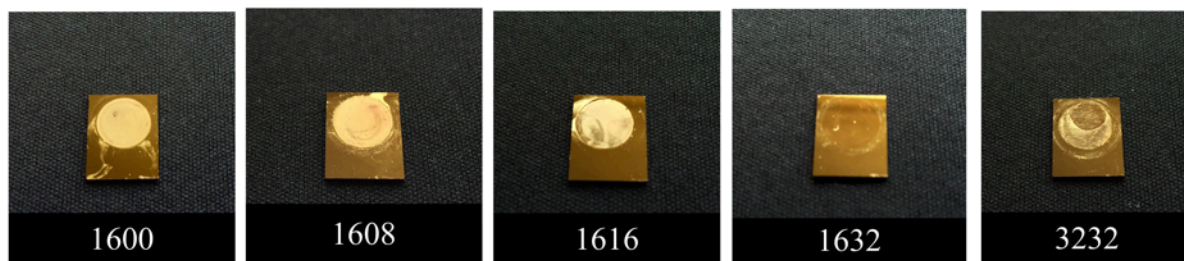
Figure S3. Digital images taken from bare gold electrode after electrodeposition: Changing monomers composition.
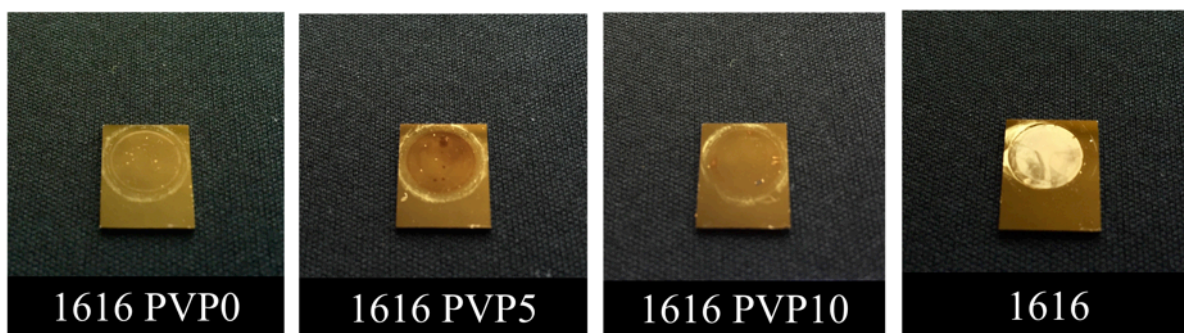
Figure S4. Digital images taken from bare gold electrode after electrodeposition: Changing amount of PVP.
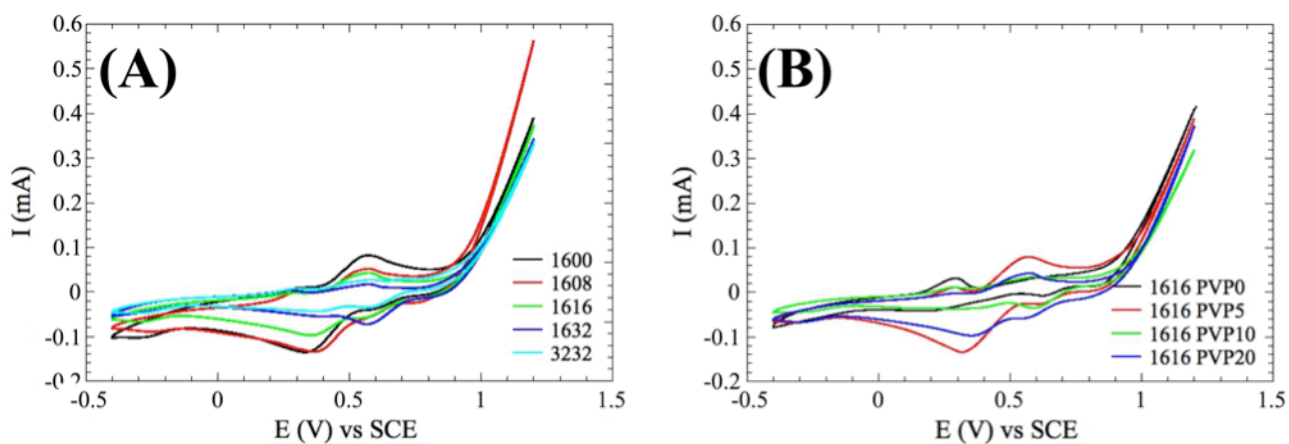
Figure S5. Electrodeposition essay of conducting magnetic nanoparticle on bare gold: (A) varying monomers composition, and (B) sample 1616 changing amount of PVP.

CONCLUSÕES FINAIS

Nesta tese, foram abordadas diferentes técnicas para a obtenção de materiais híbridos. Inicialmente, um hidrogel pH-responsivo baseado em poli(etileno glicol) foi sintetizado e caracterizado. Observou-se que o PEG modificado com GMA atua como constituinte chave do hidrogel, sendo que algumas amostras, quando intumescidas em pH ácido, apresentaram seus poros totalmente destruídos, indicando, uma possível degradação do polímero nesse meio. As condições experimentais que levaram à síntese de hidrogéis com as melhores performances no intumescimento, foram utilizadas para obter-se um hidrogel com propriedades magnéticas e pH-responsivas. Utilizando a Prednisolona, como fármaco modelo, verificou-se que a velocidade de liberação de fármaco pode ser controlada por meio de um campo magnético externo. Além disso, os hidrogéis apresentaram baixa toxicidade e, portanto, possuem um grande potencial para ser aplicado como matriz polimérica na encapsulação de fármacos.

Em um segundo momento, objetivou-se a síntese de partículas magnéticas em tamanho submicrométrico para aplicação em biossensores. Inicialmente, otimizou-se os parâmetros experimentais de síntese utilizando estireno e o divinilbenzeno como referencia. Observou-se que a composição da mistura de monômeros influencia diretamente a morfologia final dos materiais nanoparticulados. Com os resultados obtidos, estabeleceu-se uma rota de síntese na polimerização em emulsão semeada, a fim de se obter partículas com propriedades elétricas e magnéticas baseadas em polipirrol. Quando as partículas foram eletro-depositadas em barras de ouro, observou-se um aumento na condutividade do substrato. Além disso, as partículas apresentaram um comportamento superparamagnético, que é essencial para ser aplicado em etapas de concentração/captura de compostos alvo bem como na sua detecção.

PERSPECTIVAS FUTURAS

A área biomédica é de extrema importância para a sociedade. A cada dia, novos materiais são desenvolvidos seja com o objetivo de otimizar procedimentos já estabelecidos ou de fornecer novas técnicas para o tratamento de doenças. Assim sendo, este trabalho oferece informações que podem ser utilizados para a obtenção de novos materiais híbridos magnéticos para diferentes finalidades. Embora os materiais obtidos durante este trabalho de doutorado apresentem morfologia e propriedades distintas, as suas aplicações são semelhantes. Por exemplo, ambos os materiais podem ser aplicados para a liberação controlada de fármacos, sensores e áreas intermediárias à estas aplicações.

Por este motivo, novos materiais podem ser obtidos investigando somente os hidrogéis magnéticos de PEG ou somente as partículas magnéticas de polipirrol com tamanho submicrométrico. Além disso, ambos os materiais podem ser combinados para a obtenção, por exemplo, de nanogéis do tipo *core-shell* com propriedades elétricas e magnéticas para aplicações voltadas tanto para terapia quanto para o diagnóstico de doenças.

Ainda há muitos caminhos para serem trilhados, em especial, ao que concerne o desenvolvimento de novos materiais. Nessa longa caminhada, muito passos foram dados e serviram como base de orientação no desenvolvimento de novas tecnologias. Assim sendo, acredito que esta tese possa vir a ter um papel importante na pesquisa, na obtenção de novos materiais e em suas aplicações.

REFERÊNCIAS

1. KICKELBICK, G., Hybrid Materials - Past, Present and Future. **Hybrid Materials**, 1: 39-51, 2014.

2. TENORIO-NETO, E. T.,JAMSHAID, T.,EISSA, M.,KUNITA, M. H.,ZINE, N.,AGUSTI, G.,FESSI, H.,EL-SALHI, A. E.,ELAISSARI, A., TGA and magnetization measurements for determination of composition and polymer conversion of magnetic hybrid particles. **Polymers for Advanced Technologies**, 26: 1199-1208, 2015.

3. JAMSHAID, T.,TENORIO-NETO, E. T.,EISSA, M.,ZINE, N.,EL-SALHI, A. E.,KUNITA, M. H.,ELAISSARI, A., Preparation and characterization of submicron hybrid magnetic latex particles. **Polymers for Advanced Technologies**, 26: 1102-1108, 2015.

4. WISE, N.,GROB, T.,MORTEN, K.,THOMPSON, I.,SHEARD, S., Magnetophoretic velocities of superparamagnetic particles, agglomerates and complexes. **Journal of Magnetism and Magnetic Materials**, 384: 328-334, 2015.

5. LIMA-TENORIO, M. K.,TENORIO-NETO, E. T.,GUILHERME, M. R.,GARCIA, F. P.,NAKAMURA, C. V.,PINEDA, E. A. G.,RUBIRA, A. F., Water transport properties through starch-based hydrogel nanocomposites responding to both pH and a remote magnetic field. **Chemical Engineering Journal**, 259: 620-629, 2015.

6. LIMA-TENÓRIO, M. K.,TENÓRIO-NETO, E. T.,GARCIA, F. P.,NAKAMURA, C. V.,GUILHERME, M. R.,MUNIZ, E. C.,PINEDA, E. A. G.,RUBIRA, A. F., Hydrogel nanocomposite based on starch and Co-doped zinc ferrite nanoparticles that shows magnetic field-responsive drug release changes. **Journal of Molecular Liquids**, 210, Part A: 100-105, 2015.

7. JAN, K.,KIRAT, S.,ALAN, O. N.,CARL, J.,ALAN, M.,PETER, O. B., Development of a microfluidic device for fluorescence activated cell sorting. **Journal of Micromechanics and Microengineering**, 12: 486, 2002.

8. ARRUEBO, M.,FERNANDEZ-PACHECO, R.,IBARRA, M. R.,SANTAMARIA, J., Magnetic nanoparticles for drug delivery. **Nano Today**, 2: 22-32, 2007.

9. RANZONI, A.,SABATTE, G.,VAN IJZENDOORN, L. J.,PRINS, M. W. J., One-Step Homogeneous Magnetic Nanoparticle Immunoassay for Biomarker Detection Directly in Blood Plasma. **ACS Nano**, 6: 3134-3141, 2012.

10. BAL, T.,KEPSUTLU, B.,KIZILEL, S., Characterization of protein release from poly(ethylene glycol) hydrogels with crosslink density gradients. **Journal of Biomedical Materials Research Part A**, 102: 487-495, 2014.

11. ALEXANDER, A.,AJAZUDDIN,KHAN, J.,SARAF, S.,SARAF, S., Poly(ethylene glycol)-poly(lactic-co-glycolic acid) based thermosensitive injectable hydrogels for biomedical applications. **Journal of Controlled Release**, 172: 715-729, 2013.

12. GUILHERME, M. R.,AOUADA, F. A.,FAJARDO, A. R.,MARTINS, A. F.,PAULINO, A. T.,DAVI, M. F. T.,RUBIRA, A. F.,MUNIZ, E. C., Superabsorbent hydrogels based on polysaccharides for application in agriculture as soil conditioner and nutrient carrier: A review. **European Polymer Journal**, 72: 365-385, 2015.

13. GIBAS, I.,JANIK, H., Synthetic polymer hydrogels for biomedical applications. **Chemistry & Chemical Technology**, 4: 297-304, 2010.

14. AHMED, E. M., Hydrogel: Preparation, characterization, and applications: A review. **Journal of Advanced Research**, 6: 105-121, 2015.

15. ZHU, J. M.,MARCHANT, R. E., Design properties of hydrogel tissue-engineering scaffolds. **Expert Review of Medical Devices**, 8: 607-626, 2011.

16. DASH, R.,CATETO, C. A.,RAGAUSKAS, A. J., Synthesis of a co-cross-linked nanocomposite hydrogels from poly(methyl vinyl ether-co-maleic acid)-polyethylene glycol and nanofibrillated cellulose. **Cellulose**, 21: 529-534, 2014.

17. CALÓ, E.,KHUTORYANSKIY, V. V., Biomedical applications of hydrogels: A review of patents and commercial products. **European Polymer Journal**, 65: 252-267, 2015.

18. LI, Z.,SHEN, J.,MA, H.,LU, X.,SHI, M.,LI, N.,YE, M., Preparation and characterization of pH- and temperature-responsive nanocomposite double

network hydrogels. **Materials Science and Engineering: C**, 33: 1951-1957, 2013.

19. CHEN, J.,LIU, M.,LIU, H.,MA, L.,GAO, C.,ZHU, S.,ZHANG, S., Synthesis and properties of thermo- and pH-sensitive poly(diallyldimethylammonium chloride)/poly(N,N-diethylacrylamide) semi-IPN hydrogel. **Chemical Engineering Journal**, 159: 247-256, 2010.

20. ALTHANS, D.,SCHRADER, P.,ENDERS, S., Solubilisation of quercetin: Comparison of hyperbranched polymer and hydrogel. **Journal of Molecular Liquids**, 196: 86-93, 2014.

21. TENORIO-NETO, E. T.,GUILHERME, M. R.,LIMA-TENORIO, M. K.,SCARIOT, D. B.,NAKAMURA, C. V.,RUBIRA, A. F.,KUNITA, M. H., Synthesis and characterization of a pH-responsive poly(ethylene glycol)-based hydrogel: acid degradation, equilibrium swelling, and absorption kinetic characteristics. **Colloid and Polymer Science**, 293: 3611-3622, 2015.

22. ZHU, J., Bioactive modification of poly(ethylene glycol) hydrogels for tissue engineering. **Biomaterials**, 31: 4639-4656, 2010.

23. KOETTING, M. C.,PETERS, J. T.,STEICHEN, S. D.,PEPPAS, N. A., Stimulus-responsive hydrogels: Theory, modern advances, and applications. **Materials Science and Engineering: R: Reports**, 93: 1-49, 2015.

24. TRUONG, V.,BLAKEY, I.,WHITTAKER, A. K., Hydrophilic and Amphiphilic Polyethylene Glycol-Based Hydrogels with Tunable Degradability Prepared by "Click" Chemistry. **Biomacromolecules**, 13: 4012-4021, 2012.

25. POURMOAZZEN, Z.,BAGHERI, M.,ENTEZAMI, A. A.,KOSHKI, K. N., pH-responsive micelles composed of poly(ethylene glycol) and cholesterol-modified poly(monomethyl itaconate) as a nanocarrier for controlled and targeted release of piroxicam. **Journal of Polymer Research**, 20: 1-12, 2013.

26. PENG, L.,LIU, T.,LIU, S.,HAN, Y.,LI, X.,GUANG, N.,SHENG, W., Sol–gel transition of novel temperature responsive ABA triblock copolymer P(MEO2MA-co-HMAM)-b-PEG-b-P(MEO2MA-co- HMAM). **Journal of Polymer Research**, 22: 1-12, 2015.

27. LEE, B. H.,KIM, M. H.,LEE, J. H.,SELIKTAR, D.,CHO, N. J.,TAN, L. P., Modulation of Huh7.5 Spheroid Formation and Functionality Using Modified PEG-Based Hydrogels of Different Stiffness. **Plos One**, 10: 20, 2015.

28. BENCHERIF, S. A.,SRINIVASAN, A.,SHEEHAN, J. A.,WALKER, L. M.,GAYATHRI, C.,GIL, R.,HOLLINGER, J. O.,MATYJASZEWSKI, K.,WASHBURN, N. R., End-group effects on the properties of PEG-co-PGA hydrogels. **Acta Biomaterialia**, 5: 1872-1883, 2009.

29. JO, S.,SHIN, H.,SHUNG, A. K.,FISHER, J. P.,MIKOS, A. G., Synthesis and Characterization of Oligo(poly(ethylene glycol) fumarate) Macromer. **Macromolecules**, 34: 2839-2844, 2001.

30. WANG, Y. P.,YAN, L. S.,LI, B.,QI, Y. X.,XIE, Z. G.,JING, X. B.,CHEN, X. S.,HUANG, Y. B., Protein-Resistant Biodegradable Amphiphilic Graft Copolymer Vesicles as Protein Carriers. **Macromolecular Bioscience**, 15: 1304-1313, 2015.

31. O'LENICK, T. G.,JIANG, X.,ZHAO, B., Thermosensitive Aqueous Gels with Tunable Sol−Gel Transition Temperatures from Thermo- and pH-Responsive Hydrophilic ABA Triblock Copolymer. **Langmuir**, 26: 8787-8796, 2010.

32. ALMANY, L.,SELIKTAR, D., Biosynthetic hydrogel scaffolds made from fibrinogen and polyethylene glycol for 3D cell cultures. **Biomaterials**, 26: 2467-2477, 2005.

33. ZHENG, Y.,NGUYEN, M. K.,HE, C.,HUYNH, C. T.,LEE, D. S., pH- and temperature-sensitive PCL-grafted poly(β-amino ester)-poly(ethylene glycol)-poly(β-amino ester) copolymer hydrogels. **Macromolecular Research**, 18: 1096-1102, 2010.

34. PARK, S.,LEE, Y.,KIM, D. N.,PARK, S.,JANG, E.,KOH, W.-G., Entrapment of enzyme-linked magnetic nanoparticles within poly(ethylene glycol) hydrogel microparticles prepared by photopatterning. **Reactive and Functional Polymers**, 69: 293-299, 2009.

35. WANG, Q. F.,REN, L.,XU, C. X.,ZHAI, Z. C.,ZHOU, J. A.,YAO, Y. C.,XIA, H.,WANG, Y. J., Synthesis and Characterization of Glucosamine Modified Poly(ethylene glycol) Hydrogels via Photopolymerization. **Journal of Applied Polymer Science**, 128: 89-96, 2013.

36. TSAI, B. H.,LIN, C. H.,LIN, J. C., Synthesis and property evaluations of photocrosslinkable chitosan derivative and its photocopolymerization with poly(ethylene glycol). **Journal of Applied Polymer Science**, 100: 1794-1801, 2006.

37. PAHIMANOLIS, N.,SORVARI, A.,LUONG, N. D.,SEPPÄLÄ, J., Thermoresponsive xylan hydrogels via copper-catalyzed azide-alkyne cycloaddition. **Carbohydrate Polymers**, 102: 637-644, 2014.

38. VAN HOVE, A. H.,WILSON, B. D.,BENOIT, D. S. W., Microwave-assisted Functionalization of Poly(ethylene glycol) and On-resin Peptides for Use in Chain Polymerizations and Hydrogel Formation. **Jove-Journal of Visualized Experiments**: 16, 2013.

39. LIU, C. B.,GONG, C. Y.,HUANG, M. J.,WANG, J. W.,PAN, Y. F.,DE ZHANG, Y.,LI, G. Z.,GOU, M. L.,WANG, K.,TU, M. J.,WEI, Y. Q.,QIAN, Z. Y., Thermo reversible gel-sol behavior of biodegradable PCL-PEG-PCL triblock copolymer in aqueous solutions. **Journal of Biomedical Materials Research Part B-Applied Biomaterials**, 84B: 165-175, 2008.

40. MA, D.,ZHANG, L.-M., Fabrication and Modulation of Magnetically Supramolecular Hydrogels. **The Journal of Physical Chemistry B**, 112: 6315-6321, 2008.

41. BENCHERIF, S. A.,SHEEHAN, J. A.,HOLLINGER, J. O.,WALKER, L. M.,MATYJASZEWSKI, K.,WASHBURN, N. R., Influence of cross-linker chemistry on release kinetics of PEG-co-PGA hydrogels. **Journal of Biomedical Materials Research Part A**, 90A: 142-153, 2009.

42. LI, S. M.,RASHKOV, I.,ESPARTERO, J. L.,MANOLOVA, N.,VERT, M., Synthesis, Characterization, and Hydrolytic Degradation of PLA/PEO/PLA Triblock Copolymers with Long Poly(l-lactic acid) Blocks. **Macromolecules**, 29: 57-62, 1996.

43. DU, H.,ZHA, G.,GAO, L.,WANG, H.,LI, X.,SHEN, Z.,ZHU, W., Fully biodegradable antibacterial hydrogels via thiol-ene "click" chemistry. **Polymer Chemistry**, 5: 4002-4008, 2014.

44. BADIGER, M. V.,MCNEILL, M. E.,GRAHAM, N. B., Porogens in the preparation of microporous hydrogels based on poly(ethylene oxides). **Biomaterials**, 14: 1059-1063, 1993.

45. CHEN, Z.,ZHAO, M.,LIU, K.,WAN, Y.,LI, X.,FENG, G., Novel chitosan hydrogel formed by ethylene glycol chitosan, 1,6-diisocyanatohexan and polyethylene glycol-400 for tissue engineering scaffold: in vitro and in vivo

evaluation. **Journal of Materials Science: Materials in Medicine**, 25: 1903-1913, 2014.

46. BERDICHEVSKI, A.,SHACHAF, Y.,WECHSLER, R.,SELIKTAR, D., Protein composition alters in vivo resorption of PEG-based hydrogels as monitored by contrast-enhanced MRI. **Biomaterials**, 42: 1-10, 2015.

47. KAR, M.,VERNON SHIH, Y.-R.,VELEZ, D. O.,CABRALES, P.,VARGHESE, S., Poly(ethylene glycol) hydrogels with cell cleavable groups for autonomous cell delivery. **Biomaterials**, 77: 186-197, 2016.

48. KHOUSHABI, A.,SCHMOCKER, A.,PIOLETTI, D. P.,MOSER, C.,SCHIZAS, C.,MANSON, J. A.,BOURBAN, P. E., Photo-polymerization, swelling and mechanical properties of cellulose fibre reinforced poly(ethylene glycol) hydrogels. **Composites Science and Technology**, 119: 93-99, 2015.

49. YANG, X.,JI, X.,SHI, C.,LIU, J.,WANG, H.,LUAN, Y., Investigation on the ion pair amphiphiles and their in vitro release of amantadine drug based on PLGA–PEG–PLGA gel. **Journal of Nanoparticle Research**, 16: 1-14, 2014.

50. GONG, C.,SHI, S.,WU, L.,GOU, M.,YIN, Q.,GUO, Q.,DONG, P.,ZHANG, F.,LUO, F.,ZHAO, X.,WEI, Y.,QIAN, Z., Biodegradable in situ gel-forming controlled drug delivery system based on thermosensitive PCL–PEG–PCL hydrogel. Part 2: Sol–gel–sol transition and drug delivery behavior. **Acta Biomaterialia**, 5: 3358-3370, 2009.

51. HENNINK, W. E.,VAN NOSTRUM, C. F., Novel crosslinking methods to design hydrogels. **Advanced Drug Delivery Reviews**, 64, Supplement: 223-236, 2012.

52. ULLAH, F.,OTHMAN, M. B. H.,JAVED, F.,AHMAD, Z.,AKIL, H. M., Classification, processing and application of hydrogels: A review. **Materials Science and Engineering: C**, 57: 414-433, 2015.

53. MAITRA, J.,SHUKLA, V. K., Cross-linking in Hydrogels - A review. **American Journal of Polymer Science**, 6: 25-31, 2014.

54. JABBARI, E.,KHADEMHOSSEINI, A., Biologically-Responsive Hybrid Biomaterials: A Reference for Material Scientists and Bioengineers. World Scientific. 2010.

55. PONNUMALLAYAN, P.,FEE, C. J., Reversible and Rapid pH-Regulated Self-Assembly of a Poly(ethylene glycol)–Peptide Bioconjugate. **Langmuir**, 30: 14250-14256, 2014.

56. CIRILLO, G.,HAMPEL, S.,SPIZZIRRI, U. G.,PARISI, O. I.,PICCI, N.,IEMMA, F., Carbon Nanotubes Hybrid Hydrogels in Drug Delivery: A Perspective Review. **Biomed Research International**: 17, 2014.

57. PAPAPHILIPPOU, P.,CHRISTODOULOU, M.,MARINICA, O.-M.,TACULESCU, A.,VEKAS, L.,CHRISSAFIS, K.,KRASIA-CHRISTOFOROU, T., Multiresponsive Polymer Conetworks Capable of Responding to Changes in pH, Temperature, and Magnetic Field: Synthesis, Characterization, and Evaluation of Their Ability for Controlled Uptake and Release of Solutes. **ACS Applied Materials & Interfaces**, 4: 2139-2147, 2012.

58. LI, Y. H.,HUANG, G. Y.,ZHANG, X. H.,LI, B. Q.,CHEN, Y. M.,LU, T. L.,LU, T. J.,XU, F., Magnetic Hydrogels and Their Potential Biomedical Applications. **Advanced Functional Materials**, 23: 660-672, 2013.

59. MEENACH, S. A.,ANDERSON, A. A.,SUTHAR, M.,ANDERSON, K. W.,HILT, J. Z., Biocompatibility analysis of magnetic hydrogel nanocomposites based on poly(N-isopropylacrylamide) and iron oxide. **Journal of Biomedical Materials Research Part A**, 91A: 903-909, 2009.

60. FRIMPONG, R. A.,FRASER, S.,HILT, J. Z., Synthesis and temperature response analysis of magnetic-hydrogel nanocomposites. **Journal of Biomedical Materials Research Part A**, 80A: 1-6, 2007.

61. MEENACH, S. A.,OTU, C. G.,ANDERSON, K. W.,HILT, J. Z., Controlled synergistic delivery of paclitaxel and heat from poly(β-amino ester)/iron oxide-based hydrogel nanocomposites. **International Journal of Pharmaceutics**, 427: 177-184, 2012.

62. WANG, Q.,LIU, S.,SHENG, W.,GUANG, N.,LI, X., Synthesis and sol-gel transition of novel temperature responsive aba triblock-graft copolymers based on PCL and PEG analogues. **Macromolecular Research**, 23: 607-617, 2015.

63. CAO, H.,WANG, Q.,LI, M.,CHEN, Z., Synthesis of stimuli-responsive poly(ethylene glycol) diacrylate/methacrylic acid-based nanogels and their application as drug delivery vehicle. **Colloid and Polymer Science**, 293: 441-451, 2015.

64. LUTZ, J.-F.,HOTH, A., Preparation of Ideal PEG Analogues with a Tunable Thermosensitivity by Controlled Radical Copolymerization of 2-(2-

Methoxyethoxy)ethyl Methacrylate and Oligo(ethylene glycol) Methacrylate. **Macromolecules**, 39: 893-896, 2006.

65. XIA, M.,WU, W.,LIU, F.,THEATO, P.,ZHU, M., Swelling behavior of thermosensitive nanocomposite hydrogels composed of oligo(ethylene glycol) methacrylates and clay. **European Polymer Journal**, 69: 472-482, 2015.

66. CHEN, L.,CI, T.,YU, L.,DING, J., Effects of Molecular Weight and Its Distribution of PEG Block on Micellization and Thermogellability of PLGA–PEG–PLGA Copolymer Aqueous Solutions. **Macromolecules**, 48: 3662-3671, 2015.

67. MA, H.,HE, C.,CHENG, Y.,LI, D.,GONG, Y.,LIU, J.,TIAN, H.,CHEN, X., PLK1shRNA and doxorubicin co-loaded thermosensitive PLGA-PEG-PLGA hydrogels for osteosarcoma treatment. **Biomaterials**, 35: 8723-8734, 2014.

68. YAN, Q.,XIAO, L. Q.,TAN, L.,SUN, W.,WU, T.,CHEN, L. W.,MEI, Y.,SHI, B., Controlled release of simvastatin-loaded thermo-sensitive PLGA-PEG-PLGA hydrogel for bone tissue regeneration: in vitro and in vivo characteristics. **Journal of Biomedical Materials Research Part A**, 103: 3580-3589, 2015.

69. DE GRAAF, A. J.,AZEVEDO PRÓSPERO DOS SANTOS, I. I.,PIETERS, E. H. E.,RIJKERS, D. T. S.,VAN NOSTRUM, C. F.,VERMONDEN, T.,KOK, R. J.,HENNINK, W. E.,MASTROBATTISTA, E., A micelle-shedding thermosensitive hydrogel as sustained release formulation. **Journal of Controlled Release**, 162: 582-590, 2012.

70. WARSON, H., Modern Superabsorbent Polymer Technology, Edited by F L Buchholz and A T Graham, Wiley-VCH, New York, 1998, PP xvii + 279, ISBN price £85.00. **Polymer International**, 49: 1548-1548, 2000.

71. GUPTA, P.,VERMANI, K.,GARG, S., Hydrogels: from controlled release to pH-responsive drug delivery. **Drug Discovery Today**, 7: 569-579, 2002.

72. BETANCOURT, T.,PARDO, J.,SOO, K.,PEPPAS, N. A., Characterization of pH-responsive hydrogels of poly(itaconic acid-g-ethylene glycol) prepared by UV-initiated free radical polymerization as biomaterials for oral delivery of bioactive agents. **Journal of Biomedical Materials Research Part A**, 93A: 175-188, 2010.

73. KOETTING, M. C.,PEPPAS, N. A., pH-Responsive poly(itaconic acid-co-N-vinylpyrrolidone) hydrogels with reduced ionic strength loading solutions offer

improved oral delivery potential for high isoelectric point-exhibiting therapeutic proteins. **International Journal of Pharmaceutics**, 471: 83-91, 2014.

74. SHENG, W. J.,LIU, T.,LIU, S. X.,WANG, Q. Q.,LI, X.,GUANG, N., Temperature and pH responsive hydrogels based on polyethylene glycol analogues and poly(methacrylic acid) via click chemistry. **Polymer International**, 64: 1415-1424, 2015.

75. HE, X.,FAN, J. W.,ZHANG, F. W.,LI, R. C.,POLLACK, K. A.,RAYMOND, J. E.,ZOU, J.,WOOLEY, K. L., Multi-responsive hydrogels derived from the self-assembly of tethered allyl-functionalized racemic oligopeptides. **Journal of Materials Chemistry B**, 2: 8123-8130, 2014.

76. LI, G.,ZHANG, H.,FORTIN, D.,XIA, H.,ZHAO, Y., Poly(vinyl alcohol)–Poly(ethylene glycol) Double-Network Hydrogel: A General Approach to Shape Memory and Self-Healing Functionalities. **Langmuir**, 31: 11709-11716, 2015.

77. KOETTING, M. C.,GUIDO, J. F.,GUPTA, M.,ZHANG, A.,PEPPAS, N. A., pH-responsive and enzymatically-responsive hydrogel microparticles for the oral delivery of therapeutic proteins: Effects of protein size, crosslinking density, and hydrogel degradation on protein delivery. **Journal of Controlled Release**, 221: 18-25, 2016.

78. STEVENS, K. R.,MILLER, J. S.,BLAKELY, B. L.,CHEN, C. S.,BHATIA, S. N., Degradable hydrogels derived from PEG-diacrylamide for hepatic tissue engineering. **Journal of Biomedical Materials Research Part A**, 103: 3331-3338, 2015.

79. PAPAVASILIOU, G.,SOKIC, S.,TURTURRO, M., Biotechnology - Molecular Studies and Novel Applications for Improved Quality of Human Life. ed. R.H. Sammour: In Tech. 2012. 250.

80. WALTERS, K. A.,ROBERTS, M. S., Dermatologic, Cosmeceutic, and Cosmetic Development: Therapeutic and Novel Approaches. CRC Press. 2007.

81. LIN, C.-H.,YEH, Y.-H.,LIN, W.-C.,YANG, M.-C., Novel silicone hydrogel based on PDMS and PEGMA for contact lens application. **Colloids and Surfaces B: Biointerfaces**, 123: 986-994, 2014.

82. LIN, C.-H.,CHO, H.-L.,YEH, Y.-H.,YANG, M.-C., Improvement of the surface wettability of silicone hydrogel contact lenses via layer-by-layer self-assembly technique. **Colloids and Surfaces B: Biointerfaces**, 136: 735-743, 2015.

83. TANG, Q. W.,WU, J. H.,SUN, H.,FAN, S. J.,HU, D.,LIN, J. M., Synthesis of Polyacrylate/Poly(ethylene glycol) Hydrogel and its Absorption Properties for Heavy Metal Ions and Dye. **Polymer Composites**, 30: 1183-1189, 2009.

84. YUAN, Z. C.,WANG, Y.,HAN, X.,CHEN, D. J., The adsorption behaviors of the multiple stimulus-responsive poly(ethylene glycol)-based hydrogels for removal of RhB dye. **Journal of Applied Polymer Science**, 132: 8, 2015.

85. SAGLE, A. C.,JU, H.,FREEMAN, B. D.,SHARMA, M. M., PEG-based hydrogel membrane coatings. **Polymer**, 50: 756-766, 2009.

86. AMIDON, G. L.,LEE, P. I.,TOPP, E. M., Transport Processes in Pharmaceutical Systems. Taylor & Francis. 1999.

87. TAJIMA, H.,YOSHIDA, Y.,ABIKO, S.,YAMAGIWA, K., Size adjustment of spherical temperature-sensitive hydrogel beads by liquid–liquid dispersion using a Kenics static mixer. **Chemical Engineering Journal**, 156: 479-486, 2010.

88. LIU, H.,ZHEN, M.,WU, R., Ionic-Strength- and pH-Responsive Poly[acrylamide-co-(maleic acid)] Hydrogel Nanofibers. **Macromolecular Chemistry and Physics**, 208: 874-880, 2007.

89. VALADE, D.,WONG, L. K.,JEON, Y. J.,JIA, Z. F.,MONTEIRO, M. J., Polyacrylamide hydrogel membranes with controlled pore sizes. **Journal of Polymer Science Part a-Polymer Chemistry**, 51: 129-138, 2013.

90. HERTZ, J.,ROBINSON, R.,VALENZUELA, D. A.,LAVIK, E. B.,GOLDBERG, J. L., A tunable synthetic hydrogel system for culture of retinal ganglion cells and amacrine cells. **Acta Biomaterialia**, 9: 7622-7629, 2013.

91. WU, Y.,WEI, W.,ZHOU, M.,WANG, Y.,WU, J.,MA, G.,SU, Z., Thermal-sensitive hydrogel as adjuvant-free vaccine delivery system for H5N1 intranasal immunization. **Biomaterials**, 33: 2351-2360, 2012.

92. KONO, H., Characterization and properties of carboxymethyl cellulose hydrogels crosslinked by polyethylene glycol. **Carbohydrate Polymers**, 106: 84-93, 2014.

93. GAVIRA, J. A.,CERA-MANJARRES, A.,ORTIZ, K.,MENDEZ, J.,JIMENEZ-TORRES, J. A.,PATIÑO-LOPEZ, L. D.,TORRES-LUGO, M., Use of Cross-Linked Poly(ethylene glycol)-Based Hydrogels for Protein Crystallization. **Crystal Growth & Design**, 14: 3239-3248, 2014.

94. NGUYEN, M. K.,ALSBERG, E., Bioactive factor delivery strategies from engineered polymer hydrogels for therapeutic medicine. **Progress in Polymer Science**, 39: 1235-1265, 2014.

95. BUREK, M.,CZUBA, Z. P.,WASKIEWICZ, S., Novel acid-degradable and thermo-sensitive poly(N-isopropylacrylamide) hydrogels cross-linked by α,α-trehalose diacetals. **Polymer**, 55: 6460-6470, 2014.

96. REIS, A. V.,FAJARDO, A. R.,SCHUQUEL, I. T. A.,GUILHERME, M. R.,VIDOTTI, G. J.,RUBIRA, A. F.,MUNIZ, E. C., Reaction of Glycidyl Methacrylate at the Hydroxyl and Carboxylic Groups of Poly(vinyl alcohol) and Poly(acrylic acid): Is This Reaction Mechanism Still Unclear? **The Journal of Organic Chemistry**, 74: 3750-3757, 2009.

97. SIEPMANN, J.,PEPPAS, N. A., Modeling of drug release from delivery systems based on hydroxypropyl methylcellulose (HPMC). **Advanced Drug Delivery Reviews**, 48: 139-157, 2001.

98. DOKOUMETZIDIS, A.,PAPADOPOULOU, V.,MACHERAS, P., Analysis of Dissolution Data Using Modified Versions of Noyes–Whitney Equation and the Weibull Function. **Pharmaceutical Research**, 23: 256-261, 2006.

99. COSTA, P.,SOUSA LOBO, J. M., Modeling and comparison of dissolution profiles. **European Journal of Pharmaceutical Sciences**, 13: 123-133, 2001.

100. PAPADOPOULOU, V.,KOSMIDIS, K.,VLACHOU, M.,MACHERAS, P., On the use of the Weibull function for the discernment of drug release mechanisms. **International Journal of Pharmaceutics**, 309: 44-50, 2006.

101. COSTA, D.,VALENTE, A. J. M.,MIGUEL, M. G.,QUEIROZ, J., Gel Network Photodisruption: A New Strategy for the Codelivery of Plasmid DNA and Drugs. **Langmuir**, 27: 13780-13789, 2011.

102. SITTA, D. L. A.,GUILHERME, M. R.,DA SILVA, E. P.,VALENTE, A. J. M.,MUNIZ, E. C.,RUBIRA, A. F., Drug release mechanisms of chemically cross-linked albumin microparticles: Effect of the matrix erosion. **Colloids and Surfaces B: Biointerfaces**, 122: 404-413, 2014.

103. KUNITA, M. H.,GUILHERME, M. R.,FILHO, L. C.,MUNIZ, E. C.,FRANCESCHI, E.,DARIVA, C.,RUBIRA, A. F., Solid-state radical grafting reaction of glycidyl methacrylate and poly(4-methyl-1-pentene) in supercritical

carbon dioxide: Surface morphology and adhesion. **Journal of Colloid and Interface Science**, 361: 331-337, 2011.

104. CONTRERAS-LÓPEZ, D.,SALDÍVAR-GUERRA, E.,LUNA-BÁRCENAS, G., Copolymerization of isoprene with polar vinyl monomers: Reactivity ratios, characterization and thermal properties. **European Polymer Journal**, 49: 1760-1772, 2013.

105. WANG, S. S.,SHAO, L.,SONG, Z. Q.,ZHAO, J. R.,FENG, Y., Preparation of epoxy functionalized PP with unique structure and its post-ring open reaction. **Journal of Applied Polymer Science**, 124: 4827-4837, 2012.

106. WANG, X.,SHEN, Y.,LAI, X., Micromorphology and mechanism of polyurethane/polyacrylate membranes modified with epoxide group. **Progress in Organic Coatings**, 77: 268-276, 2014.

107. LIU, X.,XIANG, S.,YUE, Y.,SU, X.,ZHANG, W.,SONG, C.,WANG, P., Preparation of poly(acrylamide-co-acrylic acid) aqueous latex dispersions using anionic polyelectrolyte as stabilizer. **Colloids and Surfaces A: Physicochemical and Engineering Aspects**, 311: 131-139, 2007.

108. SOUCEK, M. D.,YI, Y., Synthesis and Characterization of Water Soluble Carboxymethyl Chitosan Grafted with Glycidyl Methacrylate. **Journal of Macromolecular Science Part a-Pure and Applied Chemistry**, 48: 562-568, 2011.

109. KOLYA, H.,TRIPATHY, T., Grafted Polysaccharides Based on Acrylamide and N,N-Dimethylacrylamide: Preparation and Investigation of Their Flocculation Performances. **Journal of Applied Polymer Science**, 127: 2786-2795, 2013.

110. KOLYA, H.,TRIPATHY, T., Hydroxyethyl Starch-g-Poly-(N,N-dimethylacrylamide-co-acrylic acid): An efficient dye removing agent. **European Polymer Journal**, 49: 4265-4275, 2013.

111. CROCKFORD, C.,GEEN, H.,TITMAN, J. J., Two-dimensional MAS–NMR spectra which correlate fast and slow magic angle spinning sideband patterns. **Chemical Physics Letters**, 344: 367-373, 2001.

112. HUNG, I.,GAN, Z., An efficient amplification pulse sequence for measuring chemical shift anisotropy under fast magic-angle spinning. **Journal of Magnetic Resonance**, 213: 196-199, 2011.

113. SHAHID, S. A.,QIDWAI, A. A.,ANWAR, F.,ULLAH, I.,RASHID, U., Improvement in the Water Retention Characteristics of Sandy Loam Soil Using a Newly Synthesized Poly(acrylamide-co-acrylic Acid)/AlZnFe2O4 Superabsorbent Hydrogel Nanocomposite Material. **Molecules**, 17: 9397-9412, 2012.

114. RASHIDZADEH, A.,OLAD, A.,SALARI, D.,REYHANITABAR, A., On the preparation and swelling properties of hydrogel nanocomposite based on Sodium alginate-g-Poly (acrylic acid-co-acrylamide)/Clinoptilolite and its application as slow release fertilizer. **Journal of Polymer Research**, 21: 1-15, 2014.

115. ÇAYKARA, T.,AKÇAKAYA, İ., Synthesis and network structure of ionic poly(N,N-dimethylacrylamide-co-acrylamide) hydrogels: Comparison of swelling degree with theory. **European Polymer Journal**, 42: 1437-1445, 2006.

116. PATEL, Y. N.,PATEL, M. P., A new fast swelling poly[DAPB-co-DMAAm-co-AASS] superabsorbent hydrogel for removal of anionic dyes from water. **Chinese Chemical Letters**, 24: 1005-1007, 2013.

117. LI, P.,XU, K.,TAN, Y.,LU, C.,LI, Y.,WANG, P., A novel fabrication method of temperature-responsive poly(acrylamide) composite hydrogel with high mechanical strength. **Polymer**, 54: 5830-5838, 2013.

118. POON, Y. F.,CAO, Y.,ZHU, Y.,JUDEH, Z. M. A.,CHAN-PARK, M. B., Addition of β-Malic Acid-Containing Poly(ethylene glycol) Dimethacrylate To Form Biodegradable and Biocompatible Hydrogels. **Biomacromolecules**, 10: 2043-2052, 2009.

119. GIAMMONA, G.,PITARRESI, G.,CRAPARO, F. E.,CAVALLARO, G.,BUSCEMI, S., New biodegradable hydrogels based on a photo-cross-linkable polyaspartamide and poly(ethylene glycol) derivatives. Release studies of an anticancer drug. **Colloid and Polymer Science**, 279: 771-783, 2001.

120. LEE, C.-Y.,TEYMOUR, F.,CAMASTRAL, H.,TIRELLI, N.,HUBBELL, J. A.,ELBERT, D. L.,PAPAVASILIOU, G., Characterization of the Network Structure of PEG Diacrylate Hydrogels Formed in the Presence of N-Vinyl Pyrrolidone. **Macromolecular Reaction Engineering**, 8: 314-328, 2014.

121. ALTAF, K.,ASHCROFT, I. A.,SALEH, N.,HAGUE, R., Environmental aging of epoxy based stereolithography parts Part 1-Moisture transport. **Plastics Rubber and Composites**, 41: 120-128, 2012.

122. KATOCH, S.,SHARMA, V.,KUNDU, P. P., Water sorption and diffusion through saturated polyester and their nanocomposites synthesized from glycolyzed PET waste with varied composition. **Chemical Engineering Science**, 65: 4378-4387, 2010.

123. WU, Q. X.,LI, M. Z.,YAO, S. J., Performances of NaCS-WSC protein drug microcapsules with different degree of substitution of NaCS using sodium polyphosphate as cross-linking agent. **Cellulose**, 21: 1897-1908, 2014.

124. SONG, F.,WANG, X.-L.,WANG, Y.-Z., Poly (N-isopropylacrylamide)/poly (ethylene oxide) blend nanofibrous scaffolds: Thermo-responsive carrier for controlled drug release. **Colloids and Surfaces B: Biointerfaces**, 88: 749-754, 2011.

125. CURCIO, M.,ALTIMARI, I.,SPIZZIRRI, U. G.,CIRILLO, G.,VITTORIO, O.,PUOCI, F.,PICCI, N.,IEMMA, F., Biodegradable gelatin-based nanospheres as pH-responsive drug delivery systems. **Journal of Nanoparticle Research**, 15: 11, 2013.

126. XU, T.,FARRIS, R. J., Stresses associated with diffusion in polyimide and polyacrylics films. **Journal of Applied Polymer Science**, 99: 2661-2670, 2006.

127. WIND, M. M.,LENDERINK, H. J. W., A capacitance study of pseudo-fickian diffusion in glassy polymer coatings. **Progress in Organic Coatings**, 28: 239-250, 1996.

128. SITTA, D. L. A.,GUILHERME, M. R.,GARCIA, F. P.,CELLET, T. S. P.,NAKAMURA, C. V.,MUNIZ, E. C.,RUBIRA, A. F., Covalent Albumin Microparticles as an Adjuvant for Production of Mucosal Vaccines against Hepatitis B. **Biomacromolecules**, 14: 3231-3237, 2013.

129. DA SILVA, E. P.,SITTA, D. L. A.,FRAGAL, V. H.,CELLET, T. S. P.,MAURICIO, M. R.,GARCIA, F. P.,NAKAMURA, C. V.,GUILHERME, M. R.,RUBIRA, A. F.,KUNITA, M. H., Covalent TiO2/pectin microspheres with Fe3O4 nanoparticles for magnetic field-modulated drug delivery. **International Journal of Biological Macromolecules**, 67: 43-52, 2014.

130. FIEL, S. B.,VINCKEN, W., Systemic corticosteroid therapy for acute asthma exacerbations. **Journal of Asthma**, 43: 321-331, 2006.

131. THROWER, B. W., Relapse Management in Multiple Sclerosis. **Neurologist**, 15: 1-5, 2009.

132. PROSAPIO, V.,DE MARCO, I.,REVERCHON, E., PVP/corticosteroid microspheres produced by supercritical antisolvent coprecipitation. **Chemical Engineering Journal**, 292: 264-275, 2016.

133. HU, T. T.,CAO, H.,YANG, C. L.,ZHANG, L. J.,JIANG, X. H.,GAO, X.,YANG, F.,HE, G.,SONG, X. R.,TONG, A. P.,GAO, G.,GONG, C. Y.,LI, R.,ZHANG, X. N.,WANG, X. C.,ZHENG, Y., LHD-Modified Mechanism-Based Liposome Coencapsulation of Mitoxantrone and Prednisolone Using Novel Lipid Bilayer Fusion for Tissue-Specific Colocalization and Synergistic Antitumor Effects. **ACS Applied Materials & Interfaces**, 8: 6586-6601, 2016.

134. MAHER, H. M.,ALZOMAN, N. Z.,SHEHATA, S. M., Simultaneous determination of selected tyrosine kinase inhibitors with corticosteroids and antiemetics in rat plasma by solid phase extraction and ultra-performance liquid chromatography–tandem mass spectrometry: Application to pharmacokinetic interaction studies. **Journal of Pharmaceutical and Biomedical Analysis**, 124: 216-227, 2016.

135. KUMRIA, R.,NAIR, A. B.,GOOMBER, G.,GUPTA, S., Buccal films of prednisolone with enhanced bioavailability. **Drug Delivery**, 23: 471-478, 2016.

136. DI COLO, G.,BAGGIANI, A.,ZAMBITO, Y.,MOLLICA, G.,GEPPI, M.,SERAFINI, M. F., A new hydrogel for the extended and complete prednisolone release in the GI tract. **International Journal of Pharmaceutics**, 310: 154-161, 2006.

137. VAN DER VALK, F. M.,VAN WIJK, D. F.,LOBATTO, M. E.,VERBERNE, H. J.,STORM, G.,WILLEMS, M. C. M.,LEGEMATE, D. A.,NEDERVEEN, A. J.,CALCAGO, C.,MANI, V.,RAMACHANDRAN, S.,PARIDAANS, M. P. M.,OTTEN, M. J.,DALLINGA-THIE, G. M.,FAYAD, Z. A.,NIEUWDORP, M.,SCHULTE, D. M.,METSELAAR, J. M.,MULDER, W. J. M.,STROES, E. S., Prednisolone-containing liposomes accumulate in human atherosclerotic macrophages upon intravenous administration. **Nanomedicine-Nanotechnology Biology and Medicine**, 11: 1039-1046, 2015.

138. PARK, H. S.,LEE, J. Y.,CHO, S. H.,BAEK, H. J.,LEE, S. J., Colon delivery of prednisolone based on chitosan coated polysaccharide tablets. **Archives of Pharmacal Research**, 25: 964-968, 2002.

139. BAYARD, F. J. C.,THIELEMANS, W.,PRITCHARD, D. I.,PAINE, S. W.,YOUNG, S. S.,BÄCKMAN, P.,EWING, P.,BOSQUILLON, C., Polyethylene glycol-drug ester conjugates for prolonged retention of small inhaled drugs in the lung. **Journal of Controlled Release**, 171: 234-240, 2013.

140. AKIN, A.,IŞIKLAN, N., Microwave assisted synthesis and characterization of sodium alginate-graft-poly(N,N′-dimethylacrylamide). **International Journal of Biological Macromolecules**, 82: 530-540, 2016.

141. MORALES-WIEMER, E. A.,MACOSSAY, J.,BUCIO, E., Radiation grafting of N,N′-dimethylacrylamide and 2-hydroxyethylmethacrylate onto polypropylene films by one step method. **Radiation Physics and Chemistry**, 84: 166-169, 2013.

142. SILVERSTEIN, R. M.,WEBSTER, F. X.,KIEMLE, D. J.,BRYCE, D. L., Spectrometric Identification of Organic Compounds. Wiley. 2014.

143. TENÓRIO-NETO, E. T.,BARAKET, A.,KABBAJ, D.,ZINE, N.,ERRACHID, A.,FESSI, H.,KUNITA, M. H.,ELAISSARI, A., Submicron magnetic core conducting polypyrrole polymer shell: Preparation and characterization. **Materials Science and Engineering: C**, 61: 688-694, 2016.

144. WIŚNIEWSKA, M.,URBAN, T.,GRZĄDKA, E.,ZARKO, V. I.,GUN'KO, V. M., Comparison of adsorption affinity of polyacrylic acid for surfaces of mixed silica–alumina. **Colloid and Polymer Science**, 292: 699-705, 2014.

145. HU, S.-H.,LIU, T.-Y.,LIU, D.-M.,CHEN, S.-Y., Controlled Pulsatile Drug Release from a Ferrogel by a High-Frequency Magnetic Field. **Macromolecules**, 40: 6786-6788, 2007.

146. KORSMEYER, R. W.,GURNY, R.,DOELKER, E.,BURI, P.,PEPPAS, N. A., Mechanisms of solute release from porous hydrophilic polymers. **International Journal of Pharmaceutics**, 15: 25-35, 1983.

147. RITGER, P. L.,PEPPAS, N. A., A simple equation for description of solute release I. Fickian and non-fickian release from non-swellable devices in the form of slabs, spheres, cylinders or discs. **Journal of Controlled Release**, 5: 23-36, 1987.

148. TENORIO-NETO, E. T.,SILVA, E. L.,CELLET, T. S. P.,SILVA, E. P.,FRANCESCHI, E.,FILHO, L. C.,RUBIRA, A. F.,KUNITA, M. H., Coprecipitation of Safrole Oxide with Poly(3-hydroxybutyrate-co-3-

hydroxyvalerate) in Supercritical Carbon Dioxide. **Journal of the Brazilian Chemical Society**, 24: 327-335, 2013.

149.   FU, Y.,KAO, W. J., Drug release kinetics and transport mechanisms of non-degradable and degradable polymeric delivery systems. **Expert Opinion on Drug Delivery**, 7: 429-444, 2010.

150.   KOH, I.,JOSEPHSON, L., Magnetic Nanoparticle Sensors. **Sensors**, 9: 8130-8145, 2009.

151.   AHSAN, A.,AZIZ, A.,ARSHAD, M. A.,ALI, O.,NAUMAN, M.,AHMAD, N. M.,ELAISSARI, A., Smart magnetically engineering colloids and biothin films for diagnostics applications. **Journal of Colloid Science and Biotechnology**, 2: 19-26, 2013.

152.   HÄFELI, U.,SCHÜTT, W.,TELLER, J.,ZBOROWSKI, M., Scientific and Clinical Applications of Magnetic Carriers. Springer US. 2013.

153.   VILKNER, T.,JANASEK, D.,MANZ, A., Micro total analysis systems. Recent developments. **Analytical Chemistry**, 76: 3373-3385, 2004.

154.   MONTAGNE, F.,MONDAIN-MONVAL, O.,PICHOT, C.,ELAISSARI, A., Highly magnetic latexes from submicrometer oil in water ferrofluid emulsions. **Journal of Polymer Science Part a-Polymer Chemistry**, 44: 2642-2656, 2006.

155.   MONTAGNE, F.,BRACONNOT, S.,MONDAIN-MONVAL, O.,PICHOT, C.,ELAISSARI, A., Colloidal and physicochemical characterization of highly magnetic O/W magnetic emulsions. **Journal of Dispersion Science and Technology**, 24: 821-832, 2003.

156.   ELAISSARI, A., Colloidal Polymers: Synthesis and Characterization. Taylor & Francis. 2003.

157.   HIDALGO-ALVAREZ, R., Structure and Functional Properties of Colloidal Systems. CRC Press. 2009.

158.   AHMED, N.,FESSI, H.,ELAISSARI, A., Theranostic applications of nanoparticles in cancer. **Drug Discovery Today**, 17: 928-934, 2012.

159.   JAMSHAID, T.,EISSA, M.,ZINE, N.,EL-SALHI, A. E.,AHMAD, N. M.,ELAISSARI, A., *Soft Hybrid Nanoparticles: from Preparation to Biomedical Applications*, in *Soft Nanoparticles for Biomedical Applications*2014. p. 312-341.

160.   MEDEIROS, S. F.,LARA, B. R.,OLIVEIRA, P. F. M.,MORAES, R. M.,ALVES, G. M.,ELAISSARI, A.,SANTOS, A. M., Stimuli-Responsive and Biocompatible

Poly(N-vinylcaprolactam-co-acrylic acid)-Coated Iron Oxide Nanoparticles by Nanoprecipitation Technique. **Journal of Colloid Science and Biotechnology**, 2: 180-194, 2013.

161. RAHMAN, M. M.,ABDELHAMID, E., Multi-Stimuli Responsive Magnetic Core–Shell Particles: Synthesis, Characterization and Specific RNA Recognition. **Journal of Colloid Science and Biotechnology**, 1: 3-15, 2012.

162. MACKOVÁ, H.,HORÁK, D.,TRACHTOVÁ,TEPÁNKA,RITTICH, B.,PANOVÁ, A., The Use of Magnetic Poly(N-isopropylacrylamide) Microspheres for Separation of DNA from Probiotic Dairy Products. **Journal of Colloid Science and Biotechnology**, 1: 235-240, 2012.

163. ELAISSARI, A., Colloidal Biomolecules, Biomaterials, and Biomedical Applications. Taylor & Francis. 2003.

164. DUGAS, V.,ELAISSARI, A.,CHEVALIER, Y., Recognition Receptors in Biosensors. New York: Springer. 2010. 849.

165. VEYRET, R.,DELAIR, T.,PICHOT, C.,ELAISSARI, A., Amino-containing magnetic nanoemulsions: elaboration and nucleic acid extraction. **Journal of Magnetism and Magnetic Materials**, 295: 155-163, 2005.

166. JOO, J.,YIM, C.,KWON, D.,LEE, J.,SHIN, H. H.,CHA, H. J.,JEON, S., A facile and sensitive detection of pathogenic bacteria using magnetic nanoparticles and optical nanocrystal probes. **Analyst**, 137: 3609-3612, 2012.

167. BANKS, R. E.,DUNN, M. J.,HOCHSTRASSER, D. F.,SANCHEZ, J.-C.,BLACKSTOCK, W.,PAPPIN, D. J.,SELBY, P. J., Proteomics: new perspectives, new biomedical opportunities. **The Lancet**, 356: 1749-1756, 2000.

168. CHENG, J.,FORTINA, P.,SURREY, S.,KRICKA, L. J.,WILDING, P., Microchip-based devices for molecular diagnosis of genetic diseases. **Molecular Diagnosis**, 1: 183-200, 1996.

169. TUDOS, A. J.,BESSELINK, G. A. J.,SCHASFOORT, R. B. M., Trends in miniaturized total analysis systems for point-of-care testing in clinical chemistry. **Lab on a Chip**, 1: 83-95, 2001.

170. YAGER, P.,EDWARDS, T.,FU, E.,HELTON, K.,NELSON, K.,TAM, M. R.,WEIGL, B. H., Microfluidic diagnostic technologies for global public health. **Nature**, 442: 412-418, 2006.

171. MYERS, F. B.,LEE, L. P., Innovations in optical microfluidic technologies for point-of-care diagnostics. **Lab on a Chip**, 8: 2015-2031, 2008.

172. BASELT, D. R.,LEE, G. U.,NATESAN, M.,METZGER, S. W.,SHEEHAN, P. E.,COLTON, R. J., A biosensor based on magnetoresistance technology1. **Biosensors and Bioelectronics**, 13: 731-739, 1998.

173. RIFE, J. C.,MILLER, M. M.,SHEEHAN, P. E.,TAMANAHA, C. R.,TONDRA, M.,WHITMAN, L. J., Design and performance of GMR sensors for the detection of magnetic microbeads in biosensors. **Sensors and Actuators A: Physical**, 107: 209-218, 2003.

174. GIJS, M. A. M.,LACHARME, F.,LEHMANN, U., Microfluidic Applications of Magnetic Particles for Biological Analysis and Catalysis. **Chemical Reviews**, 110: 1518-1563, 2010.

175. PAMME, N., Magnetism and microfluidics. **Lab on a Chip**, 6: 24-38, 2006.

176. GIJS, M. A. M., Magnetic bead handling on-chip: new opportunities for analytical applications. **Microfluidics and Nanofluidics**, 1: 22-40, 2004.

177. LIEN, K.-Y.,LIN, J.-L.,LIU, C.-Y.,LEI, H.-Y.,LEE, G.-B., Purification and enrichment of virus samples utilizing magnetic beads on a microfluidic system. **Lab on a Chip**, 7: 868-875, 2007.

178. DANCKWARDT, N. Z.,FRANZREB, M.,GUBER, A. E.,SAILE, V., Pump-free transport of magnetic particles in microfluidic channels. **Journal of Magnetism and Magnetic Materials**, 323: 2776-2781, 2011.

179. PAMME, N.,EIJKEL, J. C. T.,MANZ, A., On-chip free-flow magnetophoresis: Separation and detection of mixtures of magnetic particles in continuous flow. **Journal of Magnetism and Magnetic Materials**, 307: 237-244, 2006.

180. HATCH, G. P.,STELTER, R. E., Magnetic design considerations for devices and particles used for biological high-gradient magnetic separation (HGMS) systems. **Journal of Magnetism and Magnetic Materials**, 225: 262-276, 2001.

181. PAMME, N.,KOYAMA, R.,MANZ, A., Counting and sizing of particles and particle agglomerates in a microfluidic device using laser light scattering: application to a particle-enhanced immunoassay. **Lab on a Chip**, 3: 187-192, 2003.

182. SCHRUM, D. P.,CULBERTSON, C. T.,JACOBSON, S. C.,RAMSEY, J. M., Microchip flow cytometry using electrokinetic focusing. **Analytical Chemistry**, 71: 4173-4177, 1999.

183. PAMME, N., On-chip bioanalysis with magnetic particles. **Current Opinion in Chemical Biology**, 16: 436-443, 2012.

184. WEST, J.,BECKER, M.,TOMBRINK, S.,MANZ, A., Micro Total Analysis Systems: Latest Achievements. **Analytical Chemistry**, 80: 4403-4419, 2008.

185. LOMBARDI, D.,DITTRICH, P. S., Droplet microfluidics with magnetic beads: a new tool to investigate drug-protein interactions. **Analytical and Bioanalytical Chemistry**, 399: 347-352, 2011.

186. LIU, Y. J.,GUO, S. S.,ZHANG, Z. L.,HUANG, W. H.,BAIGL, D.,XIE, M.,CHEN, Y.,PANG, D. W., A micropillar-integrated smart microfluidic device for specific capture and sorting of cells. **Electrophoresis**, 28: 4713-4722, 2007.

187. SCHUURMAN, T.,DE BOER, R.,PATTY, R.,KOOISTRA-SMID, M.,VAN ZWET, A., Comparative evaluation of in-house manual, and commercial semi-automated and automated DNA extraction platforms in the sample preparation of human stool specimens for a Salmonella enterica 5'-nuclease assay. **Journal of Microbiological Methods**, 71: 238-245, 2007.

188. LEB, V.,STOCHER, M.,VALENTINE-THON, E.,HOLZL, G.,KESSLER, H.,STEKAL, H.,BERG, J., Fully automated, internally controlled quantification of hepatitis B virus DNA by real-time PCR by use of the MagNA pure LC and LightCycler instruments. **Journal of Clinical Microbiology**, 42: 585-590, 2004.

189. ZHAO, W.,YAO, S.,HSING, I. M., A microsystem compatible strategy for viable Escherichia coli detection. **Biosensors and Bioelectronics**, 21: 1163-1170, 2006.

190. LUND-OLESEN, T.,DUFVA, M.,HANSEN, M. F., Capture of DNA in microfluidic channel using magnetic beads: Increasing capture efficiency with integrated microfluidic mixer. **Journal of Magnetism and Magnetic Materials**, 311: 396-400, 2007.

191. KRENKOVA, J.,FORET, F., Immobilized microfluidic enzymatic reactors. **Electrophoresis**, 25: 3550-3563, 2004.

192. SLOVAKOVA, M.,MINC, N.,BILKOVA, Z.,SMADJA, C.,FAIGLE, W.,FUTTERER, C.,TAVERNA, M.,VIOVY, J.-L., Use of self assembled magnetic beads for on-chip protein digestion. **Lab on a Chip**, 5: 935-942, 2005.

193. LADJ, R.,BITAR, A.,EISSA, M.,MUGNIER, Y.,LE DANTEC, R.,FESSI, H.,ELAISSARI, A., Individual inorganic nanoparticles: preparation, functionalization and in vitro biomedical diagnostic applications. **Journal of Materials Chemistry B**, 1: 1381-1396, 2013.

194. CASILLAS, P. E. G.,PÉREZ, C. A. M.,GONZALEZ, C. A. R., Infrared Spectroscopy of Functionalized Magnetic Nanoparticles. INTECH Open Access Publisher. 2012.

195. TEJA, A. S.,KOH, P.-Y., Synthesis, properties, and applications of magnetic iron oxide nanoparticles. **Progress in Crystal Growth and Characterization of Materials**, 55: 22-45, 2009.

196. RAHMAN, M. M.,ELAISSARI, A., *Organic–inorganic hybrid magnetic latex*, in *Hybrid Latex Particles: Preparation with (Mini)emulsion Polymerization*, A.M. van Herk, S.A.F. Bon, and K. Landfester, Editors. 2010, Springer: Berlim. p. 237-282.

197. ELAISSARI, A.,FESSI, H., Reactive and Highly Submicron Magnetic Latexes for Bionanotechnology Applications. **Macromolecular Symposia**, 288: 115-120, 2010.

198. OH, J. K.,PARK, J. M., Iron oxide-based superparamagnetic polymeric nanomaterials: Design, preparation, and biomedical application. **Progress in Polymer Science**, 36: 168-189, 2011.

199. MAHDAVI, M.,BIN AHMAD, M.,HARON, M. J.,NAMVAR, F.,NADI, B.,AB RAHMAN, M. Z.,AMIN, J., Synthesis, Surface Modification and Characterisation of Biocompatible Magnetic Iron Oxide Nanoparticles for Biomedical Applications. **Molecules**, 18: 7533-7548, 2013.

200. RAVIKUMAR, C.,KUMAR, S.,BANDYOPADHYAYA, R., Aggregation of dextran coated magnetic nanoparticles in aqueous medium: Experiments and Monte Carlo simulation. **Colloids and Surfaces A: Physicochemical and Engineering Aspects**, 403: 1-6, 2012.

201. PAUL, K. G.,FRIGO, T. B.,GROMAN, J. Y.,GROMAN, E. V., Synthesis of Ultrasmall Superparamagnetic Iron Oxides Using Reduced Polysaccharides. **Bioconjugate Chemistry**, 15: 394-401, 2004.

202. THOMAS, L. A.,DEKKER, L.,KALLUMADIL, M.,SOUTHERN, P.,WILSON, M.,NAIR, S. P.,PANKHURST, Q. A.,PARKIN, I. P., Carboxylic acid-stabilised

iron oxide nanoparticles for use in magnetic hyperthermia. **Journal of Materials Chemistry**, 19: 6529-6535, 2009.

203. AQIL, A.,VASSEUR, S.,DUGUET, E.,PASSIRANI, C.,BENOÎT, J. P.,ROCH, A.,MÜLLER, R.,JÉRÔME, R.,JÉRÔME, C., PEO coated magnetic nanoparticles for biomedical application. **European Polymer Journal**, 44: 3191-3199, 2008.

204. ANDRADE, Â.,FABRIS, J.,FERREIRA, R.,DOMINGUES, R., *Coating Nanomagnetic Particles for Biomedical Applications*, in *Biomedical Engineering Frontiers and Challenges*, R. Fazel, Editor 2011, InTech. p. 158-176.

205. RAHMAN, M. M.,ELAISSARI, A., Multi-Stimuli Responsive Magnetic Core–Shell Particles: Synthesis, Characterization and Specific RNA Recognition. **Journal of Colloid Science and Biotechnology**, 1: 3-15, 2012.

206. CARLOS, L.,MÁRTIRE, D. O.,EINSCHLAG, F. S. G.,GONZÁLEZ, M. C., *Applications of magnetite nanoparticles for heavy metal removal from wastewater*, in *Waste Water - Treatment Technologies and Recent Analytical Developments*, F.S.G. Einschlag and L. Carlos, Editors. 2013, InTech. p. 63-77.

207. IUPAC, *Compendium of Chemical Terminology*, in *The Gold Book*, A.D. McNaught and A. Wilkinson, Editors. 2006, Blackwell Scientific Publications: Oxford

208. BUD, R.,WARNER, D. J., Instruments of Science: An Historical Encyclopedia. Science Museum, London, and National Museum of American History, Smithsonian Institution. 1998.

209. MALLAKPOUR, S.,TAGHAVI, M., Kinetics and Thermal Degradation Study of Optically Active and Thermally Stable Aromatic Polyamides with Flame-Retardancy Properties. **Polym. J**, 41: 308-318, 2009.

210. DOBKOWSKI, Z.,RUDNIK, E., Lifetime prediction for polymers via the temperature of initial decomposition part 2. **Journal of Thermal Analysis and Calorimetry**, 69: 693-697, 2002.

211. OLIVEIRA, M.,DE MIRANDA SANTOS, L.,DE GOIS DA SILVA, M.,DA CUNHA, H.,DA SILVA FILHO, E.,DA SILVA LEITE, C., Preparation and characterization of composite polyaniline/poly(vinyl alcohol)/palygorskite. **Journal of Thermal Analysis and Calorimetry**, 119: 37-46, 2015.

212. CHENG, S. Z. D., Handbook of Thermal Analysis and Calorimetry: Applications to Polymers and Plastics. Vol. 3: Elsevier Science. 2002. 858.

213. SARAJI-BOZORGZAD, M.,GEISSLER, R.,STREIBEL, T.,MÜHLBERGER, F.,SKLORZ, M.,KAISERSBERGER, E.,DENNER, T.,ZIMMERMANN, R., Thermogravimetry Coupled to Single Photon Ionization Quadrupole Mass Spectrometry: A Tool To Investigate the Chemical Signature of Thermal Decomposition of Polymeric Materials. **Analytical Chemistry**, 80: 3393-3403, 2008.

214. ALSHEHRI, S. M.,AL-FAWAZ, A.,AHAMAD, T., Thermal kinetic parameters and evolved gas analysis (TG–FTIR–MS) for thiourea–formaldehyde based polymer metal complexes. **Journal of Analytical and Applied Pyrolysis**, 101: 215-221, 2013.

215. HAINES, P. J., Principles of Thermal Analysis and Calorimetry. ed. R.S.o.C. paperbacks: Royal Society of Chemistry. 2002. 220.

216. FERNÁNDEZ-BERRIDI, M. J.,GONZÁLEZ, N.,MUGICA, A.,BERNICOT, C., Pyrolysis-FTIR and TGA techniques as tools in the characterization of blends of natural rubber and SBR. **Thermochimica Acta**, 444: 65-70, 2006.

217. MOTIEE, F.,TAGHVAEI-GANJALI, S.,MALEKZADEH, M., Investigation of correlation between rheological properties of rubber compounds based on natural rubber/styrene-butadiene rubber with their thermal behaviors. **International Journal of Industrial Chemistry**, 4: 16, 2013.

218. BUSCHOW, K. H. J.,BOER, F. R., Physics of Magnetism and Magnetic Materials. Vol. 7, New York: Springer. 2003. 182.

219. MICHALOWSKY, L., Magnettechnik: Grundlagen, Werkstoffe, Anwendungen. 3rd ed Fachbuchverlag Leipzig: Vulkan-Verlag. 2006.

220. CORNELL, R. M.,SCHWERTMANN, U., The Iron Oxides: Structure, Properties, Reactions, Occurrences and Uses. 2nd ed: Wiley. 2006. 703.

221. DAVE, S. R.,GAO, X. H., Monodisperse magnetic nanoparticles for biodetection, imaging, and drug delivery: a versatile and evolving technology. **Wiley Interdisciplinary Reviews-Nanomedicine and Nanobiotechnology**, 1: 583-609, 2009.

222. MONTAGNE, F.,MONDAIN-MONVAL, O.,PICHOT, C.,MOZZANEGA, H.,ELAÏSSARI, A., Preparation and characterization of narrow sized (o/w) magnetic emulsion. **Journal of Magnetism and Magnetic Materials**, 250: 302-312, 2002.

223. BITAR, A.,KAEWSANEHA, C.,EISSA, M. M.,JAMSHAID, T.,TANGBORIBOONRAT, P.,POLPANICH, D.,ELAISSARI, A., Ferrofluids: From Preparation to Biomedical Applications. **Journal of Colloid Science and Biotechnology**, 3: 3-18, 2014.

224. MONTAGNE, F.,BRACONNOT, S.,ELAÏSSARI, A.,PICHOT, C.,DANIEL, J. C.,MANDRAND, B.,MONDAIN-MONVAL, O., Force Measurements Between Emulsion Droplets-ssDNA Conjugates: A New Tool for Medical Diagnostics. **Journal of Nanoscience and Nanotechnology**, 6: 2312-2319, 2006.

225. EISSA, M. M.,MAHBUBOR RAHMAN, M.,ZINE, N.,JAFFREZIC, N.,ERRACHID, A.,FESSI, H.,ELAISSARI, A., Reactive magnetic poly(divinylbenzene-co-glycidyl methacrylate) colloidal particles for specific antigen detection using microcontact printing technique. **Acta Biomaterialia**, 9: 5573-5582, 2013.

226. RAHMAN, M. M.,CHEHIMI, M. M.,FESSI, H.,ELAISSARI, A., Highly temperature responsive core–shell magnetic particles: Synthesis, characterization and colloidal properties. **Journal of Colloid and Interface Science**, 360: 556-564, 2011.

227. ZHANG, L.,HE, R.,GU, H. C., Oleic acid coating on the monodisperse magnetite nanoparticles. **Applied Surface Science**, 253: 2611-2617, 2006.

228. RAMIREZ, L. P.,LANDFESTER, K., Magnetic polystyrene nanoparticles with a high magnetite content obtained by miniemulsion processes. **Macromolecular Chemistry and Physics**, 204: 22-31, 2003.

229. ZHAO, S. Y.,LEE, D. K.,KIM, C. W.,CHA, R. G.,KIM, Y. H.,KANG, Y. S., Synthesis of magnetic nanoparticles of Fe3O4 and CoFe2O4 and their surface modification by surfactant adsorption. **Bulletin of the Korean Chemical Society**, 27: 237-242, 2006.

230. ZHAO, H.,SAATCHI, K.,HAFELI, U. O., Preparation of biodegradable magnetic microspheres with poly(lactic acid)-coated magnetite. **Journal of Magnetism and Magnetic Materials**, 321: 1356-1363, 2009.

231. XU, Z. Z.,WANG, C. C.,YANG, W. L.,DENG, Y. H.,FU, S. K., Encapsulation of nanosized magnetic iron oxide by polyacrylamide via inverse miniemulsion polymerization. **Journal of Magnetism and Magnetic Materials**, 277: 136-143, 2004.

232. GUO, L.,LIU, G.,HONG, R.-Y.,LI, H.-Z., Preparation and Characterization of Chitosan Poly(acrylic acid) Magnetic Microspheres. **Marine Drugs**, 8: 2212-2222, 2010.

233. YAMAURA, M.,CAMILO, R. L.,SAMPAIO, L. C.,MACÊDO, M. A.,NAKAMURA, M.,TOMA, H. E., Preparation and characterization of (3-aminopropyl)triethoxysilane-coated magnetite nanoparticles. **Journal of Magnetism and Magnetic Materials**, 279: 210-217, 2004.

234. CHEN, Y.,QIAN, Z.,ZHANG, Z., Novel preparation of magnetite/polystyrene composite particles via inverse emulsion polymerization. **Colloids and Surfaces A: Physicochemical and Engineering Aspects**, 312: 209-213, 2008.

235. XU, Y. W.,XU, H.,GU, H. C., Controllable Preparation of Epoxy-Functionalized Magnetic Polymer Latexes with Different Morphologies by Modified Miniemulsion Polymerization. **Journal of Polymer Science Part a-Polymer Chemistry**, 48: 2284-2293, 2010.

236. NGUYEN, Q. H.,QUYEN, D. H.,HOANG, T. K. N., A new route of emulsifier-free emulsion polymerization for the preparation of polymer coated magnetite nanoparticles. **Materials Science-Poland**, 32: 264-271, 2014.

237. CHEN, Y. J.,XIONG, Z. C.,ZHANG, L. Y.,ZHAO, J. Y.,ZHANG, Q. Q.,PENG, L.,ZHANG, W. B.,YE, M. L.,ZOU, H. F., Facile synthesis of zwitterionic polymer-coated core-shell magnetic nanoparticles for highly specific capture of N-linked glycopeptides. **Nanoscale**, 7: 3100-3108, 2015.

238. LIU, X. Q.,KAMINSKI, M. D.,CHEN, H. T.,TORNO, M.,TAYLOR, L.,ROSENGART, A. J., Synthesis and characterization of highly-magnetic biodegradable poly(D,L-lactide-co-glycolide) nanospheres. **Journal of Controlled Release**, 119: 52-58, 2007.

239. CASTELLO, J.,GALLARDO, M.,BUSQUETS, M. A.,ESTELRICH, J., Chitosan (or alginate)-coated iron oxide nanoparticles: A comparative study. **Colloids and Surfaces a-Physicochemical and Engineering Aspects**, 468: 151-158, 2015.

240. BRACONNOT, S.,EISSA, M. M.,ELAISSARI, A., Morphology control of magnetic latex particles prepared from oil in water ferrofluid emulsion. **Colloid and Polymer Science**, 291: 193-203, 2013.

241. FURDUI, V. I.,HARRISON, D. J., Immunomagnetic T cell capture from blood for PCR analysis using microfluidic systems. **Lab on a Chip**, 4: 614-618, 2004.

242. ELAISSARI, A.,FESSI, H., Advances in the Biomedical Applications of Reactive Colloids. **Brazilian Journal of Physics**, 39: 146-149, 2009.

243. HOOD, M. A.,MARI, M.,MUNOZ-ESPI, R., Synthetic Strategies in the Preparation of Polymer/Inorganic Hybrid Nanoparticles. **Materials**, 7: 4057-4087, 2014.

244. TIAN, R.,CHEN, X.,XU, X.,YAO, C., Electrocatalytic activity of core/shell magnetic nanocomposite. **Analytical Biochemistry**, 463: 45-53, 2014.

245. RAHMAN, M. M.,AHMAD, H.,ISLAM, M. M., Preparation and Potential Applications of Magnetically Recyclable Biocatalysis. **Journal of Colloid Science and Biotechnology**, 2: 171-179, 2013.

246. THEVENOT, J.,OLIVEIRA, H.,SANDRE, O.,LECOMMANDOUX, S., Magnetic responsive polymer composite materials. **Chemical Society Reviews**, 42: 7099-7116, 2013.

247. CUI, Y.,CHEN, X.,LI, Y.,LIU, X.,LEI, L.,ZHANG, Y.,QIAN, J., Superparamagnetic Polymer Emulsion Particles from a Soap-Free Seeded Emulsion Polymerization and their Application for Lipase Immobilization. **Applied Biochemistry and Biotechnology**, 172: 701-712, 2014.

248. WANG, W.,LIU, M.,GU, J.,ZHANG, Q.,MAYS, J. W., Convenient synthesis and morphology of latex particles composed of poly (methyl methacrylate)-b-poly (n-butyl acrylate) by 1, 1-diphenylethylene (DPE) seeded emulsion polymerization. **Journal of Polymer Research**, 21: 1-8, 2014.

249. LIU, H.,WANG, C.,GAO, Q.,LIU, X.,TONG, Z., Magnetic hydrogels with supracolloidal structures prepared by suspension polymerization stabilized by Fe2O3 nanoparticles. **Acta Biomaterialia**, 6: 275-281, 2010.

250. CHAKRABORTY, S.,JÄHNICHEN, K.,KOMBER, H.,BASFAR, A. A.,VOIT, B., Synthesis of Magnetic Polystyrene Nanoparticles Using Amphiphilic Ionic Liquid Stabilized RAFT Mediated Miniemulsion Polymerization. **Macromolecules**, 47: 4186-4198, 2014.

251. HORÁK, D.,TRCHOVÁ, M.,BENEŠ, M. J.,VEVERKA, M.,POLLERT, E., Monodisperse magnetic composite poly(glycidyl methacrylate)/La0.75Sr0.25MnO3 microspheres by the dispersion polymerization. **Polymer**, 51: 3116-3122, 2010.

252. RAMLI, R. A.,LAFTAH, W. A.,HASHIM, S., Core-shell polymers: a review. **RSC Advances**, 3: 15543-15565, 2013.

253. MEDEIROS, S. F.,SANTOS, A. M.,FESSI, H.,ELAISSARI, A., Thermally-Sensitive and Magnetic Poly(N-Vinylcaprolactam)-Based Nanogels by Inverse Miniemulsion Polymerization **Journal of Colloid Science and Biotechnology**, 1: 99-112, 2012.

254. ROMIO, A. P.,RODRIGUES, H. H.,PERES, A.,VIEGAS, A. D.,KOBITSKAYA, E.,ZIENER, U.,LANDFESTER, K.,SAYER, C.,ARAUJO, P. H. H., Encapsulation of magnetic nickel nanoparticles via inverse miniemulsion polymerization. **Journal of Applied Polymer Science**, 129: 1426-1433, 2013.

255. UGELSTAD, J.,OLSVIK, Ø.,SCHMID, R.,BERGE, A.,FUNDERUD, S.,NUSTAD, K., *Immunoaffinity Separation of Cells Using Monosized Magnetic Polymer Beads*, in *Molecular Interactions in Bioseparations*, T.T. Ngo, Editor 2013, Springer US.

256. RAHMAN, M. M.,CHEHIMI, M. M.,ELAISSARI, A., Temperature, pH and Diol Tri-Sensing Magnetic Particles for Specific Ribonucleic Acid Recognition. **Journal of Colloid Science and Biotechnology**, 3: 46-57, 2014.

257. XIE, L.,MA, S.,YANG, Q.,LAN, F.,WU, Y.,GU, Z., Double-sided coordination assembly: superparamagnetic composite microspheres with layer-by-layer structure for protein separation. **RSC Advances**, 4: 1055-1061, 2014.

258. GAO, R.,MU, X.,ZHANG, J.,TANG, Y., Specific recognition of bovine serum albumin using superparamagnetic molecularly imprinted nanomaterials prepared by two-stage core-shell sol-gel polymerization. **Journal of Materials Chemistry B**, 2: 783-792, 2014.

259. NASEER, N.,FATIMA, H.,ASGHAR, A.,FATIMA, N.,AHMED, N.,KHAN, A. U.,AHMAD, N. M., Magnetically Responsive Hybrid Polymer Colloids for Ultrasensitive Molecular Imaging. **Journal of Colloid Science and Biotechnology**, 3: 19-29, 2014.

260. KUMAR, K. S.,KUMAR, V. B.,PAIK, P., Recent Advancement in Functional Core-Shell Nanoparticles of Polymers: Synthesis, Physical Properties, and Applications in Medical Biotechnology. **Journal of Nanoparticles**, 2013: 24, 2013.

261. LATTUADA, M.,HATTON, T. A., Synthesis, properties and applications of Janus nanoparticles. **Nano Today**, 6: 286-308, 2011.

262. WALTHER, A.,MÜLLER, A. H. E., Janus Particles: Synthesis, Self-Assembly, Physical Properties, and Applications. **Chemical Reviews**, 113: 5194-5261, 2013.

263. WALTHER, A.,HOFFMANN, M.,MÜLLER, A. H. E., Emulsion Polymerization Using Janus Particles as Stabilizers. **Angewandte Chemie International Edition**, 47: 711-714, 2008.

264. YOSHIDA, M.,ROH, K. H.,MANDAL, S.,BHASKAR, S.,LIM, D. W.,NANDIVADA, H.,DENG, X. P.,LAHANN, J., Structurally Controlled Bio-hybrid Materials Based on Unidirectional Association of Anisotropic Microparticles with Human Endothelial Cells. **Advanced Materials**, 21: 4920-4925, 2009.

265. SYNYTSKA, A.,KHANUM, R.,IONOV, L.,CHERIF, C.,BELLMANN, C., Water-Repellent Textile via Decorating Fibers with Amphiphilic Janus Particles. **ACS Applied Materials & Interfaces**, 3: 1216-1220, 2011.

266. XU, S.,MA, W.-F.,YOU, L.-J.,LI, J.-M.,GUO, J.,HU, J. J.,WANG, C.-C., Toward Designer Magnetite/Polystyrene Colloidal Composite Microspheres with Controllable Nanostructures and Desirable Surface Functionalities. **Langmuir**, 28: 3271-3278, 2012.

267. CHANG, Y.-C.,CHEN, D.-H., Preparation and adsorption properties of monodisperse chitosan-bound Fe3O4 magnetic nanoparticles for removal of Cu(II) ions. **Journal of Colloid and Interface Science**, 283: 446-451, 2005.

268. RAHMAN, M. M.,MONTAGNE, F.,FESSI, H.,ELAISSARI, A., Anisotropic magnetic microparticles from ferrofluid emulsion. **Soft Matter**, 7: 1483-1490, 2011.

269. EL-MAHDY, G. A.,ATTA, A. M.,AL-LOHEDAN, H. A., Synthesis and Evaluation of Poly(Sodium 2-Acrylamido-2-Methylpropane Sulfonate-co-Styrene)/Magnetite Nanoparticle Composites as Corrosion Inhibitors for Steel. **Molecules**, 19: 1713-1731, 2014.

270. LU, S.,RAMOS, J.,FORCADA, J., Self-Stabilized Magnetic Polymeric Composite Nanoparticles by Emulsifier-Free Miniemulsion Polymerization. **Langmuir**, 23: 12893-12900, 2007.

271. LI, L.,MA, R.,IYI, N.,EBINA, Y.,TAKADA, K.,SASAKI, T., Hollow nanoshell of layered double hydroxide. **Chemical Communications**: 3125-3127, 2006.

272. GROCHALA, W.,CYRANSKI, M. K.,DERZSI, M.,MICHALOWSKI, T.,MALINOWSKI, P. J.,MAZEJ, Z.,KURZYDLOWSKI, D.,KOZMINSKI, W.,BUDZIANOWSKI, A.,LESZCZYNSKI, P. J., Crystal and electronic structure, lattice dynamics and thermal properties of Ag(i)(SO3)R (R = F, CF3) Lewis acids in the solid state. **Dalton Transactions**, 41: 2034-2047, 2012.

273. MACHIDA, M.,KAWAMURA, K.,KAWANO, T.,ZHANG, D.,IKEUE, K., Layered Pr-dodecyl sulfate mesophases as precursors of Pr2O2SO4 having a large oxygen-storage capacity. **Journal of Materials Chemistry**, 16: 3084-3090, 2006.

274. YOON, H., Current Trends in Sensors Based on Conducting Polymer Nanomaterials. **Nanomaterials**, 3: 524-549, 2013.

275. WANG, N.,LI, G.,YU, Z.,ZHANG, X.,QI, X., Conductive polypyrrole/viscose fiber composites. **Carbohydrate Polymers**, 127: 332-339, 2015.

276. YOON, H.,JANG, J., Conducting-Polymer Nanomaterials for High-Performance Sensor Applications: Issues and Challenges. **Advanced Functional Materials**, 19: 1567-1576, 2009.

277. LINA, M. C.,ALISON, B. F., Smart fabric sensors and e-textile technologies: a review. **Smart Materials and Structures**, 23: 053001, 2014.

278. SHAHNAVAZ, Z.,LORESTANI, F.,ALIAS, Y.,WOI, P. M., Polypyrrole–ZnFe2O4 magnetic nano-composite with core–shell structure for glucose sensing. **Applied Surface Science**, 317: 622-629, 2014.

279. JANG, K. S.,LEE, H.,MOON, B., Synthesis and characterization of water soluble polypyrrole doped with functional dopants. **Synthetic Metals**, 143: 289-294, 2004.

280. MONTOYA, P.,MEJÍA, S.,GONÇALES, V. R.,TORRESI, S. I. C. D.,CALDERÓN, J. A., Performance improvement of macroporous polypyrrole sensor for detection of ammonia by incorporation of magnetite nanoparticles. **Sensors and Actuators B: Chemical**, 213: 444-451, 2015.

281. RAHMAN, M. M.,LI, X. B.,LOPA, N. S.,AHN, S. J.,LEE, J. J., Electrochemical DNA Hybridization Sensors Based on Conducting Polymers. **Sensors**, 15: 3801-3829, 2015.

282. LIN, M.,CHO, M. S.,CHOE, W. S.,LEE, Y., Electrochemical analysis of copper ion using a Gly–Gly–His tripeptide modified poly(3-thiopheneacetic acid) biosensor. **Biosensors and Bioelectronics**, 25: 28-33, 2009.

283. PIMPHA, N.,CHALEAWLERT-UMPON, S.,SUNINTABOON, P., Core/shell polymethyl methacrylate/polyethyleneimine particles incorporating large amounts of iron oxide nanoparticles prepared by emulsifier-free emulsion polymerization. **Polymer**, 53: 2015-2022, 2012.

284. AGHA, H.,FLEURY, J.-B.,GALERNE, Y., Polypyrrole coating films for nanoparticles. **Colloids and Surfaces A: Physicochemical and Engineering Aspects**, 462: 217-224, 2014.

285. BLOEMEN, M.,BRULLOT, W.,LUONG, T. T.,GEUKENS, N.,GILS, A.,VERBIEST, T., Improved functionalization of oleic acid-coated iron oxide nanoparticles for biomedical applications. **Journal of Nanoparticle Research**, 14: 10, 2012.

286. DUBIS, A. T.,GRABOWSKI, S. J.,ROMANOWSKA, D. B.,MISIASZEK, T.,LESZCZYNSKI, J., Pyrrole-2-carboxylic Acid and Its Dimers: Molecular Structures and Vibrational Spectrum. **The Journal of Physical Chemistry A**, 106: 10613-10621, 2002.

287. UPADHYAY, J.,KUMAR, A.,GOGOI, B.,BURAGOHAIN, A. K., Antibacterial and hemolysis activity of polypyrrole nanotubes decorated with silver nanoparticles by an in-situ reduction process. **Materials Science and Engineering: C**, 54: 8-13, 2015.

288. YANG, Z.,SHANG, X.,ZHANG, C.,ZHU, J., Photoelectrochemical bilirubin biosensor based on Fe3O4/hydroxyapatite/molecularly imprinted polypyrrole nanoparticles. **Sensors and Actuators B: Chemical**, 201: 167-172, 2014.

289. KUCHERYAVY, P.,HE, J.,JOHN, V. T.,MAHARJAN, P.,SPINU, L.,GOLOVERDA, G. Z.,KOLESNICHENKO, V. L., Superparamagnetic Iron Oxide Nanoparticles with Variable Size and an Iron Oxidation State as Prospective Imaging Agents. **Langmuir**, 29: 710-716, 2013.